Thermokinetics synergistic effects on co-pyrolysis of coal and rice husk blends for bioenergy production

By

Maham Tauseef

Reg. No.: 00000321016

Session 2019-21

Supervised by

Dr. Abeera Ayaz Ansari

A Thesis Submitted to U.S.-Pakistan Center for Advanced Studies in Energy in partial fulfillment of the requirement for the degree of

MASTER of SCIENCE in

ENERGY SYSTEMS ENGINEERING

U.S.-Pakistan Center for Advanced Studies in Energy (USPCAS-E)

National University of Sciences and Technology (NUST)

H-12, Islamabad 44000, Pakistan

March 2022

THESIS ACCEPTANCE CERTIFICATE

Certified that final copy of MS/MPhil thesis written by Miss. **Maham Tauseef**
(Registration No. 00000321016), of U.S.-Pakistan Center for Advanced Studies in
Energy has been vetted by undersigned, found complete in all respects as per NUST
Statues/Regulations, is within similarity indices limit and accepted as partial fulfillment
for award of MS/MPhil degree. It is further certified that necessary amendments as
pointed out by GEC members of the scholar have also been incorporated in the said
thesis.

Signature: _____

Name of Supervisor: Dr. Abeera Ayaz Ansari

Date: _____

Signature (HoD): _____

Date: _____

Signature (Dean/Principal): _____

Date: _____

CERTIFICATE

This is to certify that the work in this thesis has been carried out by Miss. **Maham Tauseef** and completed under my supervision in Fossil Fuel Lab, U.S.-Pakistan Center for Advanced Studies in Energy (USPCAS-E), National University of Sciences and Technology, H-12, Islamabad, Pakistan.

Supervisor:
_____
Dr. Abeera Ayaz Ansari
USPCAS-E
NUST, Islamabad

GEC member # 1
_____
Dr. Rabia Liaquat
USPCAS-E
NUST, Islamabad

GEC member # 2:
_____
Dr. Asif Hussain Khoja
USPCAS-E
NUST, Islamabad

GEC member # 3:
_____
Dr. Muhammad Bilal Sajid
USPCAS-E
NUST, Islamabad

HoD-ESE:
_____
Dr. Rabia Liaquat
USPCAS-E
NUST, Islamabad

Dean/Principal:
_____
Prof Dr. Adeel Waqas
USPCAS-E
NUST Islamabad

ACKNOWLEDGEMENT

DEDICATION

I would like to dedicate this thesis to my loving parents, my inspirations in life, who taught me how to fight against the struggles of life. My father who supported me through every thick and thin of life, my mother who taught me to be patient and work hard until you achieve your goals, and my teachers whose guidance helped me to achieve this status in my life.

ABSTRACT

In-depth thermodynamic and kinetic, synergistic effects of the coal and rice husk blends on co-pyrolysis have been investigated for bioenergy production. The thermo-kinetic rate parameters were determined for chemical, one-dimensional diffusional, and phase interfacial reaction models especially when fitted to the Coats-Redfern method. The fitted models exhibited thermo-kinetic rate parameters. The thermogravimetric analysis in view of the thermodynamic parameters including enthalpy, Gibbs free energy, and entropy imparted the prominent degradation temperature ranges (Stage A: 200 °C-400 °C, Stage B: 410 °C-560 °C) for co-pyrolysis reactions of blends. The proportional increase of rise husk into coal for Stage A caused an increase in the apparent values of activation energy, enthalpy specifically for one-dimensional diffusional, and phase interfacial reaction models. In case of Stage B, the increasing share of rice husk into coal proved to be beneficial in decreasing values of activation energy and enthalpy. Positive synergies for 80:20 and 60:40 coal-rice husk blends were calculated. In addition to characterization analysis of all samples; co-pyrolysis and co-gasification experiments were completed in a tubular fixed bed reactor at Stage B and onwards temperatures for synergized blends. The resultant co-pyrolysis biochar samples revealed honeycomb structure useful in adsorption applications. The gas chromatography-mass spectrometry analysis of the bio-oil yields 23% phenols, 11% acids, and methoxy phenols for the 60:40 coal-rice husk blend. The product gas composition of 2% H_2, 14% CH_4, and 4% CO_2 for the 80:20 coal-rice husk blend increased to 3% H_2, 12% CH_4, and 5% CO_2 for the 60:40 blend. The co-gasification process substantially increased the production of H_2 up to 14%-17% when compared to co-pyrolysis results. The approach used in this study can be utilized to capitalize on synergy to enhance co-pyrolysis of appropriate blends and their products can be used in further future applications upon upgradation.

Keywords: Co-pyrolysis; Co-gasification; coal-biomass blends; Thermo-kinetic; Bio-oil; Bio-char;

TABLE OF CONTENTS

LIST OF FIGURES

LIST OF TABLES

LIST OF ABBREVIATIONS

C	Coal
DTG	Derived Thermogravimetric Analysis
EDS	Energy-Dispersive X-Ray Spectrometry
FTIR	Fourier Transform Infrared Spectroscopy
GCV	Gross Calorific Value
GC-MS	Gas Chromatography-Mass Spectrometry
GHG	Greenhouse Gases
PB	Pine Butter
RH	Rice Husk
SEM	Scanning Electron Microscope
TGA	Thermogravimetric Analysis
WL	Weight loss

LIST OF PUBLICATIONS

1. **"Thermokinetics Synergistic Effects on Co-Pyrolysis of Coal and Rice Husk Blends for Bioenergy Production"**. Fuel (IF 6.609, W Category, Q1) (Published)

Chapter 1

Introduction

1.1 Background of the study

Growing population, rapid increase in industrialization concurrently complying to restrict the global warming to 1.5^oC raise potential challenges to sustainability and also increase the energy demand [1]. World energy consumption predicts a strong increase in the energy demand, with the yearly consumption of energy estimated to go around 16.5 billion tons and increased by 15 % before 2030 [2]. The detrimental impacts of fossil fuels as primary energy resources on the environment are scientifically well documented, however, the economic growth rates for developing as well-developed nations necessitates their continuing consumption. The premise of ongoing research and development in the energy and environment sector is to curb the increase of CO_2 whilst offsetting the consumption of fossil fuels without creating energy crises to meet energy and emission targets for the 21st century [3]. 21st century has not yet seen any significant reduction in conventional fossil fuel demands. Therefore, natural gas, coal and oil remains the main resources to meet energy demands like, fuel production, electricity generation, heating, and energy for power plants. **Fig 1.1** depicts the energy consumption (million tons) of conventional fossil fuels (coal, oil, and natural gas), biomass and renewable energy resources in 2020 and compares it with forecasted energy consumption rate in the year 2030 and 2040.

In spite of constant improvement in exploration technologies and regular details on the detection of new resources of oil and gas, the increased production cannot meet the world's energy demand and thus a gap is present between the demand and the supply of these two energy resources [4, 5]. Fossil fuel usage has also contributed to global warming and climate change [6]. Coal still dominates the global primary energy consumption by resource; nevertheless, this conventional energy resource is producing greenhouse gases (GHGs) at an accelerated rate causing a serious threat to global energy

and environmental sustainability. Consequently, there is a vital need of global integration of conventional and renewable energy via clean utilization of coal and other fossil fuels [3].
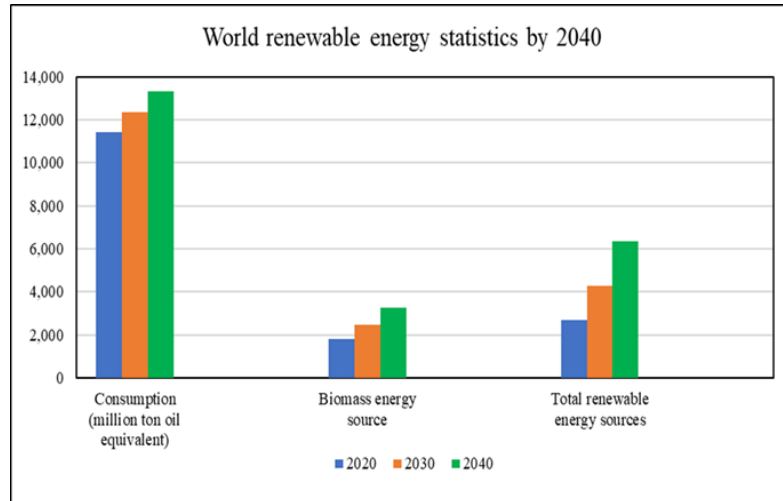
Fig 1.1 World renewable energy scenario by 2040 [7]

Coal fired power plants are still considered as the main source of production of electricity in the United States and will be used for energy generation till 2040 [8]. Coal is still expected to meet the energy demand in many nations [8], especially the developed or rapidly developing nations. Coal combustion contributes to 30-40% of share in greenhouse gas (GHGs) emissions [9]. Therefore, usage of coal needs special consideration because of the probability of continued energy generation and the potential for replacing petroleum for fuels to some extent. Due to these factors, a lot of interest has been seen in finding alternative or renewable energy resources [10] which could potentially lead to:

- Decrease in greenhouse gas (GHGs) emissions caused by deployment of coal and other fossil fuels
- Need for dependence on sustainable energy resources because of the depleting resources and varying costs of oil and natural gas.

Among such alternatives is biomass energy resource, which is readily available worldwide. Biomass is defined as an organic matter which is derived from plants and animals. It includes agricultural residue, wood residue, energy crops, industrial waste,

animal manure etc. Biomass has proven to be a reliable source of renewable energy to mitigate the emissions and other harmful effects caused by deployment of coal [11]. The deployment of renewable resources especially biomass has established prominence in the field of energy production due to incentives such as supply reliance, emissions mitigation [12], cheap and carbon neutral resource [13], diversified potential for biofuel production [14].

It has been seen that biomass accounts for around 97% of global generation of bioenergy. **Fig 1.2** represents the global bioenergy distribution in different regions. Total 62 countries are utilizing biomass resources for power generation. According to statistics, USA is the top producer of generating power through biomass, followed by Germany, Japan and Brazil and UK as major producers of biomass derived power [15].
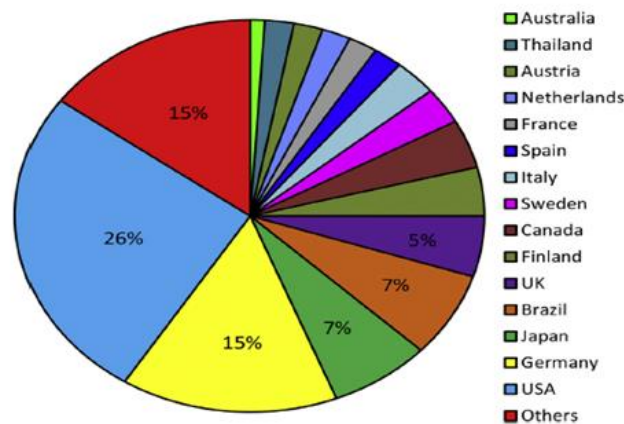
Fig 1.2 Global distribution of bio-energy [15]

Various thermochemical conversion technologies are used to obtain energy from biomass. These technologies include liquefaction, torrefaction, gasification, combustion and pyrolysis [16]. Liquefaction is a complex process and it requires high temperature and high pressure[17]. Torrefaction, on the other hand, is a technique that increases the energy density of biomass. In this process the material is heated in an inert or air atmosphere at a temperature of 200-300°C at a specified time interval [18]. The products are solids, liquids, and non-condensable gases. Energy density increases because dehydration and carboxylic reactions destroy the structure of biomass which in turn produces feedstock with high densities that can be used in co-firing processes [19]. But

the challenges of this technology are mainly associated with the handling of process gases and impurity and densification of biomass after being torrefied. After successful densification the problems of storage and handling can be overcome and can be stored easily [20]. Another technique is gasification where the biomass is heated at a temperature >700°C to obtain syngas which can be efficiently utilized to produce liquid fuels for transportation[21]. This process depends upon different parameters and takes place after various mechanisms like drying, combustion, and reduction. Some tars are also produced in gasification during syngas production. These tars undergo steam reforming to further produce syngas and in this way tar is removed from the gas [22].

Pyrolysis is a process which converts biomass into biofuels in an inert atmosphere and the products obtained are biochar, bio-oil and gases which can be further used in a number of applications[23, 24]. Decomposition of biomass can be divided into different stages such as (i) drying, (ii) primary pyrolysis, and (iii) secondary pyrolysis. In each step, the nature of components that undergo degradation are quite different. Primary pyrolysis occurs at a temperature of 250-600°C. This stage is associated with decomposition of hemicellulose, cellulose, lignin, water with some volatiles and condensable liquids. The remaining solid residue is called biochar. Basically, long chains of hemicellulose, cellulose, lignin decompose into smaller hydrocarbons. The residual biochar can be used for many agricultural purposes in soil amendment, carbon sequestration, as an activated carbon etc. Liquid product obtained from pyrolysis is known as bio-oil which may vary from yellowish brown to dark brown in color. Bio-oils are the main desired product from pyrolysis because they can replace the conventional liquid fuels in transportation sector which degrade the environment [25].

The process of pyrolysis is classified into three types namely slow, fast and flash pyrolysis[26]. Slow pyrolysis has a longer residence time of (5-30min) and lower heating rates (<10°C/s). biochar is the main product [27]. Fast pyrolysis has slightly higher heating rates (>100 C/s) with residence time of 0.5-2 seconds. Here bio-oil is the main product. However, this bio-oil is slightly unstable and acidic in nature due to the presence of aldehydes, ketones, phenols, and alcohols which are abundantly present in

biomass. For production of stable and good quality bio-oil, catalytic processes are used. This bio-oil can then be utilized for various application like in petroleum refineries[26]. Unlike the other types, Flash pyrolysis has very less residence time (<0.5 seconds) and very high heating rates (>500°C/s). this process aims to produce more liquids and gaseous products[28]. **Fig 1.3** provides further differentiation between these different types of pyrolysis.
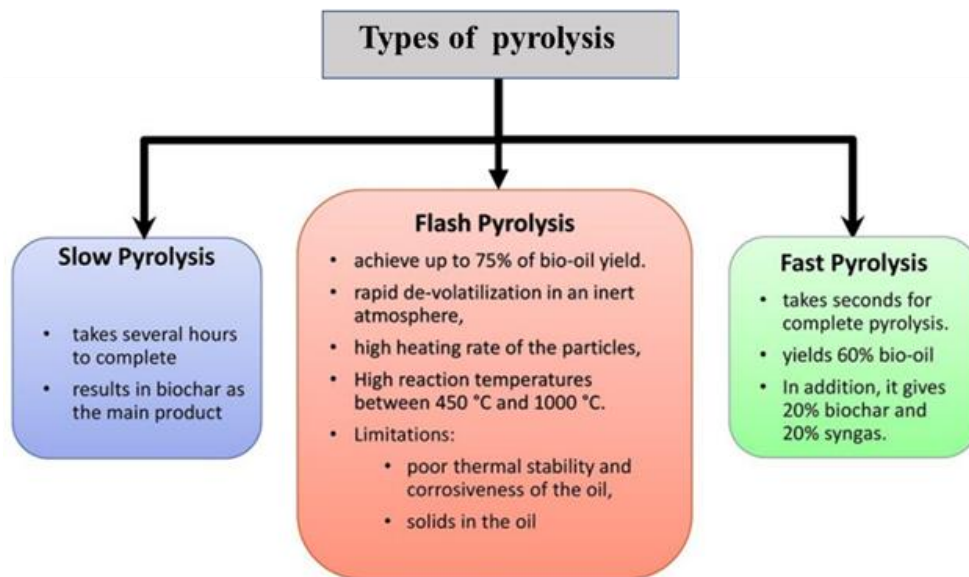
Fig 1.3 Different types of pyrolysis [29]

The thermochemical conversions routes such as combustion, pyrolysis, gasification, and liquefaction of a single type of conventional fuel have limited application when compared to the approach adopted for co-utilization of the same with biomass [16]. Co-use of fuels mitigate the limitations of sole fuel such as high moisture content, low calorific value, variation in the compositions, flexible operation, cleaner and better conversion yield. In addition a considerable interest also lies in advancement of effective techniques to recover materials and energy from wastes [30].

In case of energy generation, co-pyrolysis of biomass is considered as a favorable technology to obtain different bio-products, such as bio-oil, biochar and mixture of gaseous products [31]. It is a low energy intensive process with resulting fuels (solid, liquid and gas) ideal for various applications [32]. Co-pyrolysis include

devolatilization of biomass to form char, tar, gases, resulting in solid-gases and gases-tar reactions. Coal-biomass co-pyrolysis apart from paving the way to greater efficiency with better utilization of biomass, volume reduction of waste can also improve the quality of pyrolytic oils produced form coal only [33]. **Fig.1.4** represents the basic process of co-pyrolysis of coal-biomass blends.
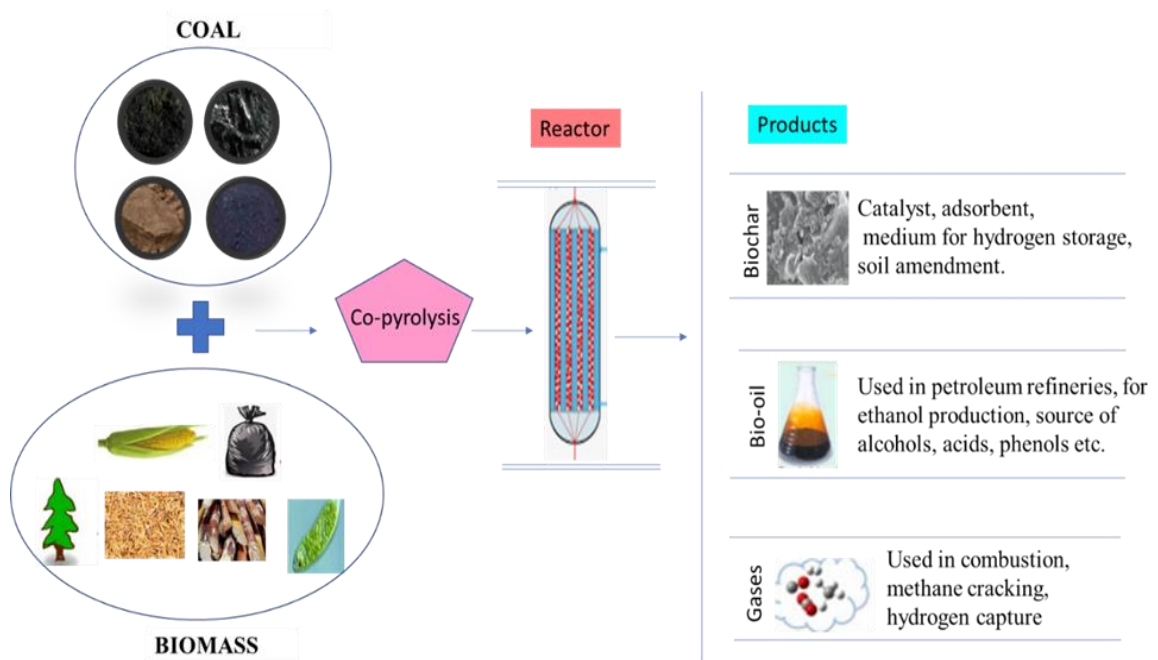
Fig 1.4 Schematic of co-pyrolysis of coal-biomass blends

The co-utilization of coal and biomass can economically be very beneficial and reliable for operating a large commercial scale energy plant. A biomass energy plant can also use the locally available coal when there is a shortage of biomass feedstock which can in turn avoid the high transportation costs of delivering that particular type of biomass from long and far distances. Similarly for coal energy plants, the costs can be decreased by blending a cheap biomass waste with coal.

Co-pyrolysis also enables densification of energy when feedstocks are blended as it overcomes the disadvantages of using biomass alone as a feedstock due to its lower calorific value, low carbon content etc. So, this shows that addition of coal to biomass can improve the energy content and decrease the supplementary energy inputs. Moreover, co-pyrolysis followed by co-gasification can produce more amount of

hydrogen. The co-gasification process can also be enhanced by different metal elements present in biomass which serve as catalytically active species[34].

In some studies co-pyrolysis of bituminous coal and woody biomass exhibited no synergy, whereas, in other bituminous and lignite coal blends with cellulose, lignin, and pine sawdust presented synergistic effect in batch pyrolysis reactor [35]. Generally, thermogravimetric analysis (TGA) is widely used for an in-depth investigation of co-pyrolysis process [36, 37]. The synergistic effect may activate due to availability of enough hydrogen (H_2) donors, free radicals and volatiles as biomass has greater H/C ratio than coal [38]. It was observed that co-pyrolysis of coal slime and coffee residue showed synergistic effect at blending ratio of 70% coffee residue and 30% coal [39]. Corn straw and lignite co-pyrolysis suggested the presence of synergistic effect, however when oxidative environment was enabled it inhibited the production of volatile matter indicating the absence of synergy [40]. Co-pyrolysis of coal gangue and coffee residue showed that blending ratio of 30% coffee residue and 70% coal gangue was considered as the ideal blend for co-pyrolysis [41]. Coal tar asphaltene and biomass co-pyrolysis revealed the presence of synergistic effect [42]. Co-pyrolysis of coal and polyethylene revealed that synergistic effect reduces the activation energy of co-pyrolysis. The study further highlighted that the distributions of H and OH radicals contributed to this interaction mechanism [43]. Thus, the thermo-kinetic behavior of the coal-biomass blends reveals the mechanistic insights of the pyrolysis process and assists in the decision-making path for suitable coal-biomass ratio.

Various kinetic models have been used to study the mechanistic behavior of blends and to assess the reactivity of these fuels with changing blending ratios, heating rates as well as type of coal and biomass [44]. Coats-Redfern is one of the model-fitting methods that has been practiced to predict behavior of coal-biomass blends, possible reaction mechanisms and to calculate the apparent values of activation energy (E_a), pre-exponential factor (A), and linear regression co-efficient (R^2) for each stage of co-pyrolysis [45, 46]. Coats-Redfern method assess the validity of various models and provides the most appropriate model for decomposition of coal-biomass blends [47]. Kinetic analysis of coal and sawdust blends by Coats-Redfern method suggested that

results were in agreement with behavior of both feedstocks [48]. So, this method can be used to assess the mechanistic behavior of blends. Various kinds of biomasses are available with different physical and chemical characteristics, amongst them rice husk (RH) as a feedstock has a great potential for co-pyrolysis due to its low cost and availability specially in agriculture-based countries. RH, usually discarded as waste material, has an effective burning efficiency. The thermochemical conversion of RH is known to produce solid residue to synthesize silica based materials for a number of applications [49]. RH is also used for bio-char and ethanol production [50].

1.2 Problem statement

Co-pyrolysis of coal and biomass has great potential to be the most prominent green technology for production of different kinds of products (solid, liquid, gas). It can utilize different types of biomass feedstocks for energy production, meanwhile reducing the consumption of coal, which causes significant environmental hazards and is a threat to sustainable future. It should be noted that biomass alone cannot be used to produce energy efficient products because of its lower calorific value, low carbon content, high moisture content etc., However, once its co-utilized with coal, the blend demonstrates significantly improved calorific value [51], increased hydrogen production and decreased GHG emissions [52]. An appropriate blending mix also needs to be identified with in-depth investigations of thermodynamic and kinetic parameters to study the complex reaction chemistry. Another main problem associated with co-pyrolysis of coal and biomass is that two types of feedstocks should interact synergistically in order to produce more gaseous and liquid products.

1.3 Research objectives

Considering all the recent advances in co-pyrolysis, this research will examine thermal, kinetic, and thermodynamic characteristics of coal-biomass blends for enhancing bio-energy production. The objectives of this research are as follows:

- To synthesize and characterize Coal-Rice Husk blends
- To study the synergistic effect in different biomass-coal blends

- To investigate the thermo-kinetic and thermo-dynamic behavior of different biomass and coal blends and determine parameters like activation energy, enthalpy, Gibbs free energy, entropy etc.

- To determine appropriate blending mix and conduct detailed characterization of co-pyrolysis products

- To enable co-gasification for enhanced syngas production

1.4 Scope and limitations of research

The aim of this study is to investigate the thermo-kinetic and thermo-dynamic behavior of various coal-RH blends during co-pyrolysis at a constant heating rate of 20°C/min and determine the understanding of blend profiles, rate parameters for chemical (F_1, $F_{1.5}$), one-dimensional diffusional (D_1), and phase interfacial (S_1) reaction models especially when fitted to the Coats-Redfern method. The blends are also characterized using ultimate analysis (CHN-S), gross calorific value (GCV), Fourier transform infrared analysis (FTIR), thermogravimetric analysis (TGA) and derived thermogravimetric analysis (DTG). Moreover, this study also attempts to carry out detailed characterization and analysis of co-pyrolysis biochar, bio-oil and product gases to understand the interactions of coal-RH blends. In this research, Rice Husk (RH) was used as biomass to be blended with coal and the effects of blending at different ratios was examined using different characterization techniques including Ultimate analysis (CHN-S), Calorific value analysis (GCV), Fourier transform infrared analysis (FTIR), Thermogravimetric (TGA) and derived thermogravimetric analysis (DTG). Kinetic and thermodynamic modeling was performed to evaluate different parameters. Synergistic effect of blends was analyzed, and the blends were pyrolyzed in tubular fixed bed reactor to obtain different kinds of products followed by co-gasification of the blends. Gas chromatography, Scanning Electron Microscopy, Electron Dispersive X-Ray Spectroscopy, TGA and FTIR was performed to evaluate the physical and chemical characteristics of biochar and bio-oil. Gas chromatography was performed to evaluate the production rate of product gases (specially hydrogen and methane) for commercial level applications. The limitations of this research include thermogravimetric analysis to

9

be performed at different heating rates, instead of a constant heating rate, which was not possible due to laboratory and time limitations.

1.5 Thesis structure

The outline of thesis structure is represented in **Fig. 1.5**

Chapter 1	• Provides an overview about world energy consumption, followed by the discussion on biomass utilization, co-pyrolysis of coal and biomass • The objectives of this research and the scope of the research was also discussed.
Chapter 2	• A comprehensive literature review was presented in this chapter. • Composition analysis of coal/biomass, different factors affecting co-pyrolysis behavior, and nature of the products were discussed in detail
Chapter 3	• This chapter covered the complete flow of research. The discussion started from preparation of blends followed by their detailed characterization. Kinetic and thermodynamic modeling followed by synergistic analysis and calculations was discussed. • At the end of the chapter, experimental setup and conditions for co-pyrolysis and co-gasification was also discussed
Chapter 4	• All the results obtained using different characterization techniques were plotted in this chapter. • Discussion on the parameters and reasons that could be responsible for these results have been elaborated
Chapter 5	• This chapter concludes complete methodology, objectives, results and a thorough discussion on obtained results. • Recommendations for upcoming research areas have also been suggested

Fig 1.5 Thesis Structure

Summary

This chapter discussed the background of the proposed work and enlightened how co-pyrolysis of coal and biomass could serve as an alternative and a clean energy source, simultaneously overcoming the disadvantages of biomass pyrolysis alone. Global energy concerns were discussed predicting the future of conventional and non-conventional energy resources to meet the energy demand. Various problems of conventional technique of biomass pyrolysis were discussed. Furthermore, innovative technique of co-pyrolysis was discussed, and it was suggested that co-pyrolysis is a promising technology to utilize the benefits of coal and biomass altogether for energy production and a cleaner future. Finally, the reason behind selection of this research, the objectives of this study and the scope of the proposed research was discussed.

References

[1] G. Bensidhom, A. Ben Hassen Trabelsi, M.A. mahmood, S. Ceylan, Insights into pyrolytic feedstock potential of date palm industry wastes: Kinetic study and product characterization, Fuel, 285 (2021) 119096.

[2] V. Khare, C. Khare, S. Nema, P. Baredar, Chapter 1-Introduction to Energy Sources, Tidal Energy Systems, (2019) 1-39.

[3] F. Sher, M.A. Pans, D.T. Afilaka, C. Sun, H. Liu, Experimental investigation of woody and non-woody biomass combustion in a bubbling fluidised bed combustor focusing on gaseous emissions and temperature profiles, Energy, 141 (2017) 2069-2080.

[4] Q. Xu, Investigation of co-gasification characteristics of biomass and coal in fluidized bed gasifiers, (2013).

[5] M. Silk, M. Ackiewicz, J. Anderson, O. Ogunsola, Overview of fundamentals of synthetic ultraclean transportation fuel production, ACS Publications2007.

[6] G.J. Velders, S.O. Andersen, J.S. Daniel, D.W. Fahey, M. McFarland, The importance of the Montreal Protocol in protecting climate, Proceedings of the National Academy of Sciences, 104 (2007) 4814-4819.

[7] A. Demirbas, Global renewable energy projections, Energy Sources, Part B, 4 (2009) 212-224.

[8] M. Balat, Influence of coal as an energy source on environmental pollution, Energy Sources, Part A: Recovery, Utilization, and Environmental Effects, 29 (2007) 581-589.

[9] G. Liu, E.D. Larson, R.H. Williams, T.G. Kreutz, X. Guo, Making Fischer− Tropsch fuels and electricity from coal and biomass: performance and cost analysis, Energy & Fuels, 25 (2011) 415-437.

[10] P. Basu, Biomass gasification and pyrolysis: practical design and theory, Academic press2010.

[11] A.A. Khan, W. de Jong, P.J. Jansens, H. Spliethoff, Biomass combustion in fluidized bed boilers: Potential problems and remedies, Fuel Processing Technology, 90 (2009) 21-50.

[12] P. McNamee, L.I. Darvell, J.M. Jones, A. Williams, The combustion characteristics of high-heating-rate chars from untreated and torrefied biomass fuels, Biomass and Bioenergy, 82 (2015) 63-72.

[13] A.A. Bhuiyan, A.S. Blicblau, A.K.M.S. Islam, J. Naser, A review on thermo-chemical characteristics of coal/biomass co-firing in industrial furnace, Journal of the Energy Institute, 91 (2018) 1-18.

[14] M.A. Munawar, A.H. Khoja, S.R. Naqvi, M.T. Mehran, M. Hassan, R. Liaquat, U.F. Dawood, Challenges and opportunities in biomass ash management and its utilization in novel applications, Renew Sust Energ Rev, 150 (2021) 111451.

[15] A. Evans, V. Strezov, T.J. Evans, Sustainability considerations for electricity generation from biomass, Renewable and Sustainable Energy Reviews, 14 (2010) 1419-1427.

[16] H.C. Ong, W.-H. Chen, A. Farooq, Y.Y. Gan, K.T. Lee, V. Ashokkumar, Catalytic thermochemical conversion of biomass for biofuel production: A comprehensive review, Renewable and Sustainable Energy Reviews, 113 (2019) 109266.

[17] W.-H. Chen, Y.-Y. Lin, H.-C. Liu, T.-C. Chen, C.-H. Hung, C.-H. Chen, H.C. Ong, A comprehensive analysis of food waste derived liquefaction bio-oil properties for industrial application, Applied Energy, 237 (2019) 283-291.

[18] M. Rudolfsson, E. Borén, L. Pommer, A. Nordin, T.A. Lestander, Combined effects of torrefaction and pelletization parameters on the quality of pellets produced from torrefied biomass, Applied Energy, 191 (2017) 414-424.

[19] A. Zheng, Z. Zhao, S. Chang, Z. Huang, F. He, H. Li, Effect of torrefaction temperature on product distribution from two-staged pyrolysis of biomass, Energy & Fuels, 26 (2012) 2968-2974.

[20] W.-H. Chen, B.-J. Lin, B. Colin, J.-S. Chang, A. Pétrissans, X. Bi, M. Pétrissans, Hygroscopic transformation of woody biomass torrefaction for carbon storage, Applied Energy, 231 (2018) 768-776.

[21] D. Phillips, E.J.S. Mitchell, A.R. Lea-Langton, K.R. Parmar, J.M. Jones, A. Williams, The use of conservation biomass feedstocks as potential bioenergy resources in the United Kingdom, Bioresource Technology, 212 (2016) 271-279.

[22] G. Guan, M. Kaewpanha, X. Hao, A. Abudula, Catalytic steam reforming of biomass tar: Prospects and challenges, Renewable and Sustainable Energy Reviews, 58 (2016) 450-461.

[23] J. Lehto, A. Oasmaa, Y. Solantausta, M. Kytö, D. Chiaramonti, Review of fuel oil quality and combustion of fast pyrolysis bio-oils from lignocellulosic biomass, Applied Energy, 116 (2014) 178-190.

[24] P.K. Kanaujia, Y.K. Sharma, M.O. Garg, D. Tripathi, R. Singh, Review of analytical strategies in the production and upgrading of bio-oils derived from lignocellulosic biomass, Journal of Analytical and Applied Pyrolysis, 105 (2014) 55-74.

[25] M. Verma, S. Godbout, S.K. Brar, O. Solomatnikova, S.P. Lemay, J.-P. Larouche, Biofuels production from biomass by thermochemical conversion technologies, International Journal of Chemical Engineering, 2012 (2012).

[26] P. Bhoi, A. Ouedraogo, V. Soloiu, R. Quirino, Recent advances on catalysts for improving hydrocarbon compounds in bio-oil of biomass catalytic pyrolysis, Renewable and Sustainable Energy Reviews, 121 (2020) 109676.

[27] A. Heidari, E. Khaki, H. Younesi, H.R. Lu, Evaluation of fast and slow pyrolysis methods for bio-oil and activated carbon production from eucalyptus wastes using a life cycle assessment approach, Journal of Cleaner Production, 241 (2019) 118394.

[28] M. Balat, Mechanisms of thermochemical biomass conversion processes. Part 1: reactions of pyrolysis, Energy Sources, Part A, 30 (2008) 620-635.

[29] P.D.M.M. Rahman, M.M. Noor, R. Mamat, 8 Nazirah et al, 2014.

[30] I. Ali, S.R. Naqvi, A. Bahadar, Kinetic analysis of Botryococcus braunii pyrolysis using model-free and model fitting methods, Fuel, 214 (2018) 369-380.

[31] X. Hu, M. Gholizadeh, Biomass pyrolysis: A review of the process development and challenges from initial researches up to the commercialisation stage, Journal of Energy Chemistry, 39 (2019) 109-143.

[32] J. Jin, Y. Li, J. Zhang, S. Wu, Y. Cao, P. Liang, J. Zhang, M.H. Wong, M. Wang, S. Shan, P. Christie, Influence of pyrolysis temperature on properties and environmental safety of heavy metals in biochars derived from municipal sewage sludge, Journal of Hazardous Materials, 320 (2016) 417-426.

[33] L. Shi, Q. Liu, X. Guo, W. Wu, Z. Liu, Pyrolysis behavior and bonding information of coal — A TGA study, Fuel Processing Technology, 108 (2013) 125-132.

[34] R.C. Brown, Q. Liu, G. Norton, Catalytic effects observed during the co-gasification of coal and switchgrass, Biomass and Bioenergy, 18 (2000) 499-506.

[35] J.M. Jones, M. Kubacki, K. Kubica, A.B. Ross, A. Williams, Devolatilisation characteristics of coal and biomass blends, Journal of Analytical and Applied Pyrolysis, 74 (2005) 502-511.

[36] G. Liu, H. Song, J. Wu, Thermogravimetric study and kinetic analysis of dried industrial sludge pyrolysis, Waste Management, 41 (2015) 128-133.

[37] Y. Zhai, W. Peng, G. Zeng, Z. Fu, Y. Lan, H. Chen, C. Wang, X. Fan, Pyrolysis characteristics and kinetics of sewage sludge for different sizes and heating rates, Journal of Thermal Analysis and Calorimetry, 107 (2012) 1015-1022.

[38] D.K. Park, S.D. Kim, S.H. Lee, J.G. Lee, Co-pyrolysis characteristics of sawdust and coal blend in TGA and a fixed bed reactor, Bioresource Technology, 101 (2010) 6151-6156.

[39] Z. Ni, H. Bi, C. Jiang, C. Wang, J. Tian, W. Zhou, H. Sun, Q. Lin, Investigation of the co-pyrolysis of coal slime and coffee industry residue based on machine learning methods and TG-FTIR: Synergistic effect, kinetics and thermodynamic, Fuel, 305 (2021) 121527.

[40] Y. Li, L. Li, Y. Liu, X. Ren, J. Chen, Y.A. Levendis, Sulfur and Nitrogen release from co-pyrolysis of coal and biomass under oxidative and non-oxidative conditions, Journal of Energy Resources Technology, 143 (2021) 061304.

[41] Z. Ni, H. Bi, C. Jiang, J. Tian, H. Sun, W. Zhou, Q. Lin, Research on the co-pyrolysis of coal gangue and coffee industry residue based on machine language: Interaction, kinetics, and thermodynamics, Sci Total Environ, 804 (2022) 150217.

[42] R. Zhou, R. Cao, Y. Liu, D. Ma, Q. Yao, J. Wang, M. Sun, X. Ma, Study on the characteristics and mechanism of fast co-pyrolysis of coal tar asphaltene and biomass, Journal of Analytical and Applied Pyrolysis, 161 (2022) 105409.

[43] D. Hong, P. Li, T. Si, X. Guo, ReaxFF simulations of the synergistic effect mechanisms during co-pyrolysis of coal and polyethylene/polystyrene, Energy, 218 (2021) 119553.

[44] Y. Ding, O.A. Ezekoye, S. Lu, C. Wang, R. Zhou, Comparative pyrolysis behaviors and reaction mechanisms of hardwood and softwood, Energy conversion and management, 132 (2017) 102-109.

[45] K. Jayaraman, M.V. Kok, I. Gokalp, Thermogravimetric and mass spectrometric (TG-MS) analysis and kinetics of coal-biomass blends, Renewable Energy, 101 (2017) 293-300.

[46] M.S. Masnadi, R. Habibi, J. Kopyscinski, J.M. Hill, X. Bi, C.J. Lim, N. Ellis, J.R. Grace, Fuel characterization and co-pyrolysis kinetics of biomass and fossil fuels, Fuel, 117 (2014) 1204-1214.

[47] I. Mian, X. Li, Y. Jian, O.D. Dacres, M. Zhong, J. Liu, F. Ma, N. Rahman, Kinetic study of biomass pellet pyrolysis by using distributed activation energy model and Coats Redfern methods and their comparison, Bioresource Technology, 294 (2019) 122099.

[48] M.G. Montiano, E. Díaz-Faes, C. Barriocanal, Kinetics of co-pyrolysis of sawdust, coal and tar, Bioresource Technology, 205 (2016) 222-229.

[49] S.R. Naqvi, Y. Uemura, N. Osman, S. Yusup, Production and evaluation of physicochemical characteristics of paddy husk bio-char for its C sequestration applications, BioEnergy Research, 8 (2015) 1800-1809.

[50] Y. Sudiyani, Muryanto,"The potential of biomass waste feedstock for bioethanol production," Proceeding of the International Conference on Sustainable Energy Engineering and Application Inna Garuda Hotel, 2012.

[51] M. Guo, J.-C. Bi, Characteristics and application of co-pyrolysis of coal/biomass blends with solid heat carrier, Fuel Processing Technology, 138 (2015) 743-749.

[52] H. Haykiri-Acma, S. Yaman, Interaction between biomass and different rank coals during co-pyrolysis, Renewable energy, 35 (2010) 288-292.

Chapter 2

Literature Review

2.1 Coal and biomass overview

2.1.1 Composition and utilization of coal

Coal is defined as the buried matter undergoes changes and transforms into more carbon rich, dense and hard material. Coal is a major energy source and can be classified into four types which include anthracite, bituminous, sub-bituminous and lignite. The characteristics of all these types are shown in **Table 2.1.** Coal consists of small aromatic rings that are connected to each other through aliphatic chains or hetero atoms [1]. Coal has been classified into different types including hard and soft coal. Coal is primarily being utilized for production of electricity along with other application depending upon the type and nature. The four major types of coal are also referred as 'ranks'. **Fig 2.1** shows the utilization pattern of various kinds of coal for various applications.
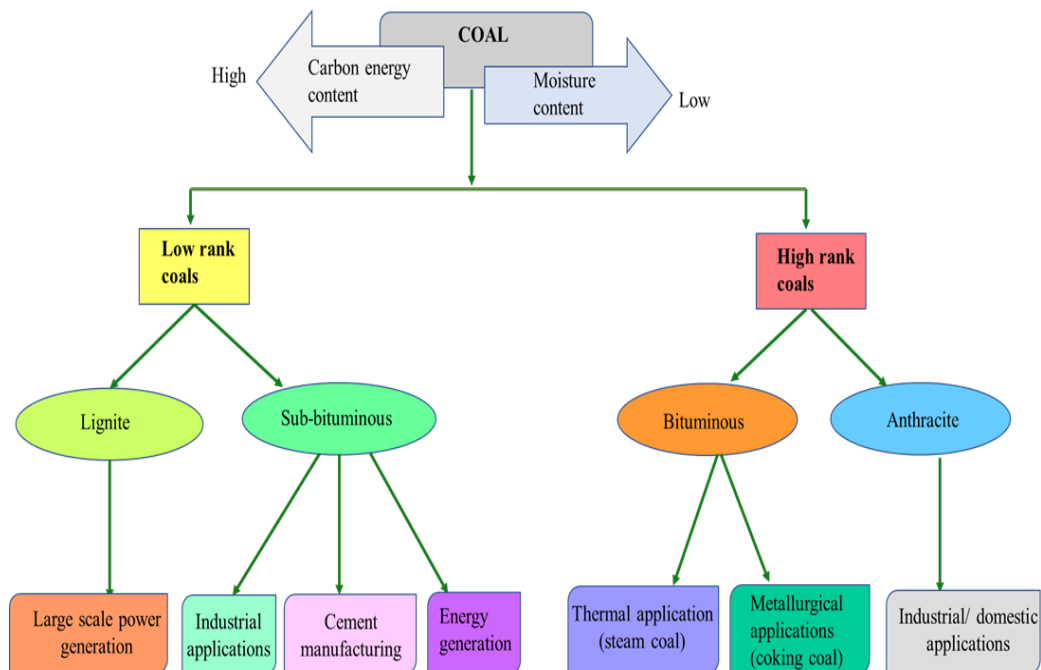
Fig 2.1 Utilization of coal (Reproduced from [2])

2.1.2 Composition and utilization of biomass

Lignocellulosic biomass is the one which is used in co-conversion processes. basically, any kind of biomass that can be burned and used as a fuel is called lignocellulosic biomass. Lignocellulosic biomass can be divided into primary, secondary, and tertiary biomass. Primary biomass is grown directly in the presence of sunlight and other natural conditions like wood, rice husk, corn cobs, rice straw, tree bark, hemp etc. [3]. Secondary biomass is produced when primary biomass undergoes certain physical, chemical, and biological changes which includes cotton, hemp, paper, linen etc. While, tertiary biomass includes residues and wastes for example municipal waste, industrial waste, construction waste, fats, oils etc. For production of bio-oil, the preferred raw material is basically biomass obtained from plants and crop residue. Biomass when used as a feedstock is a very favorable option to produce liquid and gaseous fuels. Characteristics of different types of biomasses are shown in **Table 2.2.** General utilization of biomass for various applications is presented in **Fig 2.2.**
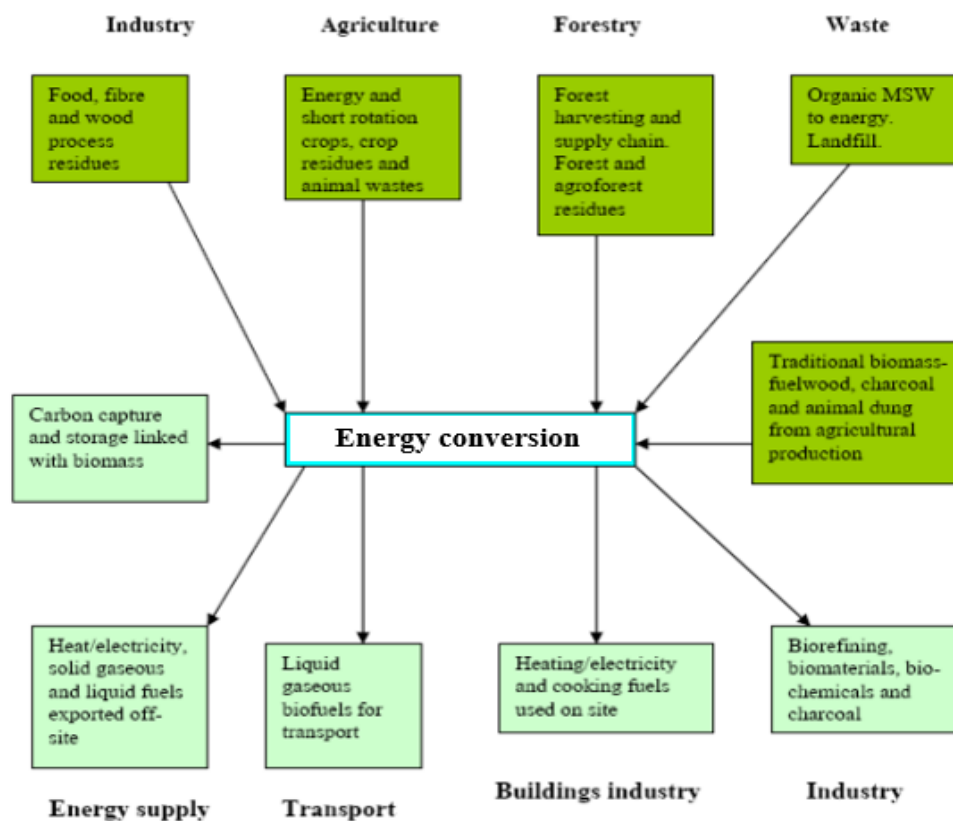
Fig 2.2 Utilization of biomass (Adapted from [4])

Table 2. 1 Composition analysis of various types of coal

Types of coal	Proximate analysis (%wt)			Ultimate analysis (%wt) dry basis					Calorific value	Ref
	VM	FC	Ash	C	H	N	S	O	CV	
Anthracite	4.2-30.4	80.3-86.8	-	84.8-94.4	2.1-3.5	<1.4	<1	1.7-6.2	30.6-36.2	[2, 3]
Bituminous	20-26.9	54.8-55.8	18.3-35	78.8-82.9	4.3-5	1.6-2	0.59-1.80	10-15.1	19.9-36.4	[4-6]
Lignite	38-54.4	36.3-50	9.4-33.3	66.8-73.2	4.5-5.1	1.0-2.0	1.3-2	16.4-22	26.5-31.7	[4, 7]
Peat	61.2-78.9	10-24.3	6.5-18.8	50.5-56.4	5.4-6	1.4-2.5	0.5-0.9	35.65-41.2	17.4-22.4	[8]

Table 2. 2 Composition analysis of various types of biomasses

Types of biomasses	Proximate analysis (%wt) dry basis			Ultimate analysis (%wt) dry basis					Calorific value	Ref
	VM	FC	Ash	C	H	N	S	O	CV	
Sawdust	84.6-91.3	14.3-19.6	0.1-1.1	45.3-52.0	6.0-6.1	0.2-0.6	0.1-1.1	41.6-47.1	17.7-20.4	[5, 6]
Rice straw	71.6-88.7	8.1-14.5	8.9-13.9	43.6-45.4	5.3-7.4	0.4-0.8	<0.1	33-50.6	16.2-18.9	[7-9]
Switch grass	76.7-80.4	14.4-14.5	5.1-8.9	39.7-49.7	4.9-6.1	0.6-0.7	<0.2	31.8-43.4	12.6-18.1	[10]
Pine chips	72.4-87	12.6-21.6	0.3-0.6	46.1-52.8	5.3-6.1	0.1-0.5	<0.3	40.5-48.4	19.0-19.8	[5, 11]
Rice husk	67.6	6.3	16.6	49.2	2.2	0.4	0.06	48.1	-	[12]
Sugarcane	82.38	8.47	2.94	45.3	7.92	0.15	-	46.6	-	[13]

2.2 Factors influencing reactivity characteristics of co-pyrolysis

The process basically takes place in a reactor in absence of air. There are various factors that influence the reactivity characteristics of co-pyrolysis, and they are listed below. Blending ratio plays a key role in the reactivity and yield of liquid products during co-pyrolysis [14, 15]. Other major factors that influence co-pyrolysis include temperature, heating rate, TGA behavior, initial weight etc. Behavior of biomass and coal during co-pyrolysis shows that lower heating rates are more suitable than higher heating rates [16].

2.2.1 Effect of temperature on co-pyrolysis

Temperature plays an important role in product type, conversion rate and yield [17]. Different products are formed at different temperatures. At increased temperature, more volatiles are released consisting of condensable and non-condensable gases. For liquid product, the temperature differs according to the reactor configuration and specifications. For coal, the optimal temperature is reported to be 500-650°C [18] and for biomass 400-500°C [19]. With temperature above these ranges more gaseous products are formed [20]. The effect of temperature on pyrolysis product distribution of Dayan Lignite coal and Legume straw biomass are shown in **Fig.2.3** [18]. In **Fig 2.3(a)** it has been depicted that for Dayan Lignite coal at 600 °C, the gaseous yield is maximum (10%) while the liquid yield is maximum (39%) at 700 °C. Temperature of 500 °C attributed to highest char yield (59.5%). While **Fig 2.3(b)** shows the product yield of Legume straw. It shows that gaseous yield is maximum at 700 °C (59%) while liquid yield is maximum at 500 °C (42%) and maximum yield of char (19%) is obtained at 500 °C. To increase the interactions between both feedstocks, the production of intermediate products is necessary.

It has also been reported that with increasing temperature, the synergy decreases [21]. If the amount of hydrogen present in coal matches that of biomass, a decrease in synergy has been observed. The reason for this can be associated with the recombination reactions from hydrogen present in biomass. If the biomass is pre-treated, maximum synergies can be observed at higher temperatures as compared to that of raw biomass and also the liquid production is influenced by the temperature and residence time [22].

21
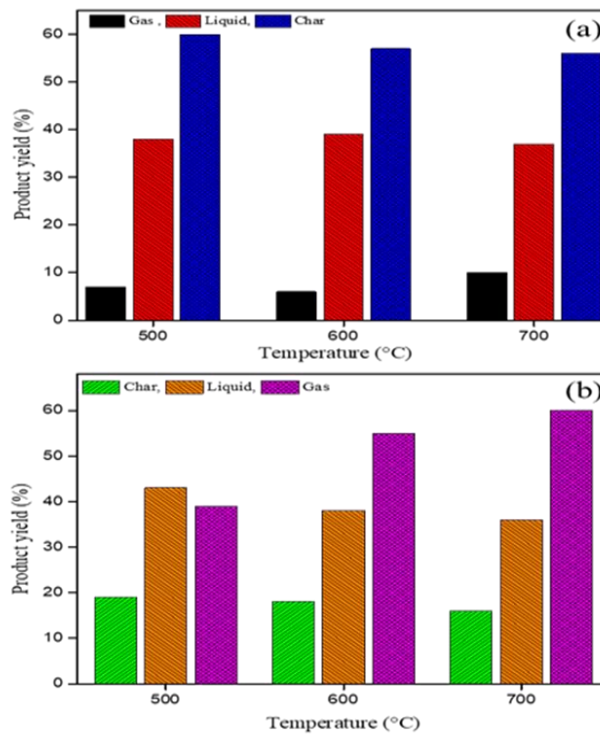
Fig 2.3 Effect of temperature on product yield (a) DL coal (b) Legume straw biomass (Reproduced from [18])

Pyrolysis of coal majorly produces solid products with some amount of liquids and gases, meanwhile biomass pyrolysis produces more liquids and solids. In co-pyrolysis of coal and biomass, the experimental product yield is in-between the yield of both feedstocks, while the calculated yield might differ because of the presence of synergistic effect [23]. With increasing temperatures, char yield decreases and volatiles increase so we can say that as temperature decreases the conversion rate of pyrolysis increases [24]. Some studies reported that biomass supported devolatilization of coal at low temperatures [25] but synergy varied with temperature. A study reported that interaction between the blends were observed at temperature > 400°C at which most of the components had undergone devolatilization and secondary reactions started taking place, thereby stopping the formation of char [26]. Another study on co-pyrolysis showed that the interactions between coal and biomass were observed at 300-500°C showing the end of devolatilization of biomass and start of decomposition of coal [27]. During the co-pyrolysis of coal and sawdust, it was observed in TGA that the synergistic

effect was seen at temperature over 400°C. In Fig. 2.4(a) the tar yield is 11.7% at lowest temperature with sawdust blending ratio of 40% and in Fig 2.4(b) the gas yield starts increasing at 400°C due to the reduced tar yield. This gas yield is 10% higher in co-pyrolysis than biomass pyrolysis alone at temperature of 400°C. In iso-thermal environment, in a fixed bed reactor, the synergistic effect produced more volatiles at temperature of 500-700°C while the maximum synergistic effect was observed at sawdust blending ratio of 60% at 600°C [24].
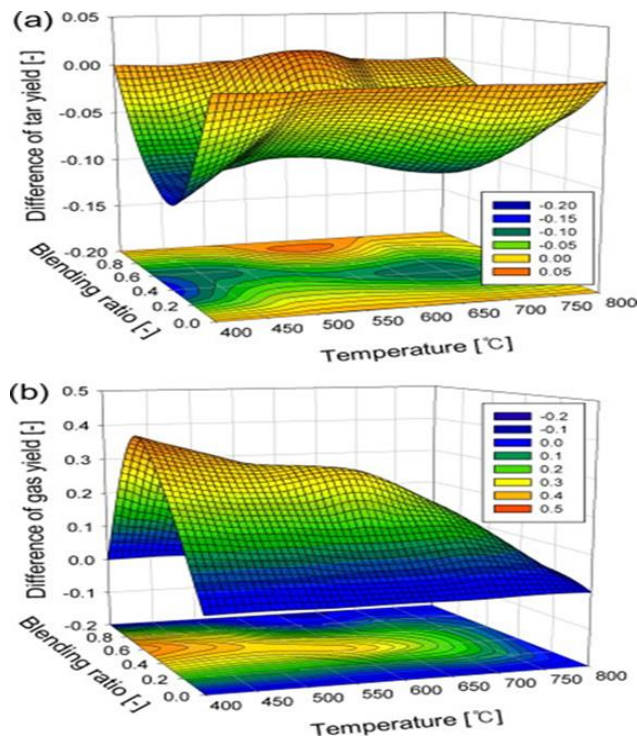
Fig 2.4 Difference between the experimental and calculated yields of (a) tar and (b) gas products (Adapted from [24])

A study conducted on lignite coal and legume straw co-pyrolysis revealed that optimum condition for synergistic effect in a free fall reactor was temperature of 600°C [18]. Few studies also showed that at temperatures up to 800°C, the difference between experimental and calculated values decreased [23]. So, this shows that for most of the blends the optimum range for synergistic effect is between 400-600°C. On increasing the temperature synergistic effect mostly decreases as the pyrolysis rate increases and hydrogen donor ability decreases.

2.2.2 Effect of blending ratios on coal-biomass co-pyrolysis

Biomass has higher H/C and O/C ratio due to higher hydrogen and oxygen content and lower carbon content respectively. The reactivity can be explained by the DTG profiles, peak degradation temperatures and decomposition rate. **Fig 2.5** illustrates the DTG profiles of blends from energy grass and lignite [28]. It shows that the blending ratios affect the peak shapes and decomposition temperatures. The degradation rate increases with increasing the share of biomass in the blend and consequently H/C ratios, volatile matter and O/C ratios increase with biomass [27]. Some studies have also shown that decomposition rate and blending ratios are directly related to the volatile matter.
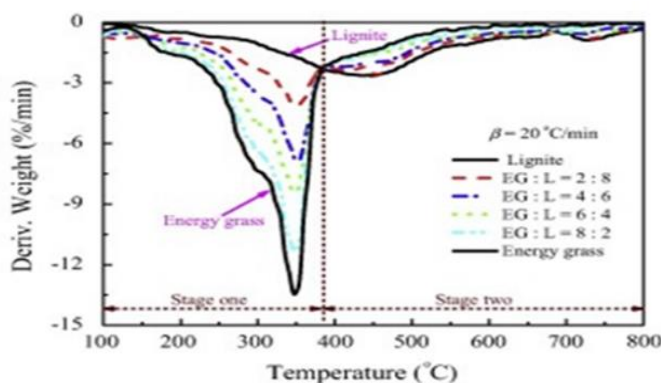
Fig 2.5 DTG profiles of blends of lignite and energy grass at various ratios (Adapted from [28])

The positive and negative synergistic effects have been observed in previous studies and most of the results show the inhibitive or negative synergistic effects. It has been observed that H acts as a donor and facilitates the degradation of coal [23, 24]. Higher oxygen content sometimes also plays some role in negative synergies because oxygen serves as a linking means which can possibly counteract the effect of hydrogen [29]. Whether the biomass is raw or torrefied it was observed that no synergies were observed [30]. Considering the decomposition temperatures considerable changes are observed on blending with torrefied biomass. The temperature of first decomposition region was shifted to a higher temperature and the regions overlapped each other. So this shows that using torrefied biomass the properties of coal and biomass become somewhat similar [31]. **Table 2.3** shows summary of some blends exhibiting synergistic behavior during co-pyrolysis.

24

2.2.3 TGA analysis of coal-biomass blends

TGA is an important parameter to analyze the weight loss with respect to temperature and time and to investigate the thermal decomposition behavior of the sample. Literature reveals that TGA analysis of biomass pyrolysis can be divided into three stages (reference?). In the initial stage, moisture loss takes place at a temperature range of >200°C. Meanwhile, the second stage is associated with the decomposition of cellulose, hemicellulose, and lignin in the temperature range of 200-600°C. In this stage, the decomposition of cellulose and hemicellulose occurs at temperature range of 200-450°C, whereas the degradation of lignin occurs from 455-600°C. Finally, the third stage is associated with degradation of complex materials and char at 600-1000°C. **Table 2.4** enlists some parameters observed through TGA for the co-pyrolysis of coal and biomass studies. These parameters include T_v (devolatilization temperature), T_f (final temperature), and DTG (derived thermogravimetric analysis) etc. Study of different blending ratios and heating rates of various blends analyzed by TGA is also depicted in **Table 2.5.**

2.2.4 Effect of initial weight on TGA

It has been reported that there exists a difference between the temperature of sample and the reactor used during co-pyrolysis [32, 33]. The initial weight of sample also plays a major role in the degradation behavior and emission of volatiles from the sample. By assessing the yield of char, the effect of weight of sample on the yield is observed. At the heating rate of 3K/min, no change was observed between the degradation temperatures, but at this lower heating rate the yield of char increased up to 18%. However, for heating rates of 41K/min and 105K/min, changes were observed between the degradation temperatures[34]. Other studies have also shown similar results [35]. It has been observed that higher heating rates around 150K/min are said to affect the char yield significantly and results in the variability of yields.

For kinetic modelling of the samples, phenomena of mass transfer is explained by Darcy law using a convective transport equation [36]. Feedstock affects the permeability and porosity. Feedstocks having pore structure of different sizes will emit volatiles at different rates. However it was observed that when biomass was torrefied

25

before co-pyrolysis the penetrability increased (10^{-11} m^2 for char) and thus the volatile release at a faster rate [37]. It was observed that at 200°C torrefaction decreased the diffusivity mass but didn't affect the permeability [38]. It was also observed shows that with torrefaction performed increased temperature of 300°C surface area also increased. So temperature has a great role to play in mass transfer and permeability [39].

2.2.5 Effect of blending on product characteristics

The blending ratios play an important role in char formation during co-pyrolysis. It has been observed that char obtained from co-pyrolysis has a greater influence on the gross calorific value. Studies show that char obtained from biomass and coal co-pyrolysis has greater calorific value than the char obtained from coal pyrolysis alone [40]. It was observed that char produced from pyrolysis of pine cone has greater amount of oxygen and lower calorific value as compared to the char produced from co-pyrolysis [41]. Moreover, blending also has an influence on the production of tar. Tar contains aromatic compounds and their derivatives. Tar production is affected by the type of feedstock, temperature, and blend mix. It has been observed that co-pyrolysis of coal and biomass decreases the content of tar as compared to individual feedstock pyrolysis [42, 43]. Co-pyrolysis of polish coal blended with forest residue produced no synergistic effect [44]. However it was observed in another study that tar yield increased when increasing the ratio of biomass in the blend mix and thus significant effect on synergy was observed [45, 46].

Co-pyrolysis results revealed that residual mass percentage decreased on increasing the biomass percentage in the blends [47-49]. **Fig 2.6** shows the TGA behavior of coal and chlorella vulgaris blends with biomass blending ratios of 3/7, 5/5 and 7/3 respectively. It can be seen from **Fig 2.6 (a)** that with blending ratio of 7/3 the percent residual mass is about 40%, with blending ratio of 5/5 the percent residual mass is 49% and with blending ratio of 3/7 percent residual mass is 45%. The structure of coal consists of strongly linked aromatics with C=C bonds having bond energy of 1000 kJ/mol [50]. As these bonds are stronger, it is more difficult to break these bonds than those of cellulose, hemicellulose, and lignin present in biomass. The cellulose, hemicellulose and lignin are linked together by weaker bonds which have bond energy

of 380-420 kJ/mol so biomass degrades much rapidly than coal. Biomass also experiences more weight loss than coal as can be seen from **Fig 2.6 (a)** in which 7/3 blending ratio experiences weight loss of 60% and biomass blending ratio of 3/7 experiences weight loss of around 49%.
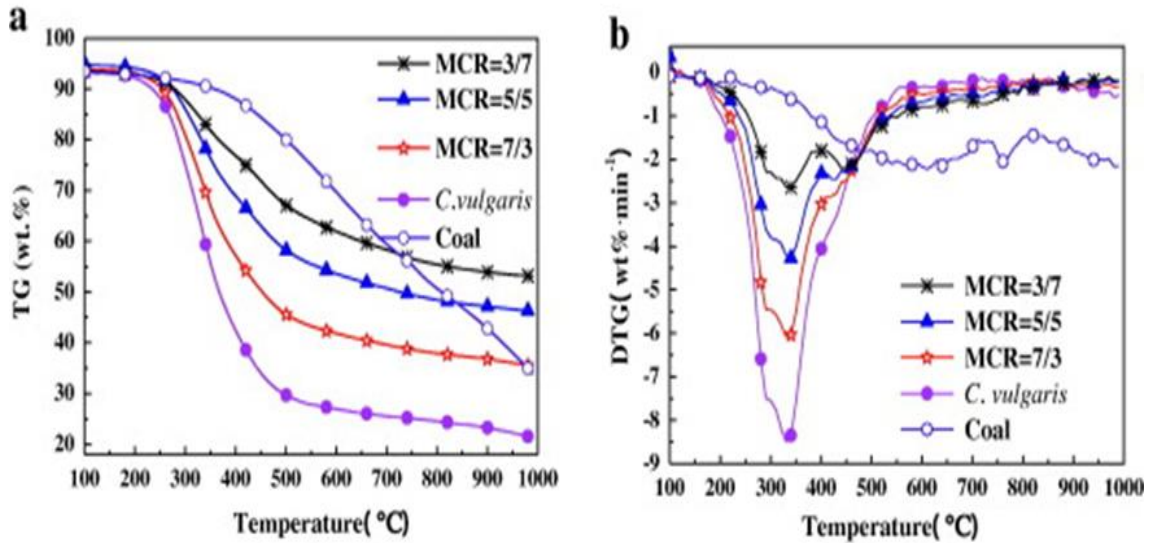
Fig 2.6 (a) TGA and (b) DTG curves of coal and chlorella vulgaris blends (Adapted from [48])

The synergistic effect also depends highly on blending ratios as well as type of feedstock. Synergistic effect is usually observed with higher biomass blending ratio as it is expected that more hydrogen donors will be supplied to coal [18, 24]. However, it was also observed that synergy is not linearly dependent on biomass percentage in the blends [18, 24, 51]. As thermal conductivity of biomass is lower than coal, higher share of biomass in the blend consequently decreases the heating rate and calorific value and also volatiles take much longer time to release from the blend [24]. This results in slow release of OH and H radicals from biomass [52]. The char residue formed during co-pyrolysis can easily gather on the molecular surface of coal that resultantly blocks the pores of molecular structure of coal by which the volatiles produced by the pyrolysis of coal so this illustrates that interaction between the solid phases shows inhibitive effect on thermal decomposition [48, 53, 54]. **Table 2.6** lists various parameters of co-pyrolysis and their effect on coal-biomass blends at different ratios

Table 2.3 Summary of some blends depicting synergistic behavior

Coal type: biomass type	Blending ratios (Coal to biomass) w/w	Heating rate (°C/min)	Temperature (°C)	Ref
Bituminous coal: saw dust	20, 40, 60, 80	10,15,20,25,30	900	[49]
Bituminous coal: cellulose	25, 50, 75	10, 20, 40	950	[55]
Lignite coal: sawdust	20, 50, 80	10	1000	[56]
African hard coal: sugarcane bagasse, corn stover	90, 80, 70, 60, 50	5, 10, 50	900	[27]
Semi-anthracite coal: chlorella vulgaris	30, 50, 70	10, 20, 40	1000	[48]
Shenhua coal: sawdust	50	10	800	[57]
Sub-bituminous coal: saw dust	60	15	800	[24]
sub-bituminous coal: Pinus Radiata sawdust	50	10, 30, 50	1200	[58]
Turkish lignite: hazelnut shell	98, 96, 94, 90, 80	20	900	[59]

Table 2.4 Some literature of parameters observed through TGA

Coal/biomass type	Blending ratios (Coal: biomass)	Temperature	Heating rate (°C/min)	T_v	T_f	DTG $_{max}$	Ref
Coal/sugarcane bagasse	90:10 80 : 20 70 : 30 60 : 40 50 : 50	25–900	20	210–390	390–450	9 to 10.8%/min	[27]
Bituminous coal/bagasse	75 : 25	25–950	10, 20, 40	318, 208,271	346, 293,461	5.8%/min 1.2%/min	[60]
Bituminous coal/sewage sludge	90 :10	25–1200	5	475	1200	0.0114	[61]
Coal/sewage sludge	10 : 90 20 : 80 30 : 70 50 : 50	25–1200	30	200	850	0.16	[62]

Table 2.5 Summary of some TGA studies of coal-biomass blends at different heating rates and blending ratios

Coal/biomass type	Blending ratios (coal: biomass)	Heating rate (°C/min)	Particle size (µm)	Temperature (°C)	Ref
Lignite coal/ safflower seed	50:50 67:33 34:66	5	500-1000	Upto 800	[63]
Lignite coal/ kernel shell, palm fruit, mesocarp fibre	80:20 40:60 50:50 60:40 20:80	10, 20, 40, 60	<212	Upto 900	[64]
Sub-bit coal/ wheat straw, wood waste	50:50 30:70 20:80 10:90	20	-	Up to 1300	[65]
Lignite coal/ olive kernel, cotton, forest residue	95:5 90:10 80:20	10	<250	850	[66]
Lignite coal/ corn cob	90:10 50:50 10:90	10	<74	up to 600	[23]
Sub-Bituminous coal, bituminous coal/ sawdust	50:50	10, 30, 50	53-75	Up to 1200	[58]
Bituminous coal/pellets, pine, olive residue, hazelnut shells, paper sludge	85:15 60:40	20	125-300	105-1000	[67]

Lignite coal/ forest residue, cotton residue, olive kernel	95:5 90:10 80:20	10/100	<450/ <250, <75	Up to 850	[68]
Lignite coal / pine chips	80:20 40:60 20:80	100	750-1200	110-900	[14]
Lignite coal/ wood waste	50:50 40:60 10:90	40	Coal = 149-210 Wood waste = 354-500	Up tp 1000	[69]
Bituminous coal/ sugarcane bagasse, corn cob	90:10 80:20 60:40	5, 10, 50	< 212	Up to 900	[51]
Lignite coal / sugar beet pulps	50:50	20	74-149	Up to 900	[70]
Sub-bituminous coal/ switch grass	75:25 50:50 25:75	25	300-355	Up to 800	[71]
Bituminous coal/yellow poplar	90:10 85:15 80:20 70:30	5, 10, 15, 20	<350	Up to 800	[72]
Semi-anthracite coal/ C. vulgaris algae	70:30 30:70 50:50	10, 20, 40	<200	Up to 1000	[48]
Lignite coal, bituminous coal, anthracite coal/ hazelnut shell	90:10	40	250	Up to 900	[73]
Bituminous coal/ macadamia	20:80	5, 10, 15, 20	250-350	Up to 1000	[74]

nut shells, wood chips	15:85 15:95 10:90				
Bituminous coal/switch grass, corn stover	80:20	5, 10, 20, 40	Coal= <400 Biomass = 400-500	Up to 800	[75]
Bituminous coal/ fungi residue	50:50 75:25 25:75	10, 20, 40	<74	Up to 1200	[76]
Anthracite coal/ Japanese cedar	50:50 75:25 25:75	20	74-149	Up to 800	[30]
Lignite coal/giant reed grass	10:90 20:80 30:70 40:60 50:50 60:40 70:30 80:20 90:10	5, 10, 15, 20, 30	<250	Up to 800	[28]
Bituminous coal/ walnut shell	50:50	10, 20, 40	-	Up to 950	[77]
Lignite coal/poplar	96:4 92:8 88:12 84:16 68:32	10, 20, 30	74-150	Up to 1000	[78]
Sub-bituminous coal/ softwood, hardwood, leaves	50:50 25:75 75:25	20	<150	Up to 800	[35]
Lignite coal, bituminous coal/ platanus wood	50:50 30:70 70:30	10, 20, 40	<74	Up to 950	[47]

Table 2.6 Thermochemical conversion parameters of coal and biomass at different ratios through co-pyrolysis

Coal type + biomass	Blending ratios	Reactor type	Temperature range (°C)	Heating rate	Product formed	Remarks	Ref
	Coal: Biomass						
Bituminous coal + saw dust (SD)	Coal: SD 0:100 80:20 60:40 40:60 100:0	Fixed bed reactor	Upto 900	10-30°C/min	Biofuels	Considerable differences were observed between experimental and calculated weight fractions. Degradation rates were slower than calculated ones	[49]
Sub-bituminous coal + pine	Coal: Pine 0:100 50:50 25:75 75:25 100:0	Drop tube	600	10°C/min	Gas	Interaction of blends depicted inhibitive effect on decomposition and the char yields were increased. positive synergy was observed on	[79]

						tar production	
Lignite + wood	70:30 30:70 50:50	Semi-batch drop tube	600-1000	-	Bio-oil	Torrefied biomass proved effective in improving bio-oil quality and yield	[80]
Lignite + sugar beet	50:50	Semi-batch drop tube	600			Volatile and ash content of blends were different than parent individual fuels. Char had higher amount of volatiles after co-pyrolysis	[70]
Sub-bit/lignite + pine	90:10 80:20 50:50	Semi-batch drop tube	600-925	-	Syngas, char	Blending with low rank coal showed better synergy	[29]
Sub-bituminous+ corn stalk	90:10 70:30 50:50 30:70 10:90	Moving bed pyrolizer	700-800	-	Char, gases, tar	On increasing ratio of corn stalk the gas and tar yield increased	[81]

Drayton coal: saw dust	95:5 90:10	Drop tube	900-1400	10^4 k/s	Gas, char, oil	No synergistic effect was observed. Product yield was proportional to biomass and coal ratio in blend	[82]
Polish coal, daw mill coal: silver birch, forest residue	67:33 51:49 48:52 27:73	Hot rod FB	850,1000	10 k/s		No synergy was observed with fluidized bed reactor. 5% higher volatile yields were observed.	[83]
Bituminous coal: switch grass	0:100 85:15 70:30 50:50 100:0	Semi batch drop tube	900		Gases, char, liquid	Linear effects were observed in product distributions	[21]
Dayan lignite: legume straw	0 to 100	Drop tube	500-700	10^4 °C/s	Biofuels	Gaseous product compositions were very different from parent fuels. Synergistic effects were also observed	[18]

Teifa Bituminous (TF) coal, Dayan brown coal (DY): pine saw dust, legume straw	0 to 100	Free fall reactor	500-700	500 °C/s	Char, gas, liquid	Significant synergy was observed with legume straw. Liquid yield with TF coal was higher than DY	[84]
Lignite coal: JiaDuoBao residue (JR)	90:10 80:20 60:40 50:50	Fluidized bed	600-850	10^4 k/s	biofuels	Synergistic effects were observed, and kinetic parameters were calculated	[85]
Yilan Sub-bituminous coal: corn cob	80:20 60:40 40:60 20:80	Fluidized bed	500-700	10-40 K/min	Bio-oil, gases, biochar	With coal blending ratios < 60%, higher oil yields were obtained. Oils contained increased the amount of alcohols, phenols, ketones and acids	[86]
Bituminous coal: saw dust	80:20 60:40 40:60 20:80	Fixed bed	800-1400		Gases, char, tar	Maximum reactivity of char was observed at	[87]

						80% blending ratio of biomass. Positive synergies were observed in vapor phase	
Bituminous coal: corn cob, bagasse, corn stover	95:5 50:50 72.5:27.5	Fixed bed	400-600	0.2-0.25 k/s	Gas, char, tar	Bending ratio had significant impact on yields while temperature and pressure had negligible effect. Synergy was observed in vapor phase.	[50]
Lignite coal: sawdust	80:20 50:50 20:80	Fixed bed	400-900		Biofuels	With increased biomass content, the synergy increased. CO and CO_2 were the major gases released.	[56]

Lignite coal: corn cob	50:50 65:35 33:67	Two stage fixed bed	0.17K/s	1000	Char, tar, gas	After interaction, tar yields decrease and gas yield increase. Potassium present in char affected the reactivity	[88]
Sub-bituminous coal:saw dust	80:20 60:40 40:60 20:80	Fixed bed		500-700	Gas, char	Maximum synergy was observed at biomass blending ratio of 60%	[24]
Lignite coal: straw	50:50	Fixed bed	0.3K/s	500-550	Gas, char, oil	Oil was obtained with lower oxygen and higher benzene content	[89]

2.3 Co-pyrolysis kinetics:

Coal-biomass pyrolysis is a complicated field [90]. A lot of attention has been given to develop the mechanistic models as first order reactions. Most of the studies have mainly focused on free radical patterns without explanation of other phenomenon. Reactor level kinetic studies require mass and heat transfer reactions however these studies do not analyze certain reactions and rate constants. So, various hybrid models were developed but for ideal conditions which are not the case in actual phenomenon [91, 92]. Various kinetic models have been developed with different reaction mechanisms to explain the mechanistic behavior of coal-biomass blends. Usually non-isothermal techniques have been adapted for experimental data for wide range of temperatures. **Table 2.7** shows some empirical models used for the assessment of kinetic behavior of blends. The accurate mechanisms of reaction for individual pyrolysis process of coal and biomass is still under debate and blending makes it more complex. In order to obtain experimental data, non-isothermal techniques are used as they can analyse a range of temperatures. Artificial Neural Network (ANN) and Monte Carlo models are used to predict relationships between co-pyrolysis but their main drawback is that they are applicable only for the fuels which they are developed. However, iso-conversional models have gained some attention in recent studies. These are called model free methods and they do not require any reaction mechanism represented in **Table 2.7**. Activation energies are represented in the table. It has been identified that activation energies of coal are higher with these models as compared to biomass pyrolysis. Another popular kinetic model is the Coats-Redfern model that is also being used for non-isothermal kinetics represented in **Table 2.8**. In non-isothermal kinetics the reaction is being done linearly at a low heating rate so results can be obtained over a longer period of time [93]. Some of the kinetic studies conducted on various studies are shown in **Table 2.9.**

2.4 Thermodynamics of co-pyrolysis:

Thermodynamic parameters including ΔH, ΔG and ΔS are calculated based on the kinetic parameters. Various studies have been conducted to analyze the thermodynamic parameters of coal-biomass blends. During co-pyrolysis of coal and

torrefied saw dust it was observed that thermodynamic parameters like ΔH, ΔG, ΔS showed a small energy barrier and the reaction chemistry was studied. Negative ΔS were observed. The system was observed to be in thermal equilibrium [94]. Thermodynamic analysis of coal and sugar cane bagasse depicted that values of entropy suggested increased depolymerization of structure of fuel [95]. Co-pyrolysis of coal and saw dust depicted a decrease in Gibbs free energy. However the Gibbs free energy of coal exhibited increased value [96]. A study on sub-bituminous coal and wood species revealed that small differences was observed between activation energy and ΔH and the effect of biomass addition was prominent in the initial stage of conversion of coal but slowly decreased upon increasing the temperature. ΔS values of blends were lower as compared to those of coal for both stages of conversion. Both positive and negative entropy changes were reported indicating the formation of complex products during thermochemical conversion [97].

2.5 Nature of co-pyrolysis products

2.5.1 Nature of co-pyrolysis oil

Condensable and non-condensable gases are released from coal-biomass blends during co-pyrolysis process [98]. The nature of composition of gases depends on the feedstock type, blend mix and reactor configuration. Oil obtained from raw biomass consists of many oxygenated species. The composition analysis of oil obtained from coal and biomass is represented in **Table 2.10**. Higher oxygen containing species in biomass than coal are the reason of lower calorific value and instability [99]. However, it is observed that torrefied biomass improves the quality and yield of bio-oil than raw biomass. It decreases the oxygen content and increases carbon content [100]. More phenolic compounds and lesser acids are observed when blending coal with torrefied biomass [101]. This is due to the fact that moisture is removed during torrefaction and cellulose and hemicellulose also degrade at a faster rate. So, this shows that blending torrefied biomass with coal is better to achieve high quality liquid products.

2.5.2 Nature of co-pyrolysis char

Pyrolysis process produces residual solid material known as char that have a large amount of carbon and is rich in energy. The yield of char is sometimes less than

the calculated yield by the additive method [18]. Char can be formed by various phenomena which include recombination reactions between the volatile matter and other reactive components, dehydration phenomena. The char produced through dehydration mechanism is known as primary char and that produced through recombination reactions is known as secondary char [102]. The recombination reactions of coal with hydrogen of biomass are referred to define the decrease in residual content and the change in char properties. Different mechanisms like dehydration, decarboxylation, de-methanation reactions result in char formation. The decrease in hydrogen and oxygen content in co-pyrolysis char are associated with the surface morphology and functionalization [39]. Many studies have reported the chemical and physical changes in coal and biomass co-pyrolysis [103-105]. During the char production process, aromatization occurs which is associated with the conversion of carbohydrates usually observed at a temperature of 300-350°C [106]. The co-pyrolysis char possesses more changes in structure and morphology as compared to coal char. However, if torrefied biomass is used instead of raw the graphitization degree decreases and amorphous content in the char structure increases [31]. The chemical composition of biomass is also said to affect the co-pyrolysis char. If torrefied biomass is used the nature of char is more significantly affected due to hemicellulose degradation [107]. Increased cellulose content in char decreases the aromatic structures and irregularity increases [108].

The alkali and alkaline earth metals (AAEM) species play a major role in structure of co-pyrolysis char. These AAEM species result in bond breakage of weaker bonds and increase the aromatic rings [109]. With higher levels of calcium (Ca) and potassium (K) the demethoxylation reactions increased [58] and hence the methoxy phenols do not have a significant effect on aromatization of structure [110].

SEM analysis has been used to observe the surface morphology of co-pyrolysis char. The structure is affected by the pyrolysis temperature [76]. It was observed that with the increase in temperature the needle like structure changed into lamellate structure due to the spreading to the carbon lattice [39]. The composition of feedstocks greatly influences these structures [106, 108].

BET analysis is performed to assess the porosity. The porosity is usually very less due to the fact the diffusion of gas is hindered by pore size. For torrefied biomass, CO_2 adsorption process is used, and surface area is up to $170 m^2/g$ [111, 112]. The porous structure of torrefied biomass hinders the diffusion reactions within the particles so it is important to investigate the reactions of biochar in presence of oxygen containing compounds and metallic compounds [113].

2.5.3 Nature of gaseous compounds

Gaseous products obtained from co-pyrolysis of coal and biomass mainly consist of CO, CO_2, H_2, CH_4 [18, 23]. Co-pyrolysis of lignite with corn cob shows that CO and CO_2 yields were similar to those of calculated ones at all temperatures [23]. In another co-pyrolysis experiment it was revealed that experimental yields of CO and CO_2 were lower than calculated ones. This is attributed to the reason that during co-pyrolysis the carbon in the feedstock favors the formation of tar or char instead of gases [18]. It was also observed that experimental yields of CO are very similar to calculated ones at lower temperatures however on increasing temperature the experimental CO yield was observed to be higher than calculated yield. The experimental yields of CO_2 were same as those of calculated ones [114]. It was observed that CH_4 production increased the synergistic effect in product gas composition that was twice or three times higher than the calculated values [23] while water was also identified to be a component of product gases which is beneficial as a reactive agent favoring the production of CH_4 . This water can also be utilized to produce hydrogen by water gas shift reaction:

$$CO_2 + H_2O = H_2 + CO$$
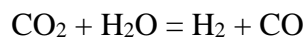
This new hydrogen has higher hydrogenation activity and can also be recovered for utilization in other purposes [115]. It also enhances the efficiency of co-pyrolysis process. So, the presence of water can be very beneficial for co-pyrolysis process in industrial and commercial utilization as it allows the usage of coal and biomass having large amounts of moisture without drying.

Table 2.7 Kinetic studies on co-pyrolysis through different models

Model	Feedstock	Parameters	Ref
Monte Carlo simulation models	tetradecylcyclohexane	Yield, weight	[116]
Thermogravimetry (Arrhenius equation, 1st order model) + Distributed activation energy model(DAEM)	Lignite + energy grass, coal+poplar	E_a, A, Yield	[28]
Miura integral method+ DAEM	NA	E_a, A, Yield	[78]
Flynn-Wall Ozawa and Kissinger-Akhira-Sunose method	NA		[117]
Kissinger method	Coal+wood	E_a, A, Yield	[74]
Coats-Redfern integral method, (5 models of various reaction mechanisms)	NA	E_a, A, Yield	[71]
Coats-Redfern integral method, (1st and nth models of various reaction mechanisms)	NA	E_a, A, Yield	[30]
Coats-Redfern integral method, (17 models of various reaction mechanisms)+ (ANN)	NA	E_a, A, Yield	[118]

Table 2.8 Some literature on Coats-Redfern method used for kinetic modelling of various blends

Blend ratios (biomass wt%)	Heating Rate (°C/min)	Reaction mechanism/model	Numerical method	E_α (α) (kJ/mol)		Ref
				Biomass	Coal	
25/50/75	25	Stage 1: Zhuravlev diffusion model, Stage 2: 1st order chemical reaction Stage 3: 3-dimensional random nucleation and nuclei growth	Integral, Coats and Redfern	Stage 1: 197 Stage 2: 528 Stage 3: 400	Stage 1: 130 Stage 2: 190 Stage 3: 429	[71]
30/50/70	20	17 models based on reaction mechanism function	Integral, Coats and Redfern	200-400°C: 5-70 400-600°C: 5-28		[118]
20/50/70	10	1st order	Integral, Coats and Redfern	SD: 138 RS: 111	200	[119]
25/50/75	20	n^{th} order	Integral, Coats and Redfern	HW:100 SW:101	157	[120]

Table 2. 9 Different kinetic models used for assessing activation energy of coal-biomass blends

Coal/biomass type	Blend ratios (Coal:biomass)	Model used	Activation energy (E_a) of coal	Activation energy (E_a) of biomass	Ref
Bituminous coal/pine wood chips	50:50	Integral FWO	106	117	[121]
Subbituminous coal/oil palm fruit bunches	50:50	Kissinger method	273	210	[64]
Bituminous coal/cypress wood chips	20:80 15:85 10:90 5:95	Differential, Kissinger method	200	169	[74]
Bituminous coal: corn cob, corn stover, bagasse	90:10 80:20 70:30 60:40 50:50	Differential, Friedman method	246	Corn cob=162-190 Corn stover =160-175 Bagasse= 165-180	[27]
Bituminous coal/fungi residue	25:75 50:50 75:25	1. Integral, Kissinger method. 2. Integral, FWO	1. 169-386 2. 74-250	1. 63-206 2. 176-378	[76]

Table 2.10 Characteristics of bio-oil obtained from coal-biomass blends

Oil characteristics	Raw coal	Raw biomass	Coal-biomass blends
Carbon	80-85	42-47	73-75
Hydrogen	2-8	6-8	11-12
Nitrogen	<1.1	<0.1	1.3-1.6
Sulphur	<0.4	<0.02	-
Oxygen	6-8	46-51	12-15
HHV (MJ/kg)	46 [122]	17-20 [123]	38-40 [63]
Water content	2-5 [124]	15-30 [125]	7-20 [81]
Yield (%wt)	6-25 [124]	65-75 [126]	7-41 [84]
Chemical compounds	Phenol, toluene, xylene, amine, pyridine, light benzenes and styrene	Alcohols, phenols, aldehydes,ketones, acids, miscellaneous compounds	Combination of both types of feedstocks

Summary

This chapter compiles most of the previously available work on co-pyrolysis of coal-biomass blends. Firstly, the detailed composition of different types of coal and biomass was discussed including carbon, hydrogen, oxygen and nitrogen content, heating values, volatile matter, ash and fixed carbon content. Afterwards, the chapter emphases mainly on the factors that affect the pyrolysis behavior of blends, blending ratios and their effect, thermogravimetric behaviors, temperature effect, initial wight effect, reactivity issues. It has been observed in previous studies that as biomass blending ratio increases, the percentage of weight loss in the blends also increases. The yield of char and oil is highly affected on using the torrefied biomass with coal. Torrefaction improves the energy efficiency of biomass. Temperature also has a major effect on co-pyrolysis. At increased temperatures more volatiles are released. It has also been observed that at increased temperature the synergy decreases. At higher biomass blending the degradation rate increases. Kinetic models used for investigating the mechanistic behaviors of blends were discussed. Lastly, the nature of co-pyrolysis oil, char and product gases was discussed. Co-pyrolysis oil consists of many chemical compounds like acids, phenol, alcohols, amines, furans, ketones, aldehydes etc. Co-pyrolysis char has a very different structural morphology as compared to coal char and the structure is defined by presence of AAEM species. This char can be used for a number of applications with little modifications. The co-pyrolysis product gases consist of CO, CO_2, H_2, CH_4. Their percentage yield varies at different blending ratios and different temperatures. These gases can further be captured and utilized for future applications.

References

[1] D.G. Levine, R.H. Schlosberg, B.G. Silbernagel, Understanding the chemistry and physics of coal structure (A Review), Proceedings of the National Academy of Sciences, 79 (1982) 3365-3370.

[2] B. Kavalov, S.D. Peteves, The future of coal, DG JRC Institute for Energy, European Commission, Petten, (2007).

[3] A. Bokhari, L.F. Chuah, L.Z.Y. Michelle, S. Asif, M. Shahbaz, M.M. Akbar, A. Inayat, F. Jamil, S.R. Naqvi, S. Yusup, Microwave enhanced catalytic conversion of canola-based methyl ester: optimization and parametric study, Advanced Biofuels, Elsevier2019, pp. 153-166.

[4] A.M. Omer, Biomass energy resources utilisation and waste management, Journal of Agricultural Biotechnology and Sustainable Development, 3 (2011) 149-170.

[5] R. García, C. Pizarro, A.G. Lavín, J.L. Bueno, Spanish biofuels heating value estimation. Part I: Ultimate analysis data, Fuel, 117 (2014) 1130-1138.

[6] R. García, C. Pizarro, A.G. Lavín, J.L. Bueno, Spanish biofuels heating value estimation. Part II: Proximate analysis data, Fuel, 117 (2014) 1139-1147.

[7] Y.-F. Huang, P.-T. Chiueh, C.-H. Shih, S.-L. Lo, L. Sun, Y. Zhong, C. Qiu, Microwave pyrolysis of rice straw to produce biochar as an adsorbent for CO2 capture, Energy, 84 (2015) 75-82.

[8] S. Li, X. Chen, A. Liu, L. Wang, G. Yu, Study on co-pyrolysis characteristics of rice straw and Shenfu bituminous coal blends in a fixed bed reactor, Bioresource technology, 155 (2014) 252-257.

[9] N. Worasuwannarak, T. Sonobe, W. Tanthapanichakoon, Pyrolysis behaviors of rice straw, rice husk, and corncob by TG-MS technique, Journal of Analytical and Applied Pyrolysis, 78 (2007) 265-271.

[10] D.A. Tillman, Biomass cofiring: the technology, the experience, the combustion consequences, Biomass and bioenergy, 19 (2000) 365-384.

[11] A.T. Masiá, B. Buhre, R. Gupta, T. Wall, Characterising ash of biomass and waste, Fuel Processing Technology, 88 (2007) 1071-1081.

[12] F. Pinto, J. Gominho, R.N. André, D. Gonçalves, M. Miranda, F. Varela, D. Neves, J.o. Santos, A. Lourenço, H. Pereira, Effect of rice husk torrefaction on syngas production and quality, Energy & Fuels, 31 (2017) 5183-5192.

[13] Q. Sohaib, A. Muhammad, M. Younas, Fast pyrolysis of sugarcane bagasse: Effect of pyrolysis conditions on final product distribution and properties, Energy Sources, Part A: Recovery, Utilization, and Environmental Effects, 39 (2017) 184-190.

[14] Y.G. Pan, E. Velo, L. Puigjaner, Pyrolysis of blends of biomass with poor coals, Fuel, 75 (1996) 412-418.

[15] S.R. Naqvi, Y. Uemura, S.B. Yusup, Catalytic pyrolysis of paddy husk in a drop type pyrolyzer for bio-oil production: The role of temperature and catalyst, Journal of Analytical and Applied Pyrolysis, 106 (2014) 57-62.

[16] F. Guo, X. Li, Y. Wang, Y. Liu, T. Li, C. Guo, Characterization of Zhundong lignite and biomass co-pyrolysis in a thermogravimetric analyzer and a fixed bed reactor, Energy, 141 (2017) 2154-2163.

[17] F.X. Collard, M. Carrier, J.F. Görgens, Chapter 4 - Fractionation of Lignocellulosic Material With Pyrolysis Processing, in: S.I. Mussatto (Ed.) Biomass Fractionation Technologies for a Lignocellulosic Feedstock Based Biorefinery, Elsevier, Amsterdam, 2016, pp. 81-101.

[18] L. Zhang, S. Xu, W. Zhao, S. Liu, Co-pyrolysis of biomass and coal in a free fall reactor, Fuel, 86 (2007) 353-359.

[19] D. Neves, H. Thunman, A. Matos, L. Tarelho, A. Gómez-Barea, Characterization and prediction of biomass pyrolysis products, Progress in Energy and Combustion Science, 37 (2011) 611-630.

[20] P. Morf, P. Hasler, T. Nussbaumer, Mechanisms and kinetics of homogeneous secondary reactions of tar from continuous pyrolysis of wood chips, Fuel, 81 (2002) 843-853.

[21] N.T. Weiland, N.C. Means, B.D. Morreale, Product distributions from isothermal co-pyrolysis of coal and biomass, Fuel, 94 (2012) 563-570.

[22] A. Zheng, Z. Zhao, S. Chang, Z. Huang, F. He, H. Li, Effect of torrefaction temperature on product distribution from two-staged pyrolysis of biomass, Energy & Fuels, 26 (2012) 2968-2974.

[23] T. Sonobe, N. Worasuwannarak, S. Pipatmanomai, Synergies in co-pyrolysis of Thai lignite and corncob, Fuel processing technology, 89 (2008) 1371-1378.

[24] D.K. Park, S.D. Kim, S.H. Lee, J.G. Lee, Co-pyrolysis characteristics of sawdust and coal blend in TGA and a fixed bed reactor, Bioresource technology, 101 (2010) 6151-6156.

[25] P. Yangali, A.M. Celaya, J.L. Goldfarb, Co-pyrolysis reaction rates and activation energies of West Virginia coal and cherry pit blends, Journal of Analytical and Applied Pyrolysis, 108 (2014) 203-211.

[26] C. Ulloa, A. Gordon, X. García, Thermogravimetric study of interactions in the pyrolysis of blends of coal with radiata pine sawdust, Fuel Processing Technology, 90 (2009) 583-590.

[27] A.O. Aboyade, J.F. Görgens, M. Carrier, E.L. Meyer, J.H. Knoetze, Thermogravimetric study of the pyrolysis characteristics and kinetics of coal blends with corn and sugarcane residues, Fuel Processing Technology, 106 (2013) 310-320.

[28] Y. Guan, Y. Ma, K. Zhang, H. Chen, G. Xu, W. Liu, Y. Yang, Co-pyrolysis behaviors of energy grass and lignite, Energy Conversion and Management, 93 (2015) 132-140.

[29] R.M. Soncini, N.C. Means, N.T. Weiland, Co-pyrolysis of low rank coals and biomass: Product distributions, Fuel, 112 (2013) 74-82.

[30] K.-M. Lu, W.-J. Lee, W.-H. Chen, T.-C. Lin, Thermogravimetric analysis and kinetics of co-pyrolysis of raw/torrefied wood and coal blends, Applied Energy, 105 (2013) 57-65.

[31] Q. He, Q. Guo, L. Ding, Y. Gong, J. Wei, G. Yu, Co-pyrolysis behavior and char structure evolution of raw/torrefied rice straw and coal blends, Energy & Fuels, 32 (2018) 12469-12476.

[32] M. Grønli, M.J. Antal, G. Varhegyi, A round-robin study of cellulose pyrolysis kinetics by thermogravimetry, Industrial & Engineering Chemistry Research, 38 (1999) 2238-2244.

[33] R. Narayan, M.J. Antal, Thermal lag, fusion, and the compensation effect during biomass pyrolysis, Industrial & engineering chemistry research, 35 (1996) 1711-1721.

[34] S. Völker, T. Rieckmann, Thermokinetic investigation of cellulose pyrolysis — impact of initial and final mass on kinetic results, Journal of Analytical and Applied Pyrolysis, 62 (2002) 165-177.

[35] Q. He, L. Ding, Y. Gong, W. Li, J. Wei, G. Yu, Effect of torrefaction on pinewood pyrolysis kinetics and thermal behavior using thermogravimetric analysis, Bioresource Technology, 280 (2019) 104-111.

[36] D.A. Granados, F. Chejne, P. Basu, A two dimensional model for torrefaction of large biomass particles, Journal of Analytical and Applied Pyrolysis, 120 (2016) 1-14.

[37] M.G. Grønli, M.C. Melaaen, Mathematical model for wood pyrolysis comparison of experimental measurements with model predictions, Energy & Fuels, 14 (2000) 791-800.

[38] P. Rousset, P. Perré, P. Girard, Modification of mass transfer properties in poplar wood (P. robusta) by a thermal treatment at high temperature, Holz als Roh-und Werkstoff, 62 (2004) 113-119.

[39] L.D. Mafu, H.W.J.P. Neomagus, R.C. Everson, C.A. Strydom, M. Carrier, G.N. Okolo, J.R. Bunt, Chemical and structural characterization of char development during lignocellulosic biomass pyrolysis, Bioresource Technology, 243 (2017) 941-948.

[40] F. Paradela, F. Pinto, I. Gulyurtlu, I. Cabrita, N. Lapa, Study of the co-pyrolysis of biomass and plastic wastes, Clean Technologies and Environmental Policy, 11 (2009) 115-122.

[41] M. Brebu, S. Ucar, C. Vasile, J. Yanik, Co-pyrolysis of pine cone with synthetic polymers, Fuel, 89 (2010) 1911-1918.

[42] I. Narváez, J. Corella, A. Orio, Fresh tar (from a biomass gasifier) elimination over a commercial steam-reforming catalyst. Kinetics and effect of different variables of operation, Industrial & Engineering Chemistry Research, 36 (1997) 317-327.

[43] C. Brage, Q. Yu, G. Chen, K. Sjöström, Tar evolution profiles obtained from gasification of biomass and coal, Biomass and Bioenergy, 18 (2000) 87-91.

[44] A.-G. Collot, Y. Zhuo, D. Dugwell, R. Kandiyoti, Co-pyrolysis and co-gasification of coal and biomass in bench-scale fixed-bed and fluidised bed reactors, Fuel, 78 (1999) 667-679.

[45] R.N. André, F. Pinto, C. Franco, M. Dias, I. Gulyurtlu, M. Matos, I. Cabrita, Fluidised bed co-gasification of coal and olive oil industry wastes, Fuel, 84 (2005) 1635-1644.

[46] M.P. Aznar, M.A. Caballero, J.A. Sancho, E. Francés, Plastic waste elimination by co-gasification with coal and biomass in fluidized bed with air in pilot plant, Fuel processing technology, 87 (2006) 409-420.

[47] H. Meng, S. Wang, L. Chen, Z. Wu, J. Zhao, Thermal behavior and the evolution of char structure during co-pyrolysis of platanus wood blends with different rank coals from northern China, Fuel, 158 (2015) 602-611.

[48] C. Chen, X. Ma, Y. He, Co-pyrolysis characteristics of microalgae Chlorella vulgaris and coal through TGA, Bioresource Technology, 117 (2012) 264-273.

[49] S. Li, X. Chen, A. Liu, L. Wang, G. Yu, Co-pyrolysis characteristic of biomass and bituminous coal, Bioresource Technology, 179 (2015) 414-420.

[50] A.O. Aboyade, M. Carrier, E.L. Meyer, H. Knoetze, J.F. Görgens, Slow and pressurized co-pyrolysis of coal and agricultural residues, Energy Conversion and Management, 65 (2013) 198-207.

[51] A.O. Aboyade, M. Carrier, E.L. Meyer, J.H. Knoetze, J.F. Görgens, Model fitting kinetic analysis and characterisation of the devolatilization of coal blends with corn and sugarcane residues, Thermochimica Acta, 530 (2012) 95-106.

[52] M. Blesa, V. Fierro, J. Miranda, R. Moliner, J. Palacios, Effect of the pyrolysis process on the physicochemical and mechanical properties of smokeless fuel briquettes, Fuel Processing Technology, 74 (2001) 1-17.

[53] H. Darmstadt, M. Garcia-Perez, A. Chaala, N.-Z. Cao, C. Roy, Co-pyrolysis under vacuum of sugar cane bagasse and petroleum residue: properties of the char and activated char products, Carbon, 39 (2001) 815-825.

[54] W.-p. Yan, Y.-y. Chen, Experimental study on co-pyrolysis characteristics of lignite mixed with biomass mixture, Journal of Power Engineering, 26 (2006) 865-893.

[55] Z. Wu, S. Wang, J. Zhao, L. Chen, H. Meng, Thermochemical behavior and char morphology analysis of blended bituminous coal and lignocellulosic biomass model compound co-pyrolysis: Effects of cellulose and carboxymethylcellulose sodium, Fuel, 171 (2016) 65-73.

[56] Y. Song, A. Tahmasebi, J. Yu, Co-pyrolysis of pine sawdust and lignite in a thermogravimetric analyzer and a fixed-bed reactor, Bioresource Technology, 174 (2014) 204-211.

[57] H. Shui, C. Shan, Z. Cai, Z. Wang, Z. Lei, S. Ren, C. Pan, H. Li, Co-liquefaction behavior of a sub-bituminous coal and sawdust, Energy, 36 (2011) 6645-6650.

[58] C.A. Ulloa, A.L. Gordon, X.A. García, Thermogravimetric study of interactions in the pyrolysis of blends of coal with radiata pine sawdust, Fuel Processing Technology, 90 (2009) 583-590.

[59] H. Haykiri-Acma, S. Yaman, Synergy in devolatilization characteristics of lignite and hazelnut shell during co-pyrolysis, Fuel, 86 (2007) 373-380.

[60] Z. Wu, S. Wang, J. Zhao, L. Chen, H. Meng, Synergistic effect on thermal behavior during co-pyrolysis of lignocellulosic biomass model components blend with bituminous coal, Bioresource technology, 169 (2014) 220-228.

[61] J. Alvarez, G. Lopez, M. Amutio, M. Artetxe, I. Barbarias, A. Arregi, J. Bilbao, M. Olazar, Characterization of the bio-oil obtained by fast pyrolysis of sewage sludge in a conical spouted bed reactor, Fuel Processing Technology, 149 (2016) 169-175.

[62] Y.-F. Huang, C.-H. Shih, P.-T. Chiueh, S.-L. Lo, Microwave co-pyrolysis of sewage sludge and rice straw, Energy, 87 (2015) 638-644.

[63] Ö. Onay, E. Bayram, Ö.M. Koçkar, Copyrolysis of seyitömer− lignite and safflower seed: influence of the blending ratio and pyrolysis temperature on product yields and oil characterization, Energy & fuels, 21 (2007) 3049-3056.

[64] S.S. Idris, N.A. Rahman, K. Ismail, A.B. Alias, Z.A. Rashid, M.J. Aris, Investigation on thermochemical behaviour of low rank Malaysian coal, oil palm biomass and their blends during pyrolysis via thermogravimetric analysis (TGA), Bioresource Technology, 101 (2010) 4584-4592.

[65] H. Vuthaluru, Thermal behaviour of coal/biomass blends during co-pyrolysis, Fuel processing technology, 85 (2004) 141-155.

[66] E. Kastanaki, D. Vamvuka, P. Grammelis, E. Kakaras, Thermogravimetric studies of the behavior of lignite–biomass blends during devolatilization, Fuel Processing Technology, 77-78 (2002) 159-166.

[67] E. Biagini, F. Barontini, L. Tognotti, Devolatilization of biomass fuels and biomass components studied by TG/FTIR technique, Industrial & Engineering Chemistry Research, 45 (2006) 4486-4493.

[68] D. Vamvuka, E. Kakaras, E. Kastanaki, P. Grammelis, Pyrolysis characteristics and kinetics of biomass residuals mixtures with lignite☆, Fuel, 82 (2003) 1949-1960.

[69] A.K. Sadhukhan, P. Gupta, T. Goyal, R.K. Saha, Modelling of pyrolysis of coal–biomass blends using thermogravimetric analysis, Bioresource Technology, 99 (2008) 8022-8026.

[70] M. Yılgın, N. Deveci Duranay, D. Pehlivan, Co-pyrolysis of lignite and sugar beet pulp, Energy Conversion and Management, 51 (2010) 1060-1064.

[71] M.S. Masnadi, R. Habibi, J. Kopyscinski, J.M. Hill, X. Bi, C.J. Lim, N. Ellis, J.R. Grace, Fuel characterization and co-pyrolysis kinetics of biomass and fossil fuels, Fuel, 117 (2014) 1204-1214.

[72] H.M. Jeong, M.W. Seo, S.M. Jeong, B.K. Na, S.J. Yoon, J.G. Lee, W.J. Lee, Pyrolysis kinetics of coking coal mixed with biomass under non-isothermal and isothermal conditions, Bioresource Technology, 155 (2014) 442-445.

[73] H. Haykiri-Acma, S. Yaman, Interaction between biomass and different rank coals during co-pyrolysis, Renewable Energy, 35 (2010) 288-292.

[74] N. Vhathvarothai, J. Ness, Q.J. Yu, An investigation of thermal behaviour of biomass and coal during copyrolysis using thermogravimetric analysis, International journal of energy research, 38 (2014) 1145-1154.

[75] G. Agarwal, B. Lattimer, Physicochemical, kinetic and energetic investigation of coal–biomass mixture pyrolysis, Fuel Processing Technology, 124 (2014) 174-187.

[76] Z. Wu, S. Wang, J. Zhao, L. Chen, H. Meng, Thermal behavior and char structure evolution of bituminous coal blends with edible fungi residue during co-pyrolysis, Energy & fuels, 28 (2014) 1792-1801.

[77] Y. Zhang, D. Fan, Y. Zheng, Comparative study on combined co-pyrolysis/gasification of walnut shell and bituminous coal by conventional and congruent-mass thermogravimetric analysis (TGA) methods, Bioresource Technology, 199 (2016) 382-385.

[78] S. Qiu, S. Zhang, X. Zhou, Q. Zhang, G. Qiu, M. Hu, Z. You, L. Wen, C. Bai, Thermal behavior and organic functional structure of poplar-fat coal blends during co-pyrolysis, Renewable Energy, 136 (2019) 308-316.

[79] C. Quan, S. Xu, Y. An, X. Liu, Co-pyrolysis of biomass and coal blend by TG and in a free fall reactor, Journal of Thermal Analysis and Calorimetry, 117 (2014) 817-823.

[80] J. Meng, J. Park, D. Tilotta, S. Park, The effect of torrefaction on the chemistry of fast-pyrolysis bio-oil, Bioresource Technology, 111 (2012) 439-446.

[81] M. Guo, J.-C. Bi, Characteristics and application of co-pyrolysis of coal/biomass blends with solid heat carrier, Fuel Processing Technology, 138 (2015) 743-749.

[82] B. Moghtaderi, C. Meesri, T.F. Wall, Pyrolytic characteristics of blended coal and woody biomass, Fuel, 83 (2004) 745-750.

[83] A.G. Collot, Y. Zhuo, D.R. Dugwell, R. Kandiyoti, Co-pyrolysis and co-gasification of coal and biomass in bench-scale fixed-bed and fluidised bed reactors, Fuel, 78 (1999) 667-679.

[84] L.-g. Wei, L. Zhang, S.-p. Xu, Effects of feedstock on co-pyrolysis of biomass and coal in a free-fall reactor, Journal of Fuel Chemistry and Technology, 39 (2011) 728-734.

[85] Y. Mao, L. Dong, Y. Dong, W. Liu, J. Chang, S. Yang, Z. Lv, P. Fan, Fast co-pyrolysis of biomass and lignite in a micro fluidized bed reactor analyzer, Bioresource Technology, 181 (2015) 155-162.

[86] J. Wang, Q. Yan, J. Zhao, Z. Wang, J. Huang, S. Gao, S. Song, Y. Fang, Fast co-pyrolysis of coal and biomass in a fluidized-bed reactor, Journal of Thermal Analysis and Calorimetry, 118 (2014) 1663-1673.

[87] S. Li, X. Chen, L. Wang, A. Liu, G. Yu, Co-pyrolysis behaviors of saw dust and Shenfu coal in drop tube furnace and fixed bed reactor, Bioresource Technology, 148 (2013) 24-29.

[88] M. Wang, J. Tian, D.G. Roberts, L. Chang, K. Xie, Interactions between corncob and lignite during temperature-programmed co-pyrolysis, Fuel, 142 (2015) 102-108.

[89] H. Zhao, Q. Song, S. Liu, Y. Li, X. Wang, X. Shu, Study on catalytic co-pyrolysis of physical mixture/staged pyrolysis characteristics of lignite and straw over an catalytic

beds of char and its mechanism, Energy Conversion and Management, 161 (2018) 13-26.

[90] J.E. White, W.J. Catallo, B.L. Legendre, Biomass pyrolysis kinetics: a comparative critical review with relevant agricultural residue case studies, Journal of analytical and applied pyrolysis, 91 (2011) 1-33.

[91] P. Mellin, E. Kantarelis, W. Yang, Computational fluid dynamics modeling of biomass fast pyrolysis in a fluidized bed reactor, using a comprehensive chemistry scheme, Fuel, 117 (2014) 704-715.

[92] Q. Xue, T.J. Heindel, R.O. Fox, A CFD model for biomass fast pyrolysis in fluidized-bed reactors, Chemical Engineering Science, 66 (2011) 2440-2452.

[93] K. Jayaraman, M.V. Kok, I. Gokalp, Thermogravimetric and mass spectrometric (TG-MS) analysis and kinetics of coal-biomass blends, Renewable Energy, 101 (2017) 293-300.

[94] L. Florentino-Madiedo, M.F. Vega, E. Díaz-Faes, C. Barriocanal, Evaluation of synergy during co-pyrolysis of torrefied sawdust, coal and paraffin. A kinetic and thermodynamic study, Fuel, 292 (2021) 120305.

[95] S. Saeed, M. Saleem, A. Durrani, Thermal performance analysis and synergistic effect on co-pyrolysis of coal and sugarcane bagasse blends pretreated by trihexyltetradecylphosphonium chloride, Fuel, 278 (2020) 118240.

[96] M. Bhattacharyya, K.P. Shadangi, P. Mahanta, K. Mohanty, Co-pyrolysis of coal-biomass: study on reaction kinetics and thermodynamics, Biofuels, Bioproducts and Biorefining, (2021).

[97] K. Konwar, H.P. Nath, N. Bhuyan, B.K. Saikia, R.C. Borah, A.C. Kalita, N. Saikia, Effect of biomass addition on the devolatilization kinetics, mechanisms and thermodynamics of a northeast Indian low rank sub-bituminous coal, Fuel, 256 (2019) 115926.

[98] N. Jendoubi, F. Broust, J.M. Commandre, G. Mauviel, M. Sardin, J. Lédé, Inorganics distribution in bio oils and char produced by biomass fast pyrolysis: The key role of aerosols, Journal of Analytical and Applied Pyrolysis, 92 (2011) 59-67.

[99] A.V. Bridgwater, Review of fast pyrolysis of biomass and product upgrading, Biomass and Bioenergy, 38 (2012) 68-94.

[100] G. Lyu, S. Wu, H. Zhang, Estimation and comparison of bio-oil components from different pyrolysis conditions, Frontiers in Energy Research, 3 (2015) 28.

[101] W. Cai, Q. Liu, D. Shen, J. Wang, Py-GC/MS analysis on product distribution of two-staged biomass pyrolysis, Journal of Analytical and Applied Pyrolysis, 138 (2019) 62-69.

[102] F.-X. Collard, J. Blin, A review on pyrolysis of biomass constituents: Mechanisms and composition of the products obtained from the conversion of cellulose, hemicelluloses and lignin, Renewable and Sustainable Energy Reviews, 38 (2014) 594-608.

[103] P. Fu, S. Hu, L. Sun, J. Xiang, T. Yang, A. Zhang, J. Zhang, Structural evolution of maize stalk/char particles during pyrolysis, Bioresource Technology, 100 (2009) 4877-4883.

[104] Y. Chen, X. Zhang, W. Chen, H. Yang, H. Chen, The structure evolution of biochar from biomass pyrolysis and its correlation with gas pollutant adsorption performance, Bioresource Technology, 246 (2017) 101-109.

[105] T. Li, L. Zhang, L. Dong, P. Qiu, S. Wang, S. Jiang, C.-Z. Li, Changes in char structure during the low-temperature pyrolysis in N2 and subsequent gasification in air of Loy Yang brown coal char, Fuel, 212 (2018) 187-192.

[106] Y. Le Brech, J. Raya, L. Delmotte, N. Brosse, R. Gadiou, A. Dufour, Characterization of biomass char formation investigated by advanced solid state NMR, Carbon, 108 (2016) 165-177.

[107] A. Anca-Couce, Reaction mechanisms and multi-scale modelling of lignocellulosic biomass pyrolysis, Progress in Energy and Combustion Science, 53 (2016) 41-79.

[108] Z. Wu, W. Yang, L. Chen, H. Meng, J. Zhao, S. Wang, Morphology and microstructure of co-pyrolysis char from bituminous coal blended with lignocellulosic biomass: Effects of cellulose, hemicellulose and lignin, Applied Thermal Engineering, 116 (2017) 24-32.

[109] D.M. Keown, X. Li, J.-i. Hayashi, C.-Z. Li, Characterization of the structural features of char from the pyrolysis of cane trash using Fourier Transform− Raman spectroscopy, Energy & fuels, 21 (2007) 1816-1821.

[110] D. Fengel, G. Wegener, Wood: chemistry, ultrastructure, reactions, Walter de Gruyter2011.

[111] H. Chen, X. Chen, Y. Qin, J. Wei, H. Liu, Effect of torrefaction on the properties of rice straw high temperature pyrolysis char: Pore structure, aromaticity and gasification activity, Bioresource Technology, 228 (2017) 241-249.

[112] Y. Chen, B. Liu, H. Yang, Q. Yang, H. Chen, Evolution of functional groups and pore structure during cotton and corn stalks torrefaction and its correlation with hydrophobicity, Fuel, 137 (2014) 41-49.

[113] D. Feng, Y. Zhao, Y. Zhang, S. Sun, S. Meng, Y. Guo, Y. Huang, Effects of K and Ca on reforming of model tar compounds with pyrolysis biochars under H2O or CO2, Chemical Engineering Journal, 306 (2016) 422-432.

[114] S. Yuan, Z.-h. Dai, Z.-j. Zhou, X.-l. Chen, G.-s. Yu, F.-c. Wang, Rapid co-pyrolysis of rice straw and a bituminous coal in a high-frequency furnace and gasification of the residual char, Bioresource Technology, 109 (2012) 188-197.

[115] Z. Guo, Z. Bai, J. Bai, Z. Wang, W. Li, Co-liquefaction of lignite and sawdust under syngas, Fuel Processing Technology, 92 (2011) 119-125.

[116] S.M. Stark, M. Neurock, M.T. Klein, Strategies for modelling kinetic interactions in complex mixtures: Monte Carlo algorithms for MIMD parallel architectures, Chemical engineering science, 48 (1993) 4081-4096.

[117] Y. Lin, Y. Tian, Y. Xia, S. Fang, Y. Liao, Z. Yu, X. Ma, General distributed activation energy model (G-DAEM) on co-pyrolysis kinetics of bagasse and sewage sludge, Bioresource technology, 273 (2019) 545-555.

[118] S.R. Naqvi, Z. Hameed, R. Tariq, S.A. Taqvi, I. Ali, M.B.K. Niazi, T. Noor, A. Hussain, N. Iqbal, M. Shahbaz, Synergistic effect on co-pyrolysis of rice husk and sewage sludge by thermal behavior, kinetics, thermodynamic parameters and artificial neural network, Waste Management, 85 (2019) 131-140.

[119] J. Wang, S.-y. Zhang, X. Guo, A.-x. Dong, C. Chen, S.-w. Xiong, Y.-t. Fang, W.-d. Yin, Thermal Behaviors and Kinetics of Pingshuo Coal/Biomass Blends during Copyrolysis and Cocombustion, Energy & Fuels, 26 (2012) 7120-7126.

[120] M. Saikia, A.A. Ali, R.C. Borah, M.S. Bezbarua, B.K. Saikia, N. Saikia, Effects of biomass types on the co-pyrolysis behaviour of a sub-bituminous high-sulphur coal, Energy, Ecology and Environment, 3 (2018) 251-265.

[121] F. Ferrara, A. Orsini, A. Plaisant, A. Pettinau, Pyrolysis of coal, biomass and their blends: Performance assessment by thermogravimetric analysis, Bioresource Technology, 171 (2014) 433-441.

[122] D.S. Fardhyanti, A. Damayanti, ANALYSIS OF COAL TAR COMPOSITIONS PRODUCED FROM SUB-BITUMINOUS KALIMANTAN COAL TAR, Sainteknol: Jurnal Sains dan Teknologi, 14 (2016) 31-38.

[123] A.C. Louwes, L. Basile, R. Yukananto, J. Bhagwandas, E.A. Bramer, G. Brem, Torrefied biomass as feed for fast pyrolysis: An experimental study and chain analysis, Biomass and Bioenergy, 105 (2017) 116-126.

[124] F. Xue, D. Li, Y. Guo, X. Liu, X. Zhang, Q. Zhou, B. Ma, Technical progress and the prospect of low-rank coal pyrolysis in China, Energy Technology, 5 (2017) 1897-1907.

[125] Q. Zhang, J. Chang, T. Wang, Y. Xu, Review of biomass pyrolysis oil properties and upgrading research, Energy conversion and management, 48 (2007) 87-92.

[126] A.V. Bridgwater, G.V.C. Peacocke, Fast pyrolysis processes for biomass, Renewable and Sustainable Energy Reviews, 4 (2000) 1-73.

Chapter 3
Material and Methods

3.1 Sample collection and blend preparation

Punjab and Sindh provinces have vast cultivation areas dedicated for rice harvesting. Similarly, Punjab (eastern, central, and western Salt Range, Makerwal coalfields) and Balochistan (Sor-range-degari and Chamalang coalfields) has bituminous quality of coal. Consequently, locally sourced Rice husk (RH) and bituminous coal (C) is used for this study. The schematic of coal-RH samples in **Fig. 3.1** entailed drying in an oven at 110 °C for 24 h to remove the moisture content, followed by crushing-grinding in Hardgrove Grindability Index Tester (USA) to produce particle sizes of 0.2 mm through sieving (RX-29–10, WS Tyler).
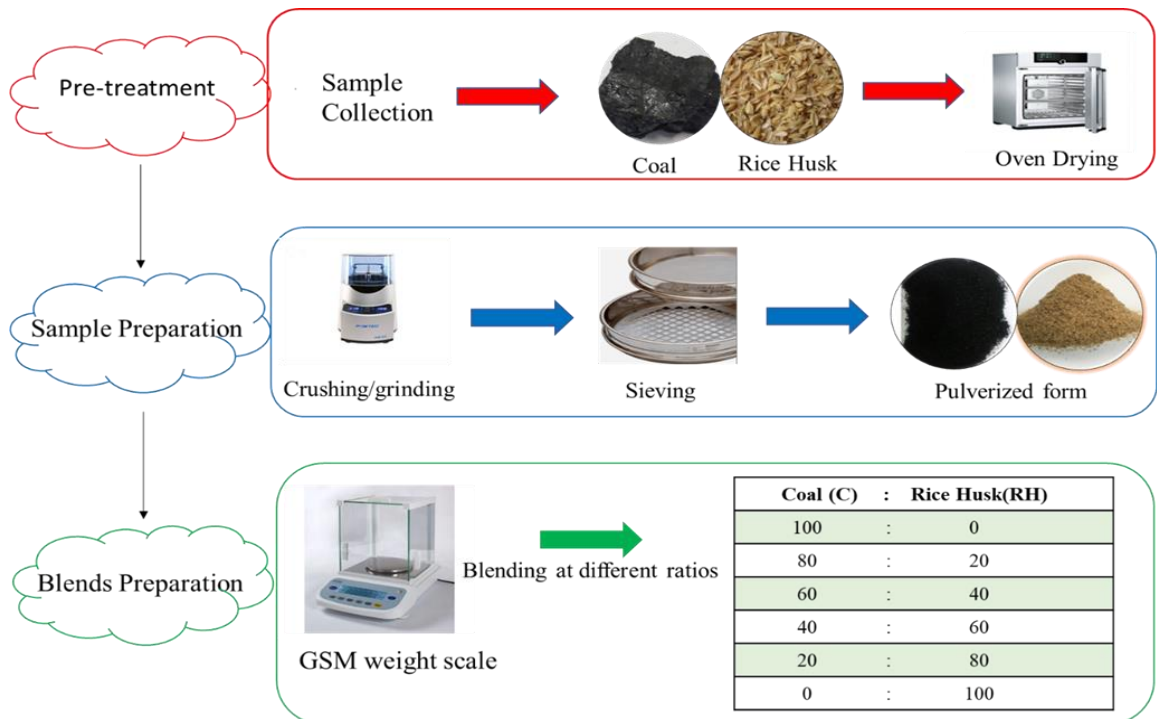

Fig 3. 1 Schematic for coal-RH blend preparation**.**

All the blends of coal-RH were prepared on weight percent basis by mixing coal with rice husk to make a 100% wt. of blend besides the pure samples. C80-RH20 represents that 80% wt. of coal was mixed with 20% wt. of rice husk, similarly, C60-RH40, C40-RH60 and C20-RH80 blends were prepared accordingly as shown in **Table 3.1**. Pure sample of coal and RH were referred as pure coal (C100) and pure rice husk (RH100) respectively.

3.2 Characterization of coal-biomass blends

The 5ECHN2200 model of CKIC series Carbon, Hydrogen Nitrogen analyzer with oxygen, helium, and nitrogen-standardized gases determined the ultimate analysis of 80 mg of each of the pure samples and blends in duplicates. 80 mg of each sample was placed in aluminum foil cup and foil was then placed on sample cup holder. Foil cup was then weighed and twisted to seal. The sealed foil cup was placed in the analyzer for analysis. The Sulphur analyzer 5E-IRS II model of CKIC make determined composition of Sulphur. 300 mg of each sample was taken, and the same procedure adopted for CHN analysis was followed. The calorific values of all samples were determined in the PAR-6200 bomb calorimeter following standard method of ASTM D5865-13. 0.5 g of each sample was placed into a crucible, crucible was then placed inside a vessel, vessel was filled with oxygen and the sample was then ignited. The sample burned and calorific value was calculated upon comparing it with the calibrant. The functional groups and chemical bonds present in the samples was determined through attenuated total reflection (ATR) module of the Fourier transform infrared (FTIR) spectroscopy allowing the direct measurement of wavelengths of 650-4500 cm^{-1} (Cary 630 model by Agilent Technologies, USA). Sample was placed in FTIR spectrometer and infrared radiation was directed towards the sample. Some of the radiation was absorbed by the sample while some was reflected. The absorbed radiation was converted into vibrational energy of molecules and the resulting signal was presented as a spectrum. Every chemical structure was distinguished upon producing a specific fingerprint. The TGA and DTG testing of the 10 mg of samples (in duplicates) from ambient to a 900 °C temperature at the 20 °C min^{-1} heating rate was completed with the 5500-0304 TGA (thermogravimetric analyzer). 8 mg of sample was placed in the pan and the pan was then placed on the sample tray. Nitrogen flow rate was set at 35

mL min^{-1} and the weight loss of blends and pure samples were recorded as a function of time and temperature under standard conditions.

3.3 Kinetic study

Coats-Redfern method has been frequently used for mechanistic analysis [1]. The coal-RH blends were analyzed for chemical (F$_1$, F$_{1.5}$), one-dimensional diffusional (D$_1$), and phase interfacial (S$_1$) reaction models to determine apparent activation energy (E$_a$), and collision frequency factor (A, pre-exponential factor) both for pyrolysis and co-pyrolysis techniques. In general, 200 °C to 600 °C is the temperature range where weight loss is attributed to moisture removal and devolatilization for the most of the blends [2]. The reaction equations for non-isothermal kinetics according to reaction kinetic theory adopted from [3, 4] are written as follows

The decomposition rate of solid to volatile state assuming Arrhenius model that the oxidation rate for mass loss is dependent only on the rate constant; mass of the sample remaining, and temperature is represented in **Eq. 1.**

$$\frac{d\alpha}{dt} = kTf(\alpha) \tag{1}$$

Where, $\frac{d\alpha}{dt}$ is the rate of conversion, k(T) is the rate constant and f(α) is the reaction model. The α is defined in **Eq. 2.**

$$\alpha = \frac{Wi - Wt}{Wi - Wf} \tag{2}$$

where, w_i is the initial mass of sample, w_t is the mass at any time(t), w_f is the final mass when degradation ends. Rate constant in **Eq. 1** is expressed in **Eq. 3** according to the Arrhenius equation.

$$k(T) = A\ exp\left(\frac{-E}{RT}\right) f(\alpha) \tag{3}$$

where, E$_a$ is the activation energy (kJ/mol), T is the temperature (K), R is universal gas constant (0.008314kJ/mol K). By substituting **Eq.3** in **Eq. 1**, the new form is represented in **Eq. 4.**

$$\frac{d\alpha}{dt} = A \exp\left(\frac{-E}{RT}\right) f(\alpha) \tag{4}$$

For TGA experiments having constant heating rate $\beta = \frac{dT}{dt}$, so equation can be expressed by the chain rule as presented in **Eq. 5.**

$$\frac{d\alpha}{dt} = \frac{A}{\beta} \exp\left(\frac{-E}{RT}\right) f(\alpha) \tag{5}$$

On applying integration to **Eq. 5,** the new equation form is shown in Eq. 6.

$$g(\alpha) = \int_0^\alpha \frac{d\alpha}{f\alpha} = \frac{A}{\beta} \int \exp\left(\frac{-E}{RT}\right) dT \tag{6}$$

While $g(\alpha)$ is the integral form of the reaction model. An exact analytical solution of the right-hand side of Eq. 6 is not possible so different method could be used to simplify this part of the equation. In case of the Coats-Redfern method the determination of three parameters including the apparent activation energy (Ea), order of reaction and Coats-Redfern constant [5] is required. This method has significance as the exact mechanism of reaction is not required in this model [6]. In this study, it was assumed that the order of reaction is equal to unity, hence the final form is expressed in **Eq. 7**:

$$\ln \left[\frac{g(\alpha)}{T^2}\right] = \ln \left[\left(\frac{AR}{\beta E}\right)\right] \times \left(\frac{1-2RT}{E}\right)\right] - \frac{E}{RT} \tag{7}$$

where, β is the heating rate, T is the temperature, A is the pre-exponential factor, R is universal gas constant. The value of E_a can be obtained from the slope of $\ln \left[\frac{g(\alpha)}{T^2}\right]$ and $\frac{1}{T}$ which gives a straight line [7]. The value of A can be obtained from the intercept of this graph. The reaction models implemented on all the blends and pure samples are illustrated in **Table 3.2** and were adopted from [8], [9].

The synergistic effect was determined by comparing the calculated values of blends with experimental values. The calculated values using **Eq. 8** were obtained by the additive model which assumed that no interactions occurred between the coal and biomass during co-pyrolysis [10].

$$Y_{calculated} = X_{coal} Y_{coal} + X_{biomass} Y_{biomass} \qquad (8)$$

Where Y_{coal} and $Y_{biomass}$ are the experimental values of coal and rice husk, while X_{coal} and $X_{biomass}$ are the mass fractions of coal and rice husk in the blends, respectively.

Deviation **(Eq. 9)** between experimental and calculated values of weight loss rates was determined to identify the presence of synergistic effect in blends [11, 12].

$$\text{Deviation} = \frac{Exp_{value} - Cal_{value}}{Exp_{value}} \times 100 \qquad (9)$$

where Exp_{value} is the value which is obtained from TGA curve and Cal_{value} is the value obtained from sum of TGA curves of individual samples as indicated in **Eq. 8**.

3.4 Thermodynamic study

Thermogravimetric analysis is also useful in determination of various thermodynamic parameters such as enthalpy (H), Gibbs free energy (G) and entropy (S) [13]. Kinetic data is used for calculation of thermodynamic parameters by using **Eq. (10-12).** The equations used for calculation of thermodynamic parameters were adopted from [14-16]

$$\Delta H = E_a - RT \qquad (10)$$

$$\Delta G = E_a - RT_m \ln[\frac{K_b T}{hA}] \qquad (11)$$

$$\Delta S = \frac{\Delta H - \Delta G}{T_m} \qquad (12)$$

Where ΔH is the change in enthalpy, ΔG is Gibbs free energy and ΔS represents change in entropy. K_b is the Boltzmann constant equal to 1.381×10^{-23} m^2 kgs^{-2} K^{-1}. T_m corresponds to the maximum decomposition temperature. h is Plank's constant having value of 6.626×10^{-34} m^2 kgs^{-1} and R is the universal gas constant.

3.5 Experimental setup for co-pyrolysis and co-gasification

The schematic of co-pyrolysis set up is presented in **Fig. 3.2.** The reactor consisted of a stainless-steel tube having 14 mm outer and 12 mm inner diameter. The selected coal-RH blend was placed in the middle section of the reactor tube sandwiched

by quartz wool. Heating was provided via an electric heater coupled with a temperature controller. Mass flow controller (MFC) (MF4603-n1-1-bv-a, Servoflo Corporation, USA) was used to regulate gas flow. Heating rate was kept constant at 20 °C/min. Post pyrolysis reactor gases were collected after the condenser, whereas liquid product was collected in a separate vessel. Feed gas and product gas were analyzed using Gas Chromatograph (GC-2010 Pro, SHIMADZU, Japan equipped with TCD column (RT-MS5A, 30 m × 0.32 mm ID, 30 μm) to detect hydrogen gas (H_2), carbon dioxide (CO_2) and methane (CH_4). After 2 h the distilled water was introduced using HPLC pump to the pre-heater to generate steam. The temperature of the reactor was elevated to 750 °C and then fixed for 2 h to analyze the co-gasification products.
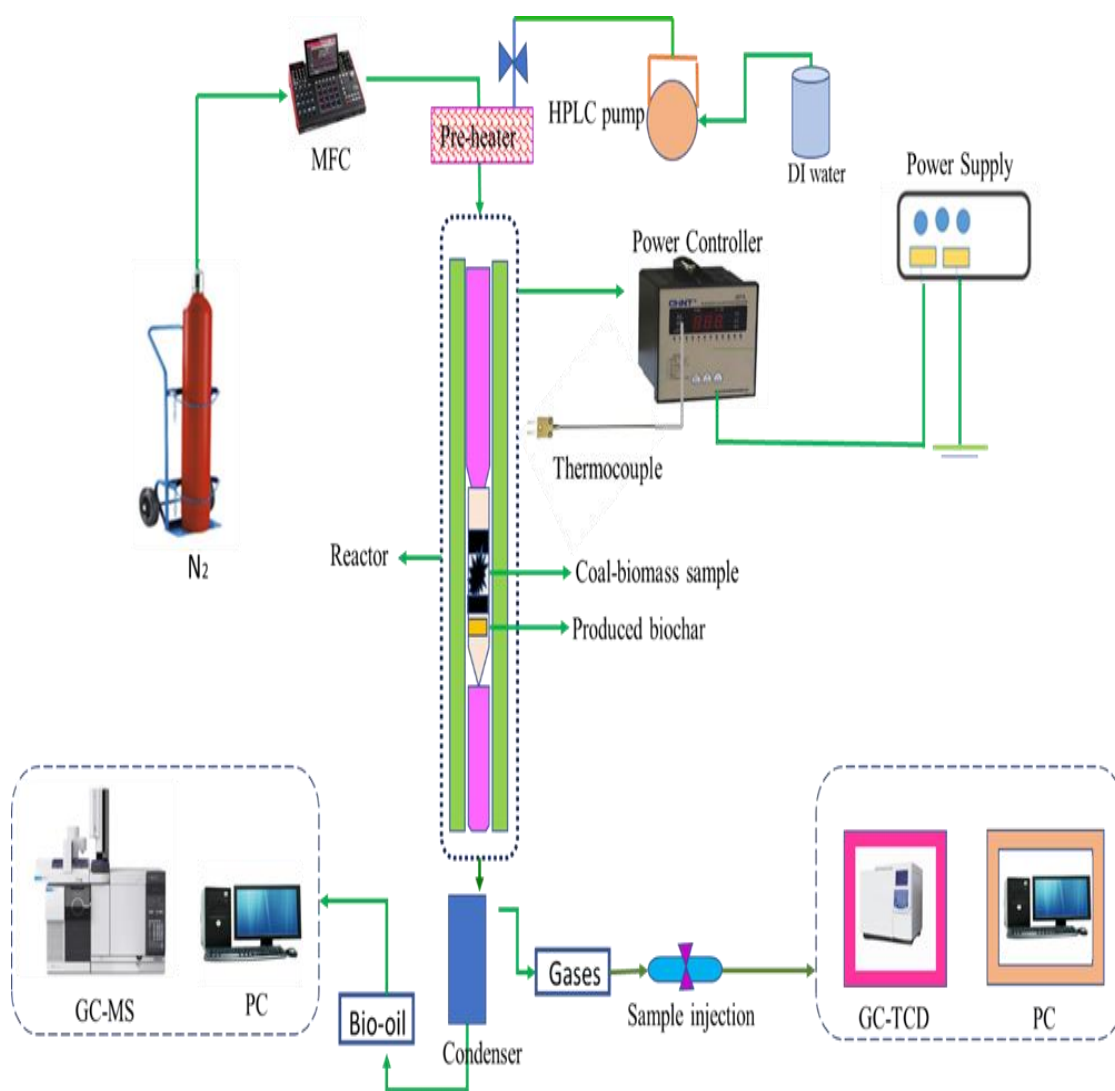
Fig 3. 2 Schematic diagram representing the setup for co-pyrolysis/co-gasification

65

Table 3.1 Sample code and percentage weight composition of the blends

Sample code	Weight (%) composition of pure samples		Weight (%) composition of blends			
	C100	RH100	C80-RH20	C60-RH40	C40-RH60	C20-RH80
Coal	100	0	80	60	40	20
Rice Husk	0	100	20	40	60	80

Table 3. 2 Reaction mechanisms and model names

Mechanism of reaction	Model name	$g(\alpha)$
Chemical reaction order	Chemical reaction order 1 (F_1)	$-\ln(1-\alpha)$
	Chemical reaction order 1.5 ($F_{1.5}$)	$2[(1-\alpha)^{-0.5}-1]$
One dimensional diffusion	Parabolic law (D_1)	α^2
Phase interfacial reaction	Shrinkage geometrical column (S_1)	$1-(1-\alpha)^{1.5}$

3.6 Characterization of pyrolysis products

3.6.1 Characterization of biochar

The characterization of biochar received after the pyrolysis was completed in SEM-EDS, TGA and FTIR to check its suitability for various catalysis and environmental applications. The morphology of biochar investigated at 20kV exposure of 3nm resolution extended to 10-20,000X, exhibited the desired micrographs through scanning electron microscopy (SEM) using (TESCAN VEGA 3, Czech Republic). The SEM images taken at different field magnifications produced better morphological structure insights. Elemental composition of biochar was examined through EDX detector (Oxford Instruments, model: 51-AD0007) [17], concurrently, the TGA and FTIR analysis as per cited conditions was also completed. The overall yield of biochar and bio-oil was calculated using **Eq. 13.**

$$\text{Product yield (wt.\%)} = \frac{W_p}{W_f} \times 100 \tag{13}$$

Where, W_p is the weight of product (g), W_f is the total weight of feedstock (g)

3.6.2 Characterization of bio-oil and product gases

The chemical composition of produced bio-oil was analyzed using GC-MS (Shimadzu P2020 NX, Japan). The sample dissolved in n-hexane solvent was loaded in the autosampler GC vial and then 1.0 µL, at a split ratio of 1:20 injected into GC-MS for analysis with helium used as a carrier gas. The initial temperature ramp for column oven was set at 5°C/min from 50 °C to 150 °C and then at rate of 10°C/min from 150°C to 290 °C. The temperature of injector and detector was set at 290 °C. Electron impact potential of 70 eV with scan range of 35-500 amu was set. The comparison of mass spectra of blends with National Institute of standards and technology (NIST) library data helped to determine the organic compounds. The product gases were analyzed in GC-TCD (Shimadzu Japan) with already reported [18] details of the used column.

Summary

This chapter discusses about various steps for the preparation of blends of Coal (C) and Rice husk (RH) at different ratios. Firstly, both the feedstocks were dried, crushed and then the blends were prepared on weight percentages. The characterization of all the blends and pure samples were carried out using CHN-S analyzer, TGA, FTIR analysis. After the characterization, Coats-Redfern method was used for the kinetic analysis using four different reaction models and their mechanisms. Thermodynamic analysis was also carried out. After these in-depth investigations, synergistic effect was determined on comparing the experimental and calculated weight loss curves of the blends.

Then the blends showing positive synergy values were pyrolyzed in the fixed bed reactor at temperature of 500°C. Fixed bed reactor contained stainless steel tube and the blend was placed in the middle section of tube for co-pyrolysis. A condenser was attached for the collection of liquid product and post pyrolysis gases were also collected. After 2 hrs of co-pyrolysis, the temperature was increased to 750°C and distilled water was introduced in order to enable co-gasification. Lastly, detailed characterization of co-pyrolysis products (biochar, bio-oil and gases) was carried out. Biochar was characterized using SEM-EDS, TGA, and FTIR analysis. Bio-oil was characterized through GC-MS analysis and produced gases including hydrogen gas (H_2), carbon dioxide (CO_2), carbon monoxide (CO), and methane (CH_4) were examined through GC-TCD analyzer.

References

[1] M. Mureddu, F. Dessì, A. Orsini, F. Ferrara, A. Pettinau, Air- and oxygen-blown characterization of coal and biomass by thermogravimetric analysis, Fuel, 212 (2018) 626-637.

[2] A. Dhaundiyal, S.B. Singh, M.M. Hanon, R. Rawat, Determination of kinetic parameters for the thermal decomposition of parthenium hysterophorus, Environmental and Climate Technologies, 22 (2018) 5-21.

[3] Y. Ma, S. Li, The pyrolysis, extraction and kinetics of Buton oil sand bitumen, Fuel Processing Technology, 100 (2012) 11-15.

[4] K.-M. Lu, W.-J. Lee, W.-H. Chen, T.-C. Lin, Thermogravimetric analysis and kinetics of co-pyrolysis of raw/torrefied wood and coal blends, Applied energy, 105 (2013) 57-65.

[5] A.W. Coats, J. Redfern, Kinetic parameters from thermogravimetric data, Nature, 201 (1964) 68-69.

[6] Z. Hameed, Z. Aman, S.R. Naqvi, R. Tariq, I. Ali, A.A. Makki, Kinetic and thermodynamic analyses of sugar cane bagasse and sewage sludge co-pyrolysis process, Energy & Fuels, 32 (2018) 9551-9558.

[7] I. Mian, X. Li, Y. Jian, O.D. Dacres, M. Zhong, J. Liu, F. Ma, N. Rahman, Kinetic study of biomass pellet pyrolysis by using distributed activation energy model and Coats Redfern methods and their comparison, Bioresource Technology, 294 (2019) 122099.

[8] V. Balasundram, N. Ibrahim, R.M. Kasmani, M.K.A. Hamid, R. Isha, H. Hasbullah, R.R. Ali, Thermogravimetric catalytic pyrolysis and kinetic studies of coconut copra and rice husk for possible maximum production of pyrolysis oil, Journal of Cleaner Production, 167 (2017) 218-228.

[9] S.R. Naqvi, Z. Hameed, R. Tariq, S.A. Taqvi, I. Ali, M.B.K. Niazi, T. Noor, A. Hussain, N. Iqbal, M. Shahbaz, Synergistic effect on co-pyrolysis of rice husk and sewage sludge by thermal behavior, kinetics, thermodynamic parameters and artificial neural network, Waste Management, 85 (2019) 131-140.

[10] D.K. Park, S.D. Kim, S.H. Lee, J.G. Lee, Co-pyrolysis characteristics of sawdust and coal blend in TGA and a fixed bed reactor, Bioresource Technology, 101 (2010) 6151-6156.

[11] H. Merdun, Z.B. Laougé, Kinetic and thermodynamic analyses during co-pyrolysis of greenhouse wastes and coal by TGA, Renewable Energy, 163 (2021) 453-464.

[12] Z. He, Z. Xia, J. Hu, L. Ma, Y. Li, Thermal decomposition and kinetics of electrically controlled solid propellant through thermogravimetric analysis, Journal of Thermal Analysis and Calorimetry, 139 (2020) 2187-2195.

[13] Y.S. Kim, Y.S. Kim, S.H. Kim, Investigation of thermodynamic parameters in the thermal decomposition of plastic waste− waste lube oil compounds, Environmental science & technology, 44 (2010) 5313-5317.

[14] A.K. Varma, N. Lal, A.K. Rathore, R. Katiyar, L.S. Thakur, R. Shankar, P. Mondal, Thermal, kinetic and thermodynamic study for co-pyrolysis of pine needles and styrofoam using thermogravimetric analysis, Energy, 218 (2021) 119404.

[15] Y. Xu, B. Chen, Investigation of thermodynamic parameters in the pyrolysis conversion of biomass and manure to biochars using thermogravimetric analysis, Bioresource Technology, 146 (2013) 485-493.

[16] K. Konwar, H.P. Nath, N. Bhuyan, B.K. Saikia, R.C. Borah, A.C. Kalita, N. Saikia, Effect of biomass addition on the devolatilization kinetics, mechanisms and thermodynamics of a northeast Indian low rank sub-bituminous coal, Fuel, 256 (2019) 115926.

[17] U. Jamil, A. Husain Khoja, R. Liaquat, S. Raza Naqvi, W. Nor Nadyaini Wan Omar, N. Aishah Saidina Amin, Copper and calcium-based metal organic framework (MOF) catalyst for biodiesel production from waste cooking oil: A process optimization study, Energy Conversion and Management, 215 (2020) 112934.

[18] J. Raza, A.H. Khoja, S.R. Naqvi, M.T. Mehran, S. Shakir, R. Liaquat, M. Tahir, G. Ali, Methane decomposition for hydrogen production over biomass fly ash-based CeO_2 nanowires promoted cobalt catalyst, Journal of Environmental Chemical Engineering, 9 (2021) 105816.

Chapter 4

Results and Discussion

4.1 Physicochemical properties of coal-biomass blends

Ultimate analysis of blends exhibits significant differences in the carbon, hydrogen, nitrogen, and sulphur contents of the samples is shown in **Fig. 4.1**. C100 has 67.2% carbon, almost 80% more than the 37.4% carbon of RH100 in **Fig. 4.1(a).** Coal contains additional amount of carbon and less volatile content when compared to the biomass that usually has high moisture, oxygen and hydrogen contents with less carbon [1]. In the case of blends, increase in the weight percentage of coal contributes to the rise in the carbon content of the blends up to a maximum amount of 63.4% carbon for C80-RH20. On the other hand, the reduction of weight percentage of coal in the blends decreased the overall percentage of carbon present in the prepared samples. The resultant percentages of carbon detected in C60-RH40, C40-RH60, and C20-RH80 blends are 53.4%, 48.2%, and 43.6%, respectively. A 4.7% hydrogen in R100 compared to 3.5% hydrogen of C100 was determined in **Fig 4.1(b)** and correspondingly C20-RH80 exhibited the maximum hydrogen content (i.e. 4.5%) among the blends because of the increased ratio of biomass present. The lowest percentage of hydrogen (i.e. 3.7%) because of the higher weight ratio of coal was present in the C80-RH20 blend. While C60-RH40 and C40-RH60 blends contained 4.1% and 4.31% hydrogen, respectively. Nitrogen content of C100 (0.5 %) slightly higher than that of RH100 (0.2%) is usually present in the aromatic structures. The content of nitrogen in the blends in **Fig 4.1(c)** being within the range of the pure fuels decreased with reducing share of coal. The percentage of sulphur in **Fig 4.1(d)** of C100 (0.6%) and RH100 (0.3%), altered to 0.57%, 0.43%, 0.43%, and 0.41% for C80-RH20, C60-RH40, C40-RH60, and C20-RH80 blends, respectively.
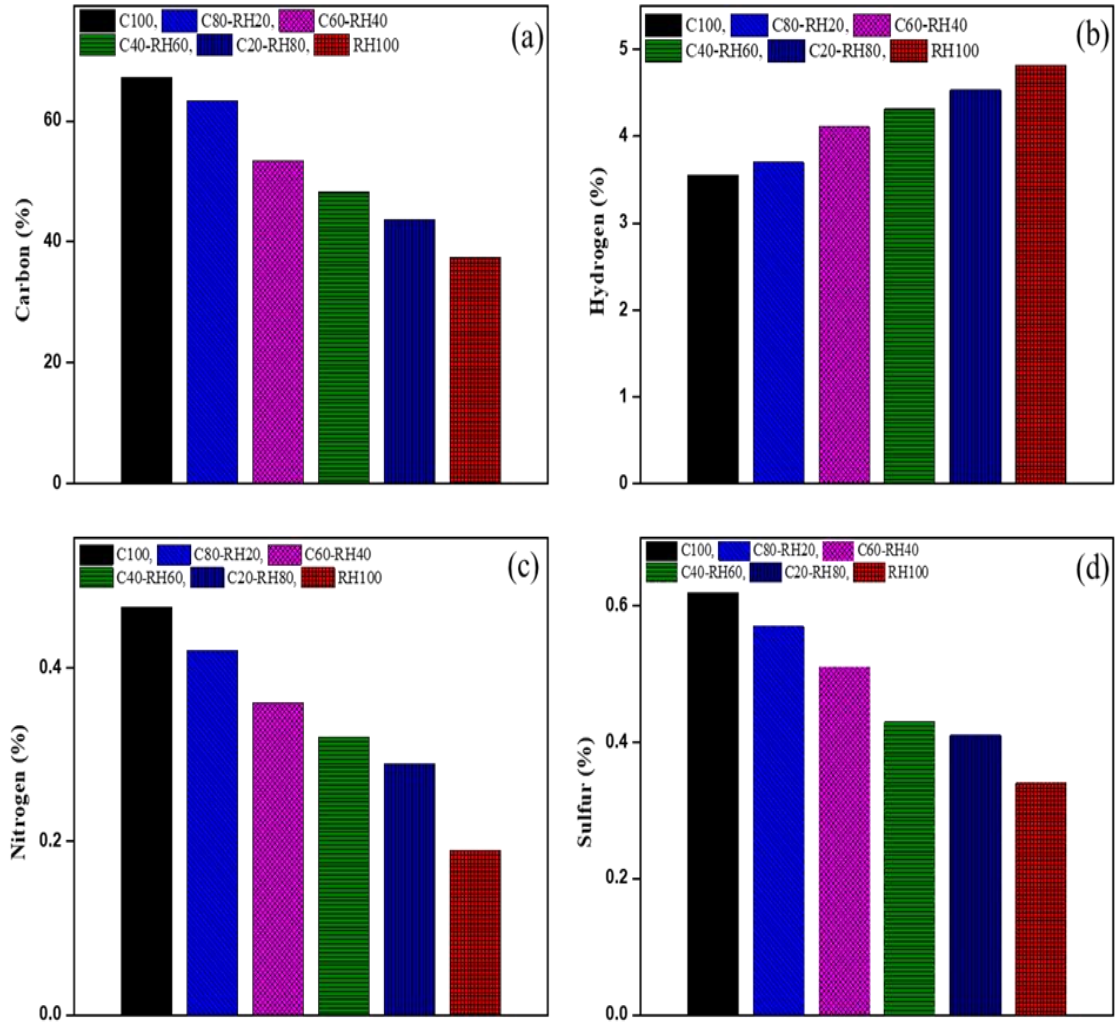
Fig 4.1 Ultimate analysis of fuel blends in terms of (a) Carbon (b) Hydrogen (c) Nitrogen (d) Sulphur

The selection criteria for a sustainable conversion process depend on the net heat release potential i.e. gross calorific value (GCV) of fuel[2][2][2][2][2][2]. Coal and RH having significantly different amounts of carbon, moisture and volatiles exhibited corresponding GCV of 29 MJ/kg and 17 MJ/kg in **Fig. 4.2**. C80-RH20 blend has the highest GCV of 28 MJ/kg almost comparable with C100, whilst C60-RH40, C40-RH60, and C20-RH80 blends have 26MJ/kg, 23MJ/kg, and 21MJ/kg values, congruently. C80-RH20, C60-RH40 blends have the potential for energy production purposes. The sensible ratios of biomass (20% and 40%) in the blends impart improvement in the overall reactivity and ignition characteristics [3].
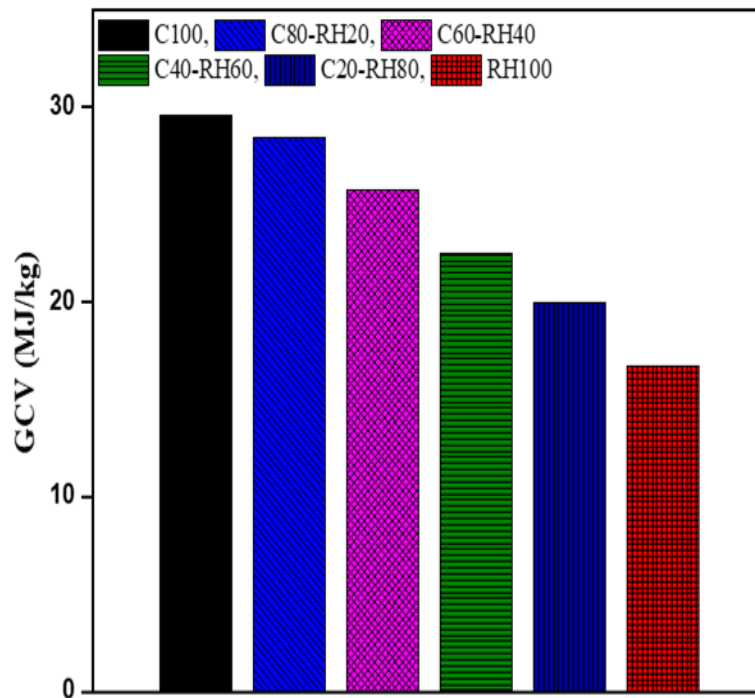
Fig 4.2 Gross Calorific value (GCV) analysis of Coal-RH blends

FTIR spectra shown in **Fig. 4.3** represents the chemical structural (functional group) differences [4] of coal, RH and blends corresponding to specific wavelengths. The oxygen-containing hydroxyl and carboxyl functional groups are present in RH, compared to the aromatic rings with some aliphatic side chains/bonds for coal. A few aromatic and aliphatic groups though present but O-H, C-O, C-H groups are abundantly detected. The most prominent peaks are obtained between the range of 1000-1700 cm^{-1}. Coal shows a peak at a wavenumber of 2800-3000 indicating aliphatic C-H stretching. Significant peak is observed between 1580-1650 cm^{-1} which shows aromatic C=C stretching. From 1300-1500 cm^{-1} coal shows aliphatic C-H deformation along with aromatic C=C stretching. This shows that the macro molecular structure of coal is composed of large number of aliphatic chains and bridge bonds [5]. Peaks with weak strength seemed over the wavenumber of 1100-1300 cm^{-1} indicating C-O stretching attributed to the deficiency of oxygen containing functional groups in coal.

However, RH100 shows peak indicating O-H stretching between 3200-3400 cm^{-1} [6]. These spectra signify the presence of hydroxyl groups and many hydrogen bonds

due to inherently detected hydrogen as identified by CHN analysis discussed above. Pure RH shows a well-defined peak at 930-1200 cm^{-1} representing C-O bond stretching [7]. This reveals the molecular structure of rice husk that contains ether bonds, alcoholic and phenolic hydroxyl groups. Aliphatic C-H stretching, and deformation is observed between 3000-2600 cm^{-1}. Weaker peak between 1600-1400 indicates presence of aromatic C=C stretching. These major differences define their pyrolysis and combustion characteristics. RH100 comprises of cellulose, hemicellulose, and lignin. Cellulose comprises of polyhydroxy aldehyde and the hydrogen atom on hydroxyl groups attract electrons on oxygen atom to form hydrogen bond. Hemicellulose on the other hand has uneven structure and excessive branched chains. Hence, functional groups of both cellulose and hemicellulose consisting of aldehyde, alcohol and hydroxyl groups contribute the detected absorption peaks. Lignin contains side chains with irregularity between recurring units and contains phenolic and alcoholic hydroxyl groups, benzene, methoxy groups etc. [5].

The impact of biomass in the blends especially with increasing the mass ratio of RH100 results in abundance of hydroxyl and oxygen containing functional groups in C20-RH80. Similarly, C80-RH20 shows abundant aromatic rings and side chains (aliphatic) whereas lesser oxygen and hydroxyl groups. These differences develop due to the differences in the base of structural units and the type of connection between these units.
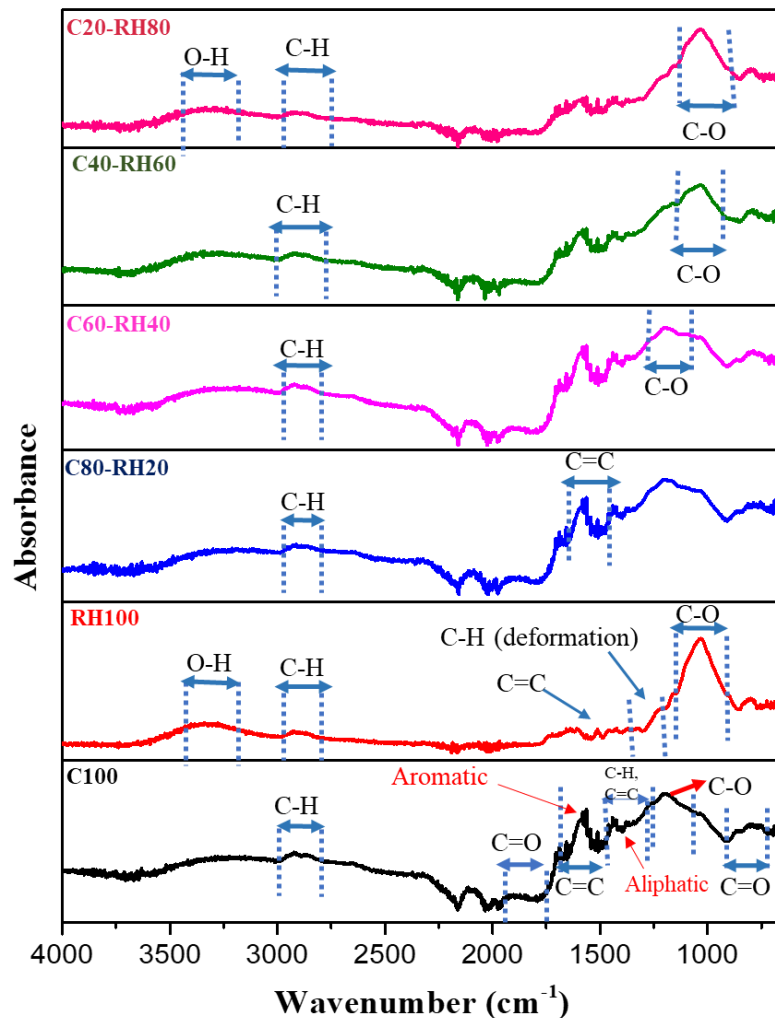
Fig 4.3 FTIR spectra of Coal-RH blends

The TGA profiles of the studied samples in nitrogen environment at heating rate of 20 °C min^{-1} represents the changes in sample composition as shown in **Fig. 4.4(a)** and redox reactions accompanied with weight loss. It has been observed that the volatiles emitted by biomass may interact with the coal char especially when the biomass and coal are within their respective major pyrolysis section regions [5]. The interaction occurs due to transfer and interactions within volatiles and char, hydrogen, alkali and alkaline earth metal and free radicals from biomass. The TGA curves indicate that weight loss of blends can be divided into three stages [8]. Three-zone specific weight losses i.e., stage-I, stage-II, stage-III can be identified in **Fig. 4.4(b).** Stage-I is attributed to the moisture loss from the fibrous structure and breakdown of low molecular weight components within 50°C to 200°C. In case of biomass, the thermal degradation (Stage-

II) includes the decomposition of cellulose, hemicellulose, and lignin [8]. At temperature range of 250°C-450°C, organic matter undergoes oxidation due to the presence of oxygen containing species and –OH functional groups [8]. In stage-I, moisture removal is associated with minimal weight loss. This moisture removal in stage-I degrades the thermal bonds in structure and creates stronger bonds in their place [9]. TGA and DTG profiles show that degradation of RH started earlier than coal. The reason attributed to this behavior is that cellulose, hemicellulose and lignin present in RH are linked together with weak ether bonds (R-O-R) having bond energy of 380-420 kJ/mol [10] that degrade at lower temperature. However structure of coal is composed of polycyclic aromatic hydrocarbons linked together by single or double bonds having high stability and high resistance towards thermal decomposition because of the bond energy of 1000 kJ/mol [11]. It is the possible reason that in (stage-II) RH started decomposing at 200 °C while degradation of coal started in stage -III at 366 °C. TGA curves reveal that bonding strength of stage-II is comparatively higher than stage-I. In the case of blends, faster degradation at higher biomass-blending ratio is exhibited compared to those with smaller blending ratios. With the increase in temperature the oxygen containing by-products reach to their burnout temperatures and this released heat, consequently breaks down the remaining organic components [12]. Aromatic hydrocarbons are much stable than ether bond, hence, biomass degrades much rapidly than coal [13].

Comparative analysis of the TGA results exhibit increase in weight loss with increasing content of biomass of the tested blends. The weight loss attributed to the Stage-II vary from 20% to a maximum of 53% in case of pure RH. The differences in the devolatilization temperatures of RH and coal are due to different structural properties attributed to the chemical and elemental composition of the parent fuels [1]. At temperature above 600 °C, complex and thermally stable components mostly inorganic start to degrade. **Table 4.1** lists the pyrolysis characteristics of each blend representing diverse temperature zones with corresponding peak temperatures.
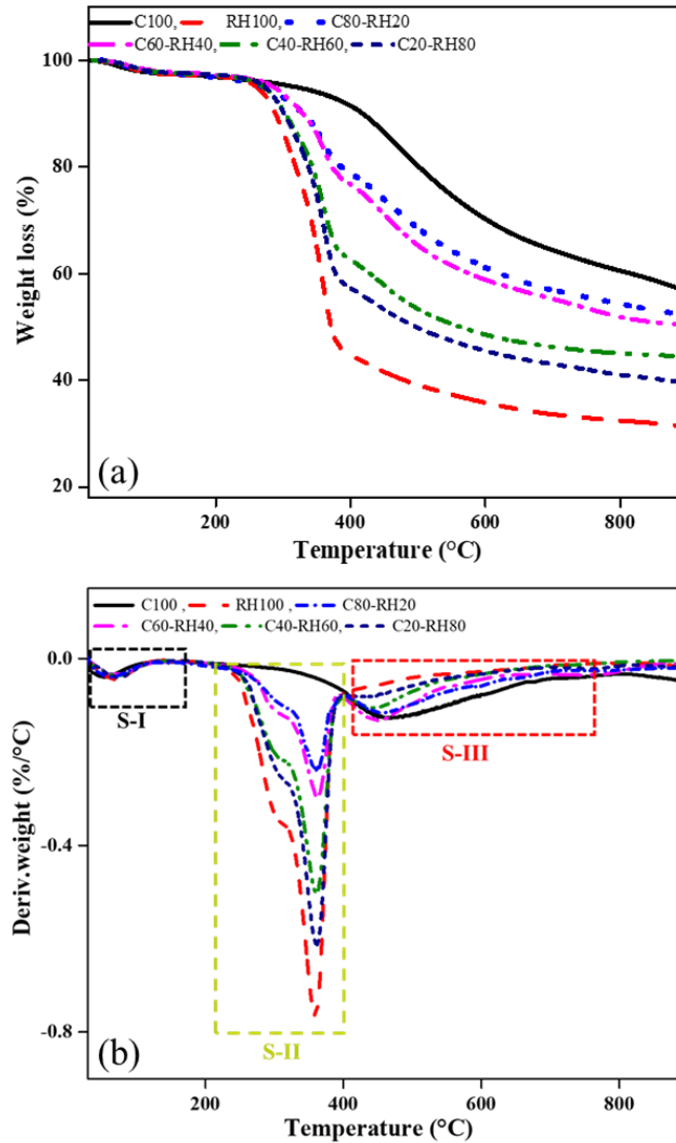
Fig 4.4 (a) TGA and (b) DTG curves of coal-rice husk blends in pyrolytic atmosphere

The DTG peaks basically indicate the points of inflection of TGA profiles and demonstrate extreme weight loss rates [14]. These curves show temperature ranges where maximum degradation takes place. **Fig. 4.4(b)** shows that reactivity of coal and RH blends is directly proportional to the DTG peaks and decreases with the increases in temperature. The peaks from raw coal pyrolysis are broader as compared to the blends profile. Coal profile reveals its low reactivity and its corresponding DTG curve does not show a significant marked peak. It is observed that reactivity increases linearly with the increase in biomass proportion. At the end of the peak after 600 °C, the slow breakdown

of the components over a wide temperature range produces residue that reaches to a constant ratio, usually referred as a long tailing section [12]. The DTG profile evaluation shows that in case of blends, the peaks shifted to lower temperatures with increase of RH blending [15]. It is evident from Fig. 6(b) that for pure RH the degradation was largest with increasing rate and was maximum at temperature of 358 °C. However, from 410 °C the degradation decreased to a very low value till 900 °C. Coal depicted a very less devotalization rate achieving maximum degradation at 460 °C. The detailed pyrolysis characteristics of each sample are illustrated in **Table 4.1**. The ignition temperatures (T_i) of blends for stage II decreased as the RH blending ratio increases. The earlier ignition temperatures are pivotal to the operations of thermochemical conversion units. Temperature in stage-II where maximum degradation took place is 358 °C for RH, 363 °C for C80-RH20, 361°C for C60-RH40, 360 °C for C40-RH60, 359 °C for C20-RH80. There is an opulent difference of 166 °C noted between pure samples (C100 = 366 °C; RH100 = 200 °C). A change of about 122 °C, 149 °C, 154 °C, and 160 °C in the ignition temperature was reported for 20 wt. %, 40 wt. %, 60 wt. %, and 80 wt. % of added biomass when compared to pure coal. This indicated that RH degrades faster and more rapidly than coal, similarly, the peak temperature (T_p) for blends decreases as the RH blending ratio increases. However, weight loss increases when ratio of RH in the blends increases i.e. C80-RH20 exhibits a total weight loss (stage II and III) of 36%, C60-RH40 reveals 45%, C40-RH60 shows 52% and C20-RH80 demonstrates a mass loss of 56%. C100 and RH100 show weight loss of 35.2% and 86% respectively. Higher residue of coal is due to its high ash content and higher carbon content [16]. So, it is rational that with increase of RH in the blend more volatiles will release, and more weight loss will be observed. The percentage of residue left and burnout temperatures at the end of pyrolysis decreases with increasing biomass-blending ratio is shown in **Table 4.1**

Table 4.1 Pyrolysis parameters of blends

	C100	**RH100**	**C80-RH20**	**C60-RH40**	**C40-RH60**	**C20-RH80**
Stage II (°C)	-	200-421	224-387	217-393	212-402	206-400
T_p (°C)	-	358	363	361	360	359
Weight loss (%)	-	53.3	16.59	19.48	20.30	39.69
Residue left	-	43.28	80.39	77.57	77.08	57.36
DTG (%/°C)	-	-0.06	-0.05	-0.076	-0.084	-0.076
Stage III (°C)	368-895	421-741	387-863	393-853	402-821	400-819
T_p (°C)	460	430	454	449	446	445
T_b (°C)	895	744	863	853	821	819
Weight loss	35.28	10.23	28.12	26	32.02	16.58
Residue left	58.13	33.05	52.27	51.57	45.06	40.75
DTG (%/°C)	-0.05	0.01	-0.008	-0.01	-0.008	-0.014

4.2 Kinetic analysis

E_a is the energy required to initiate the reaction and very important parameter in coal-RH blending analysis [17]. The temperature where maximum weight loss occurred varied according to the composition of the blend's indicative of volatilization and depolymerization reactions at dissimilar temperatures for each blend. The kinetic parameters are obtained through thermogravimetric (TGA) data of the blends and pure samples. The selection of suitable temperature ranges for each blend can have a significant impact in analyzing the kinetic parameters [18]. The best fitted model can be selected based on linear fitting of the solid-state reaction kinetic models as well as the regression coefficient of every model. Model having regression coefficient nearly equal to 0.99 can be considered as the most appropriate model for co-pyrolysis. A is the pre-exponential factor that describes the material structure [19]. Higher values of pre-exponential factors represent a complex reaction whereas the lower values represent surface reaction [20]. In case of co-pyrolysis, the blends are divided into two stages (Stage A and Stage B) of temperature for calculation of E_a depending upon their reactivity and the region where maximum decomposition occurred as shown in **Table 4.2**.The initial moisture loss stage has not been included in the kinetics calculation. **Fig. 4.5** represents the graph between 1/T and $[\frac{\ln g(\alpha)}{T^2}]$ expected to form a straight line with -E/R slope to determine the E_a for each sample as depicted in **Table 4.2.** This straight line also gives intercept to determine pre-exponential factor A (min^{-1}). **Fig.4.5(a-d)** represent the plot for model F_1, $F_{1.5}$, D_1, and S_1 respectively. It depicts the linear regression (R^2) for the extraction of various kinetic parameters for the blends at different reaction models. For stage A, model F_1 depicted higher correlation coefficient for the blends and pure samples ranging from 0.984-0.991 shown in **Fig.4.5 (a)**. While $F_{1.5}$ provided values ranging from 0.981-0.988 as depicted in **Fig. 4.5(b).** For D_1 the values of correlation coefficient ranged from 0.980-0.990 in **Fig. 4.5(c)** and for S_1 the values ranged from 0.982-0.987 in **Fig. 4.5(d)** for stage A. However, for stage B, the correlation coefficient values ranged from 0.986-0.996 for F_1 in **Fig. 4.5(a)**, Stage B. Whereas $F_{1.5}$ depicted values from 0.988-0.999 in **Fig. 4.5(b)**, Stage B. D_1 for stage B showed values from 0.956-0.975 as can be observed from in **Fig. 4.5(c)** which can be considered a good fit, however for C40-RH60 and C20-RH80 the values were 0.889 and 0.546 respectively. S_1

showed values ranging from 0.974-0.977 except for C40-RH60 and C20-RH80 showing 0.797 and 0.896 respectively in **Fig. 4.5(d)**, Stage B. For all the models, the higher apparent E_a value of RH100 is due to the presence of pore structures and usually such samples require higher temperatures [21]. All models showed linear regression in the range of 0.95-0.99 except for one-dimensional diffusional reaction model (D_1) that exhibited smaller interdependence between variables (i.e. $R^2 = 0.5$) for C20-RH80 blend in the stage B temperature range. In chemical reaction models, lower Ea values were determined in case of F_1 than $F_{1.5}$. In the case of C100, model F_1 related apparent value of 25.28 kJ/mol for Ea with linear regression of 0.986, and 30.64 kJ/mol for model $F_{1.5}$ with linear regression of 0.988 were attained. On the other hand, RH100 fuel based F_1 model yields E_a of 59.15 kJ/mol with best-fitted regression of 0.991 while $F_{1.5}$ furnishes a higher E_a of 67 kJ/mol with comparatively lower regression of 0.988. In stage A, F_1 model exhibits overall better linear regression with lower E_a as compared to $F_{1.5}$ that yields lesser regression coefficients with higher Ea. On the other hand, in stage B, model $F_{1.5}$ results in better regression coefficients with higher Ea as compared to F_1. In case of D_1, stage A exhibits higher E_a as compared to stage B however, the linear regression of stage A is lower as compared to both F_1 and $F_{1.5}$. Model F_1 shows higher values of pre-exponential factors than $F_{1.5}$ and D_1. For C100, F_1 gives the value of A which is 2.9896 min^{-1} while $F_{1.5}$ gives 10.123 min^{-1} and D_1 gives 34.46 min^{-1}. On the other hand, in the case of RH100, $F_{1.5}$ shows higher value of $1.8 \times 10^5 min^{-1}$ as compared to other models. Model D_1 exhibits much higher Ea in stage A, while phase interfacial reaction mechanism (S_1) shows the least E_a for stage A. **Fig. 4.6** illustrates that in stage B model D_1 shows higher E_a for C80-RH20 and C60-RH40 which decreases with decreasing the coal ratio in the blends. A similar trend can be observed for $F_{1.5}$ which shows higher E_a for C80-RH20 and C60-RH40 and comparatively lower E_a for C40-RH60 and C20-RH80 in stage B. This shows that these two models give higher activation values with blends having increased coal content in stage B. However, for all the models in stage A, blends having higher proportion of coal in the mix show lower Ea. In other words, the proportional increase of RH into C for Stage A caused an increase in the apparent values of activation energy (E_a). Hence, more energy will be required in the co-pyrolysis process of blends based when operated from 200 ºC to 400 ºC. Nevertheless, the

increasing share of RH into C for Stage B proved to be beneficial due to the decreasing values of E_a. It is also indicative that pyrolysis reactions easily initiate in case of higher blending ratios of RH especially for Stage B temperature range (410 ºC-560 ºC). Furthermore, in each model in **Table 4.2** with temperature ranges changing from stage A to stage B, apparent values of E_a decreased indicative of faster reaction rates in the pyrolysis process. This might be due to the additional volatile matter content of RH than Coal. Comparative analysis of the reaction models revealed similar order; D1 > F1 > F1.5 > S1 despite dissimilar values of E_a for C, RH, and their blends. In addition to the studied best-fitted models, other models describing the complex scheme of reactions for co-pyrolysis process of coal and RH blends can equally be used.
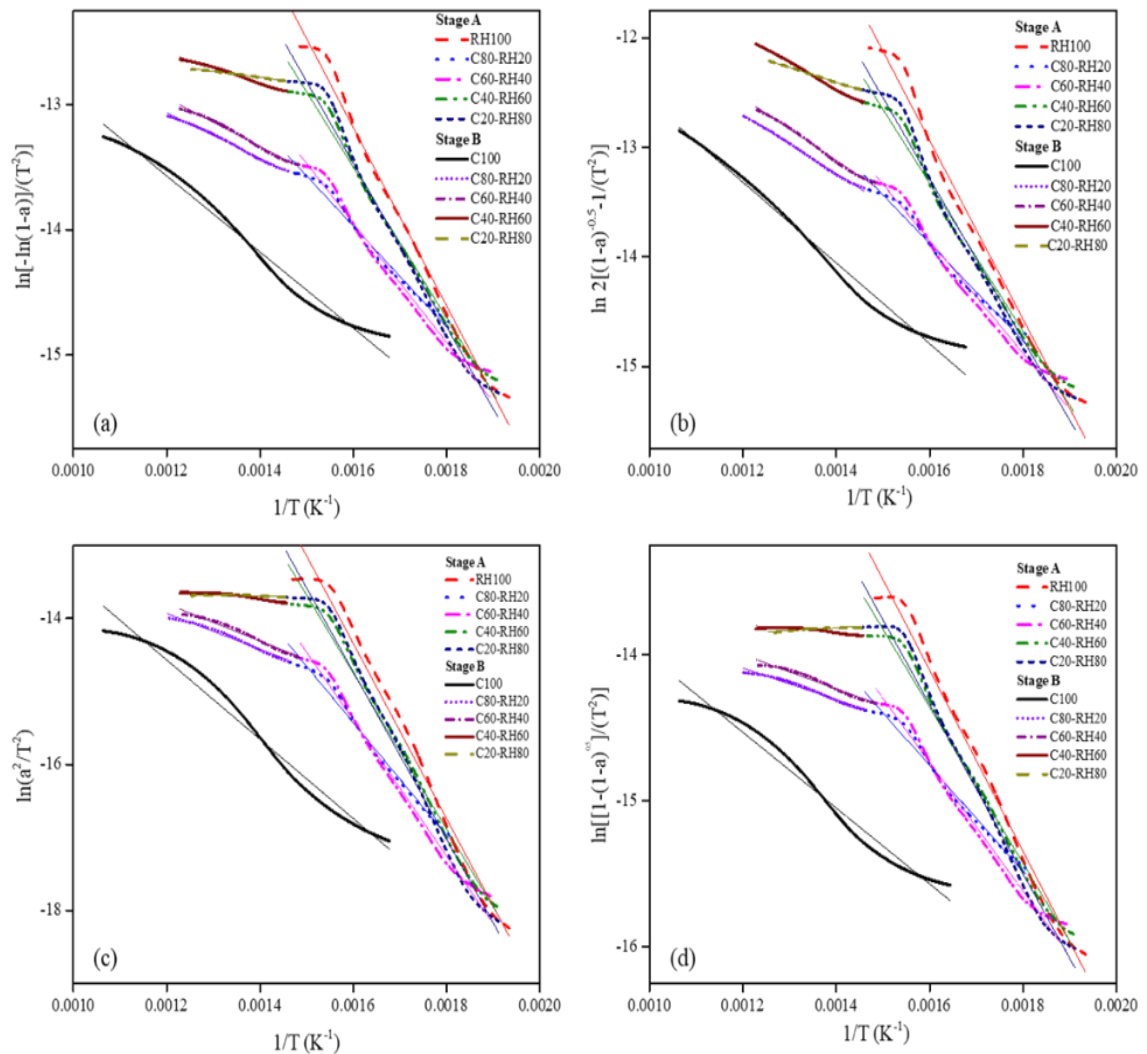
Fig 4.5 Coats Redfern plots representing models (a) F_1, (b) $F_{1.5}$, (c) D_1, (d) S_1
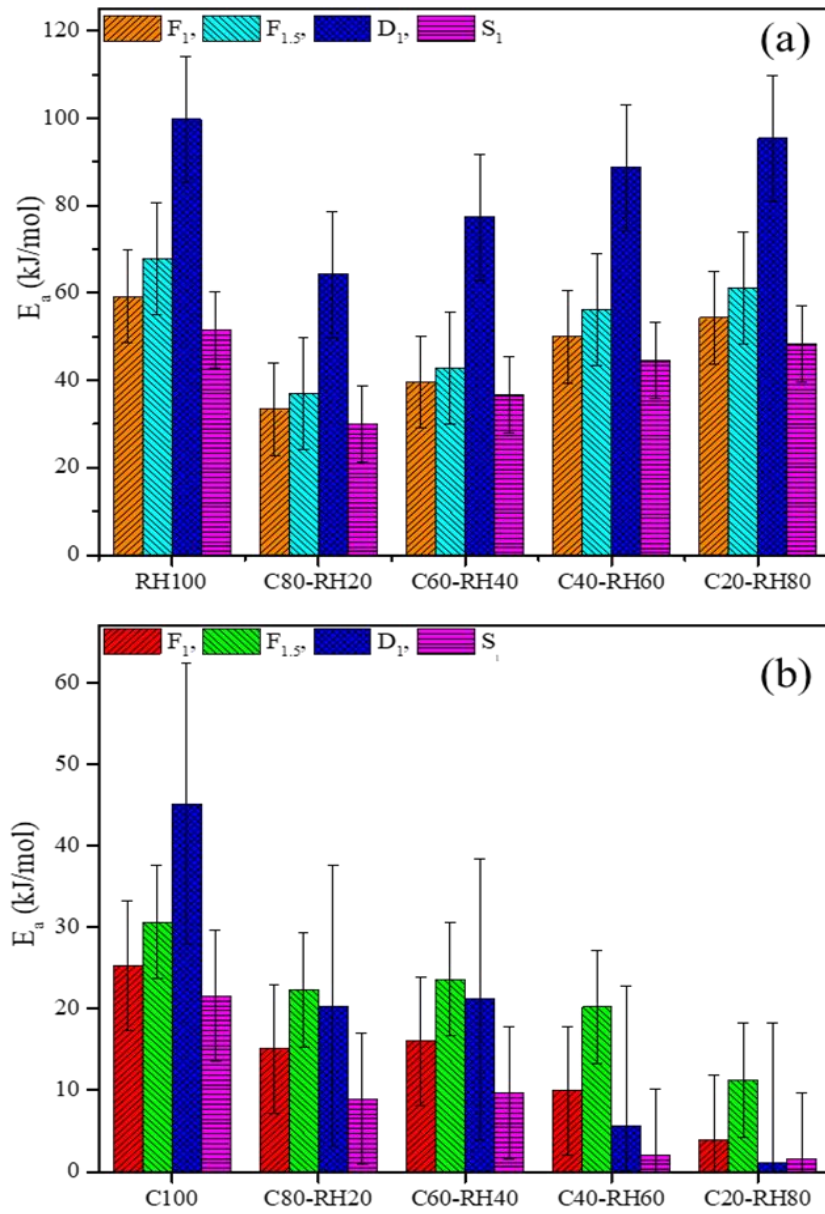
Fig 4.6 Activation energy of blends representing various models and their stages (a) stage A and (b) stage B

Table 4.2 Activation energy values of blends using different models

	STAGE A (main decomposition region)				STAGE B (main decomposition region)			
	Temperature range (°C)	E (kJ/mol)	R^2	A (min^{-1})	Temperature range (°C)	E (kJ/mol)	R^2	A (min^{-1})
F$_1$								
C100	-	-	-	-	323-667	25.28	0.986	2.9896
RH100	244-407	59.15	0.991	2.3×10^4	-	-	-	-
C80RH20	282-412	33.39	0.984	42.47	413-561	15.08	0.996	10.89
C60RH40	255-400	39.6	0.984	170.18	401-541	16.05	0.992	0.9316
C40RH60	251-412	50.03	0.989	2.5×10^3	413-541	9.93	0.993	0.03413
C20RH80	250-414	54.3	0.986	6.4×10^3	415-525	3.97	0.991	0.0524
F$_{1.5}$								
C100	-	-	-	-	323-667	30.64	0.988	10.123
RH100	244-407	67.8	0.988	1.8×10^5	-	-	-	-
C80-RH20	282-412	36.9	0.984	1×10^2	413-561	22.34	0.998	4.128
C60-RH40	255-400	42.78	0.981	3.7×10^2	401-541	23.63	0.996	6.11
C40-RH60	251-412	56.17	0.988	1×10^4	413-541	20.21	0.998	5.63
C20-RH80	250-414	76.77	0.986	3.2×10^4	415-525	11.26	0.999	0.7391
D$_1$								

C100	-	-	-	-	323-667	45.12	0.975	34.46
RH100	244-407	99.72	0.982	3×10^7	-	-	-	-
C80-RH20	282-412	64.22	0.986	7.1×10^3	413-561	20.3	0.981	0.813
C60-RH40	255-400	77.37	0.99	1.1×10^5	401-541	21.15	0.978	1.095
C40-RH60	251-412	88.74	0.984	2.1×10^6	413-541	5.605	0.889	0.0376
C20-RH80	250-414	95.33	0.98	8.5×10^6	415-525	1.079	0.546	3.5×10^{-3}
S_1								
C100	-	-	-	-	323-667	21.58	0.977	0.572
RH100	244-407	51.54	0.987	1.8×10^3	-	-	-	-
C80-RH20	282-412	30.09	0.982	9.245	413-561	8.936	0.979	0.059
C60-RH40	255-400	36.58	0.986	39.97	401-541	9.664	0.974	0.077
C40-RH60	251-412	44.44	0.986	3.2×10^2	413-541	2.11	0.797	7.048
C20-RH80	250-414	48.2	0.983	7.3×10^2	415-525	1.61	0.896	2.9×10^{-3}

4.3 Synergistic effect

The synergistic effect in the blends during pyrolysis is reflected by any positive deviation in calculated and experimental values obtained from TGA of individual fuels [22]. So, to identify the synergistic effect the theoretical data was calculated based on the assumption that all interactions between parent fuels in the blends are an additive function. Synergistic effect is explained in terms of TGA weight loss values (WL) of the blends. The comparison between experimental and calculated values of weight loss (WL) is represented in **Table 4.3**. Calculated values were obtained using Eq. 8. The deviation between experimental and calculated values is obtained using Eq. 9. The results exhibit noticeable differences between actual and calculated data and these deviations give rise to synergistic effect [23]. C80-RH20 and C60-RH40 show positive deviation representing positive synergistic effect, while C40-RH60 and C20-RH80 show slightly negative deviation representing negative synergistic effect though the difference between experimental and calculated data is very less as shown in **Table 4.3**. For C80-RH20 and C60-RH40, the experimental weight loss value is greater than calculated weight loss value which is a major indication of presence of synergistic effect [24, 25]. As experimental WL of C8-RH20 is 48% while calculated WL is 46.7%. Similarly, experimental WL for C60-RH40 is 49.5% while calculated weight loss is around 47%. So, the synergistic effect can be explained in terms of comparison of weight loss values of the blends which corresponds to release of more volatiles. In other studies [24, 26-29] synergistic effect arises due to the transfer of hydrogen radicals or due to existence of alkali and alkaline earth metals (AAEM) depending on type of biomass and its composition. This can be associated with the catalytic or non-catalytic interactions within the fuel blends. The catalytic effect arises due to the presence of various alkali and alkaline earth metals and other inorganic species while the non-catalytic effect arises due to the presence of free radicals and transfer of hydrogen from biomass [30]. The interaction between volatiles and char components as well as the interference of alkali and alkaline earth metals present in RH give rise to a synergistic effect. Moreover, the heat transfer reactions and hydrogen transfer reactions with catalytic effects of metal transfer also impacts the synergistic properties [31]. Additionally, the porous structure of char formed after devolatilization in co-pyrolysis may also lead to synergistic effect by

increasing the volatile emissions and consequently increasing the weight loss [32]. In this study, the negative synergistic effect is observed for blending at higher biomass blending ratios of C40-RH60 and C20-RH80 though the deviation is very small. This may arise due to the reason that at higher biomass blending the particles of RH and C do not completely fill into each other's interspaces [33, 34].Various other studies have also reported negative synergistic effect at higher biomass blending ratios [33, 35, 36].

Table 4.3 Deviation in experimental and calculated weight loss (WL) of blends

Sample	Experimental WL (%)	Calculated WL (%)	Deviation WL (%)
C80-RH20	48	46.7	0.027
C60-RH40	49.51	47.4	0.041
C40-RH60	56	57.0	-0.017
C20-RH80	60	61.1	-0.018

4.4 Thermodynamic analysis

The calculated thermodynamic parameters ΔH, ΔG and ΔS are illustrated in **Table 4.4.** The enthalpy change represents heat absorbed or released while keeping the pressure constant [37]. Gibbs free energy exhibits the increase in energy in the development of activated complex [38]. It can be observed from Table 4.4 that all of the models depicted positive ΔH values except in some cases for the stage B. The positive values of ΔH show that an external energy source is required to provide energy for molecules at a higher energy level to their state of transition [39]. Increased value of ΔH shows that a longer time is also required for the conversion, so high values of ΔH may change the primary reaction mechanism in co-pyrolysis [40]. In stage A and stage B of all the models, ΔH increased as activation energy increased. Among all models, ΔG values in stage B are slightly higher than in stage A, this can be interpreted to establish the disorder and changes in heat flow [41]. In all the models, ΔS exhibited negative values in both stages as shown in **Table 4.4.** This trend clearly shows that disorder which occurred in products due to bond breakage was lower as compared to the primary reactants [19]. These negative values depict organized structure of breakdown [42]

Table 4.4 Thermodynamic parameters of Coal-RH blends at various reaction models

	STAGE A (main decomposition region)				STAGE B (main decomposition region)			
	Temperature range (°C)	ΔH (kJ/mol)	ΔG (kJ/mol)	ΔS(kJ/mol)	Temperature range (°C)	ΔH (kJ/mol)	ΔG (kJ/mol)	ΔS (kJ/mol)
F_1								
C100	-	-	-	-	323-667	19.2015	527.9	-0.695
RH100	244-407	53.89	445.7	-0.62	-	-	-	-
C80-RH20	282-412	28.1	455.47	-0.672	413-561	9.06	521.41	-0.708
C60-RH40	255-400	34.32	453.5	-0.661	401-541	10.04	519.2	-0.705
C40-RH60	251-412	44.76	499.19	-0.638	413-541	3.93	523	-0.732
C20-RH80	250-414	49.02	460.4	-0.648	415-525	-1.963	518.3	-0.82
$F_{1.5}$								
C100	-	-	-	-	323-667	24.56	525.9	-0.685
RH100	244-407	62.54	443.5	-0.603	-	-	-	-
C80-RH20	282-412	31.61	454.3	-0.665	413-561	16.32	517.78	-0.693
C60-RH40	255-400	37.5	452.6	-0.654	401-541	17.62	515.58	-0.689

|								
C40-RH60	251-412	50.9	448	-0.627	413-541	14.21	512.18	-0.69
C20-RH80	250-414	71.49	462.9	-0.617	415-525	5.32	510.09	-0.796
D_1								
C100	-	-	-	-	323-667	39.04	532.94	-0.675
RH100	244-407	94.46	448.6	-0.56	-	-	-	-
C80-RH20	282-412	58.93	459.19	-0.629	413-561	14.28	525.5	-0.706
C60-RH40	255-400	72.09	457.2	-0.607	401-541	15.14	523.4	-0.704
C40-RH60	251-412	83.47	452.4	-0.582	413-541	-0.39	527.6	-0.732
C20-RH80	250-414	90.059	452.1	-0.571	415-525	-4.854	531.6	-0.846
S_1								
C100	-	-	-	-	323-667	15.5	512.7	-0.709
RH100	244-407	46.28	451.5	-0.641	-	-	-	-
C80-RH20	282-412	24.81	460.2	-0.685	413-561	2.92	529.9	-0.728
C60-RH40	255-400	31.3	458.21	-0.673	401-541	3.66	527.8	-0.726
C40-RH60	251-412	39.17	454.4	-0.655	413-541	-3.88	492.7	-0.688
C20-RH80	250-414	42.92	454.3	-0.648	415-525	-4.32	499.2	-0.794

4.5 Product analysis of co-pyrolysis

C80-RH20 and C60-RH40 were selected for co-pyrolysis in a fixed bed reactor due to the presence of a positive synergistic effect. Moreover, these two blends showed comparatively lower activation energies and higher calorific values as discussed above. The pyrolytic reactions controlled at a temperature of 500 °C produced biochar yields of 60% and 55% for C80-RH20 and C60-RH40 blends. The increase in the share of biomass decreased the char yield of the blends. These SEM micrographs in **Fig. 4.7(a-d)** exhibited honeycomb-like porous structure for C80-RH20 blend, whereas flake structure were detected in the biochar of C60-RH40 blend. SEM analyses indicate that the evaporation of volatile compounds increases the porosity and appearance of voids in the structure as expected with increasing surface area, pore volume and micropore ratio. Coal structure consists of aromatic hydrocarbons which are relatively dense having bond energies of 1000 kJ/mol. In C80-RH20 the synergy may occur due to various depolymerization, and decomposition reactions especially transfer of H_2 from RH to coal as discussed above. Heat transfer and chemical reactions also play a vital role in synergistic effects [43] especially when diverse magnitudes of holes have been observed. The pore structure facilitates the reaction and diffusion of various products and also serves as the major adsorption surface for various chemical reactions [44]. Characteristics and growth of pore structure is affected by blending ratio, pyrolysis temperature and feedstock used. Many studies have shown that a synergistic effect was observed in co-pyrolysis char due to the presence of alkali and alkaline earth metal (AAEM) species, mainly K and Ca [45]. Moreover, SEM analysis of C80-RH20 biochar confirms honey-comb shaped morphology with number of pores which shows the rapid release of volatiles from RH. SEM of C60-RH40 also shows the presence of pores which correspond to volatile release. A clear porous structure is observed which is in accordance to releasing volatiles and thus synergistic effect is confirmed [24].

EDS analysis of C80-RH20 in **Fig.4.8(a)** shows that biochar comprises of carbon (C), oxygen (O), silicon (Si), and potassium (K). It is observed that on increasing the biomass blending ratio, alkali, and alkaline earth metals increase. Potassium is

transferred from biomass to coal char so this indicates that mixing of coal and RH is beneficial and co-pyrolysis facilitates the activation of K [46]. C60-RH40 blend based biochar shown in **Fig.4.8(b)** comprising of elements of carbon (C), oxygen(O), silicon (Si), potassium (K), calcium (Ca), magnesium (Mg) depicts an increase in the catalytically active AAEM species in co-pyrolysis char [47]. The blending of coal with RH is advantageous for the release of catalytic species including K, Mg, Ca, and Si. These specific biochar exhibit additional favorable results in terms of catalytic species and suitability in future applications as well. The SEM-EDS analysis shows that the produced co-pyrolysis biochar has potential for several applications where it can be applied as an adsorbent, storage medium for carbon and hydrogen, catalyst for biodiesel production, to improve soil quality, as a habitat for microorganisms and can also work as a semiconductor [48].

TGA analysis of co-pyrolysis chars, was also performed as shown in **Fig 4.8(c).** Biochar after co-pyrolysis shows less weight loss than their actual blends and hence show stability. The comparative analysis of the chemical structure of biochars exhibited a decrease in the amorphous carbon structure with an increase of coal mass fraction in C80-RH20 blend [46]. The most dominant peak at a wavenumber of 3542 cm^{-1} signifies the O-H bond stretching. Peak observed at a wavenumber of 1614 cm^{-1} indicates C=C stretching, whereas 1170-1130 cm^{-1} wavelength range represent ester based C-O stretching. FTIR spectra of biochar from C60-RH40 shows that increased content of biomass increased amorphous structure [49]. The observed two peaks represent O-H bond stretching for 3500-3300 cm^{-1} and C-O bond stretching for 1200-1000 cm^{-1}. Co-pyrolysis char from C60RH40 includes less significant aromatic ring structures as compared to C80RH20 [50].
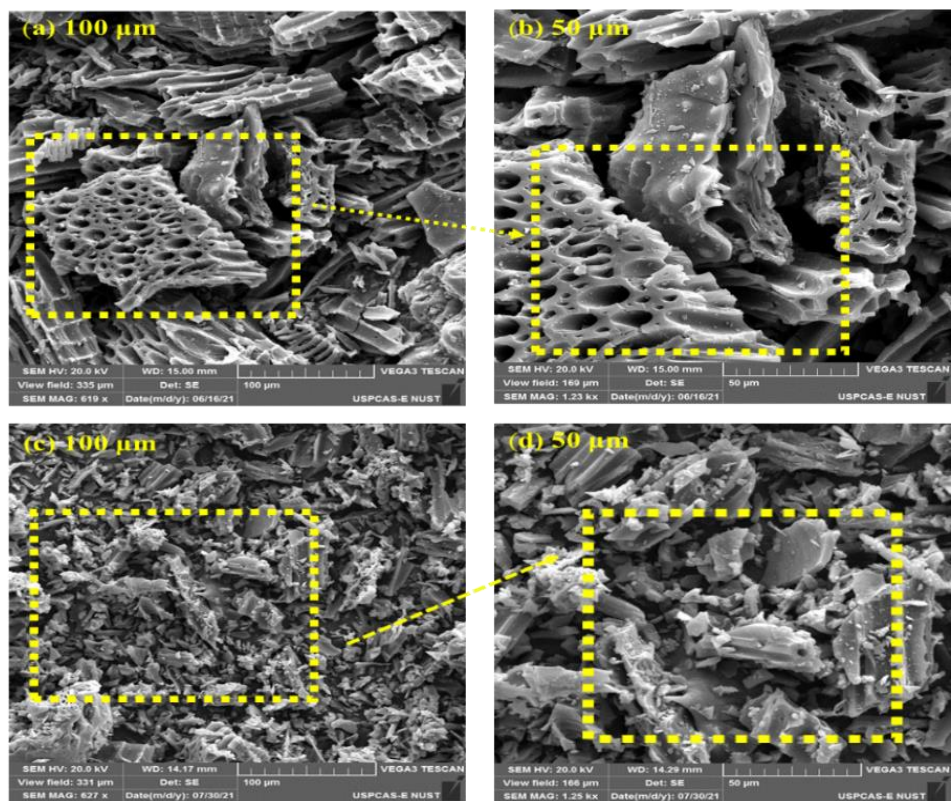
**Fig 4.7** SEM images of biochar from C80-RH20 (a-b) and C60-RH40 (c-d)
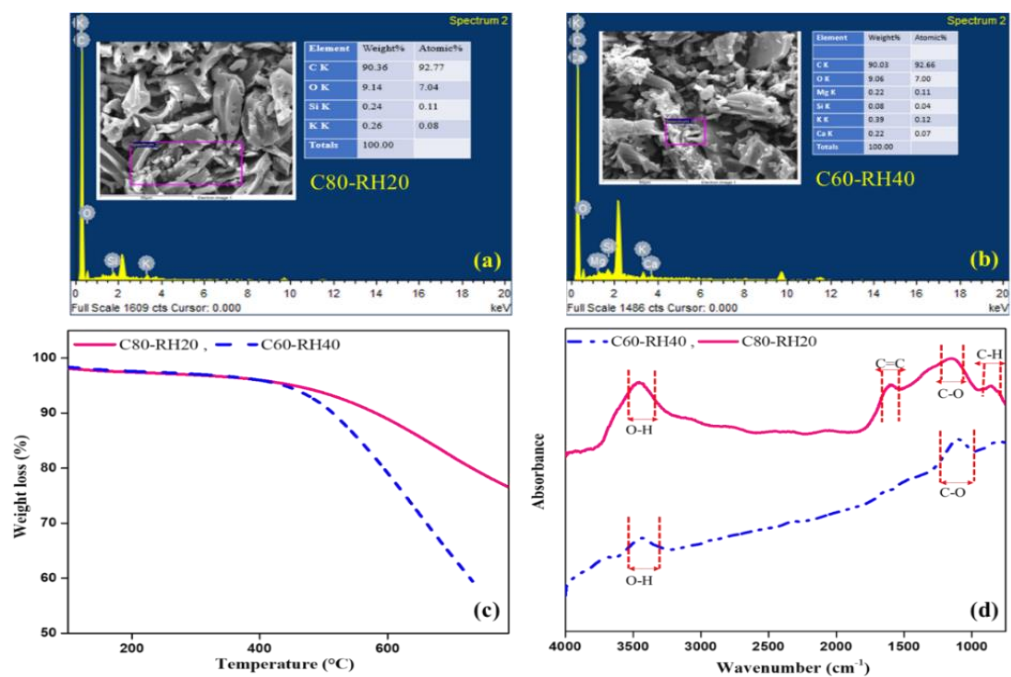
Fig 4.8 Characteristics of biochar produced from (a) C80-RH20 and (b) C60-RH40 via EDS analysis and their (c) TGA and (d) FTIR analysis

The chemical composition of the liquid product obtained at 500 °C for both C80-RH20 and C60-RH40 was analyzed by GC-MS. The peaks presented by chromatogram were interpreted using NIST search software. The analysis conducted determines that bio-oil is composed of acids, phenols, alcohols, furans, amines and esters. The composition of both samples of bio-oil was different because of the blending ratios as shown in Fig. 4.9. In the case of C80-RH20 blend, 15% bio-oil whereas, 20% from C80-RH20 blend was obtained. Major compounds identified in bio-oil obtained from C80-RH20 were phenols (22%) and acids (11%), similarly, phenols (23%) and acids (11%) were also present in the bio-oil from C60-RH40 blend. Other compounds identified in C80-RH20 were esters (3.1%), furans (0.14%) and amines (1%). While, in C60-RH40 the bio-oil also consisted of esters (3%), furans (0.3%), amines (0.5%) and alcohols (0.33%). The analysis shows that different types and amounts of fatty acids and esters were formed by the interaction of coal and RH. RH contains oxygenated compounds that mainly comprise phenols, furans and acids having more than two oxygen-containing functional groups [51]. It has been reported that liquid products majorly from pyrolysis of RH consisted of phenols, organic acids and ketones [52]. Another report revealed that compounds detected by GC-MS from pyrolysis of rice husk were classified into ketones, aldehydes, phenols, alcohols, esters, furans and acids [51]. C60-RH40 exhibited higher amounts of phenols, alcohols and furans than C80-RH20 because C60-RH40 has higher share of RH in it as compared to C80-RH20, and biomass pyrolysis oils have higher concentration of phenols, acids, alcohols as compared to coal pyrolysis oil evident from other studies [53, 54]. It has already been reported in literature that blending of biomass with coal increases the calorific value of co-pyrolytic oils as compared to non-co-pyrolytic oils as coal has higher GCV than biomass [55]. RH100 also has higher hydrogen (4.7%) than coal (3.5%) as discussed above in CHN analysis and FTIR analysis where hydroxyl (-OH) groups in RH are abundant as compared to coal. This is also a reason of higher concentration of phenols in biomass pyrolysis as compared to coal pyrolysis and consequently the blend having higher biomass share will depict higher concentrations of phenols and acids. **Fig. 4.10** shows the retention time with respect to intensity of various chemical compounds identified through GC-MS**. Fig. 4.10(a-b)** represent spectra of C80-RH20 and C60-RH40 respectively. The major

absorption peaks are represented in the spectra with their chemical structures. **Table 4.5** lists the compounds present in bio-oils according to the relative peak number.
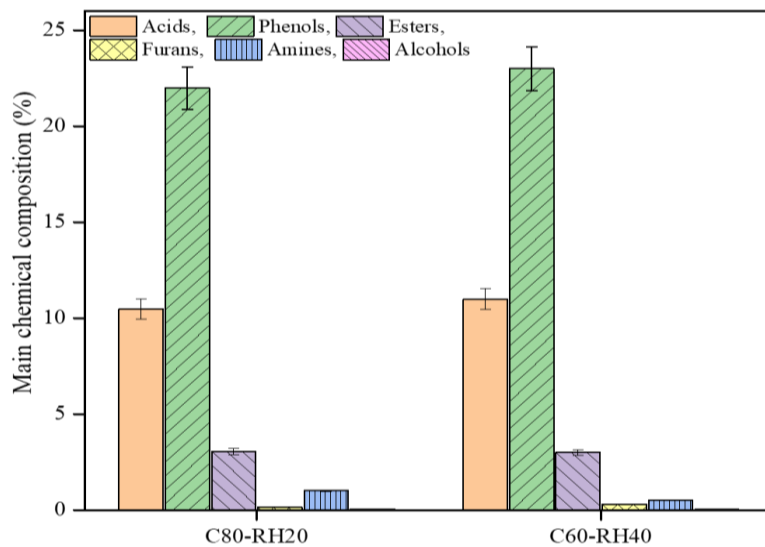
**Fig 4.9** Composition analysis of bio-oils from C80-RH20 and C60-RH40
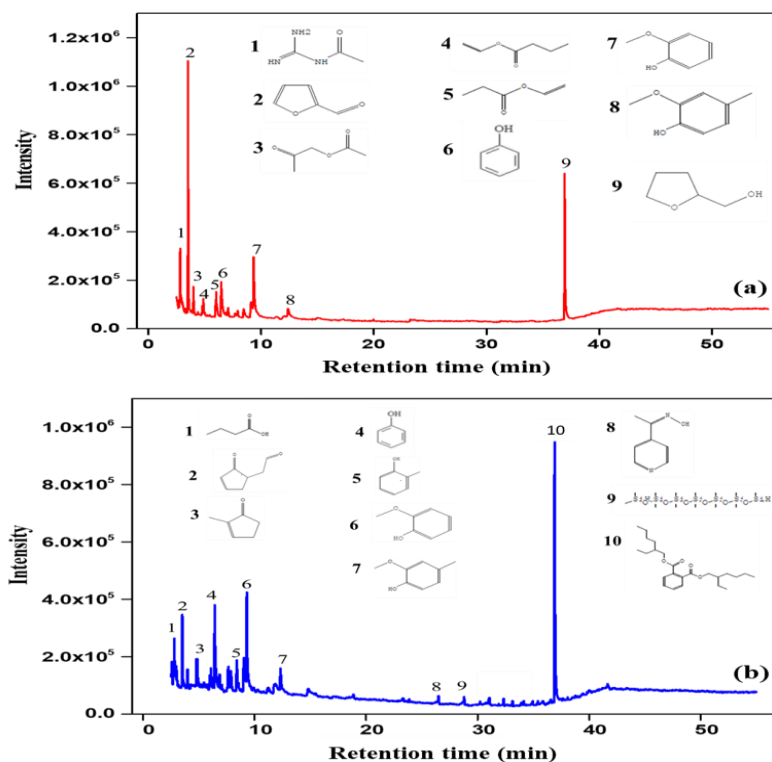
Fig 4.10 GC-MS chromatograms of (a) C80-RH20 bio-oil (b) C60-RH40 bio-oil

94

Table 4. 5 Chemical compounds identified at various peaks in C80-RH20 bio-oil and C60-RH40 bio-oil

Peak Number	Compounds identified in C80-RH20 bio-oil	Compounds identified in C60RH40 bio-oil
1	Acetamide, N-(aminoiminomethyl)	Butanoic acid
2	Furfural	3-Cyclopentene-1-acetaldehyde, 2-oxo
3	2-Propanone, 1-(acetyloxy)	2-Cyclopenten-1-one,2 methyl
4	Vinyl butyrate	Phenol
5	Propanoic acid, ethenyl ester	Phenol, 2-methyl-
6	Phenol	Phenol, 2-methoxy-
7	Phenol, 2-methoxy-	Creosol
8	Creosol	Ethanone,1-(4-pyridinyl)-, oxime
9	2-Furanmethanol, tetrahydro-	Heptasiloxane,1,1,3,3,5,5,7, 7,9,9,11,11,13,13-tetradecamethyl
10	-	Bis(2-ethylhexyl) phthalate

The gaseous product analysis of C80-RH20 and C60-RH40 was carried out using a GC-TCD analyzer. The temperature of the fixed bed reactor was kept at 500 °C (Stage B range) in an inert atmosphere for pyrolysis for Cycle 1 (2 h) with product analysis presented in **Fig. 4.11(a).** After 2 h, co-gasification was enabled, referred to as Cycle 2. It can be observed that produced gases were composed of H_2, CO_2, CH_4. Major constituents of gaseous fraction were H_2, CO_2 and CH_4. These experimental results depict that production of gases is greatly influenced by the mixing ratio of blend. The release of CO_2 during initial pyrolysis mainly occurred due to decarboxylation reactions of hemicellulose and other components like fats, lignin, phenols and other inorganics present in biomass [56]. In the case of C80-RH20, Cycle 1 exhibited CH_4 as the major gas with 13% production and H_2 as the minor gas with 1% production. In addition to cited measurements 5% production of CO_2 and 6-7% production of CO was also achieved during co-pyrolysis. However, when co-gasification is enabled in Cycle 2, methane production drastically decreased (from 13% to 4%) and hydrogen production significantly increased to 15%. Production of CO_2 decreased from 4% to 1% whereas CO production increased to 11%. The products yield also get influenced by the content of ash, depending upon the mineral composition of each blend [57]. However, when co-gasification is enabled in Cycle 2, CH_4 production drastically decreased (from 12% to 5%) and H_2 production increased to 15%. Production of CO_2 also reduced from 5% to 1%, whereas CO yield increased indicative of the progression of reverse water gas shift reaction. According to studies presented in literature it was observed that during co-pyrolysis of peat (PT) and pine branch (PB) the blends having less biomass share (3PT:1PB) reported 9% CO and that having higher biomass ratio (1PT:3PB) depicted considerably less amount of CO (7%). CO_2 was reported to be 40% in 3PT:1PB and 36% in 1PT:3PB. Similarly for 3PT:1PB, 19% CH_4 was observed and for 1PT:3PB 22% CH_4 was observed [58]. This shows that increasing biomass share in blend decreased the amount of CO and CO_2 while increased CH_4. The results presented in this study are also in accordance with the fact that in blend having higher biomass ratio (C60-RH40), the production of CO and CO_2 decreased as compared to blend having lesser biomass ratio (C80-RH20). The gaseous production of H_2 also increased in C60-RH40 as compared to

C80-RH20 due to greater concentration of hydrogen in RH evident from CHN and FTIR analysis. In case of C60-RH40, **Fig. 4.11(b),** Cycle 1 represented CH_4 yield of 11% with H_2 yield noted at 2%. CO_2 and CO yields were around 4% and 6% respectively. The Cycle 2 exhibited higher amount of H_2 (17%) while CH_4 yield significantly decreased. It is also observed that production of CO_2 (2%) decreased in co-gasification as compared to co-pyrolysis while CO increased to 9%. On comparing C80-RH20 and C60-RH40, C60-RH40 blend resulted in higher amount of H_2 (17%) produced due to larger share of biomass in the blend, as RH has greater hydrogen content. These results indicated that H_2 yield increases as CH_4 production decreases and blending also helps in the reduction of CO_2 emissions. The H_2/CO >1 for both blends is encouraging as higher H_2 is beneficial for downstream conversion to various chemicals. It is imperative that further future research is carried out to fully exploit these by-products for other commercial-level applications. **Table 4.6** shows a brief discussion some of the previous research conducted on co-pyrolysis of coal and biomass blends
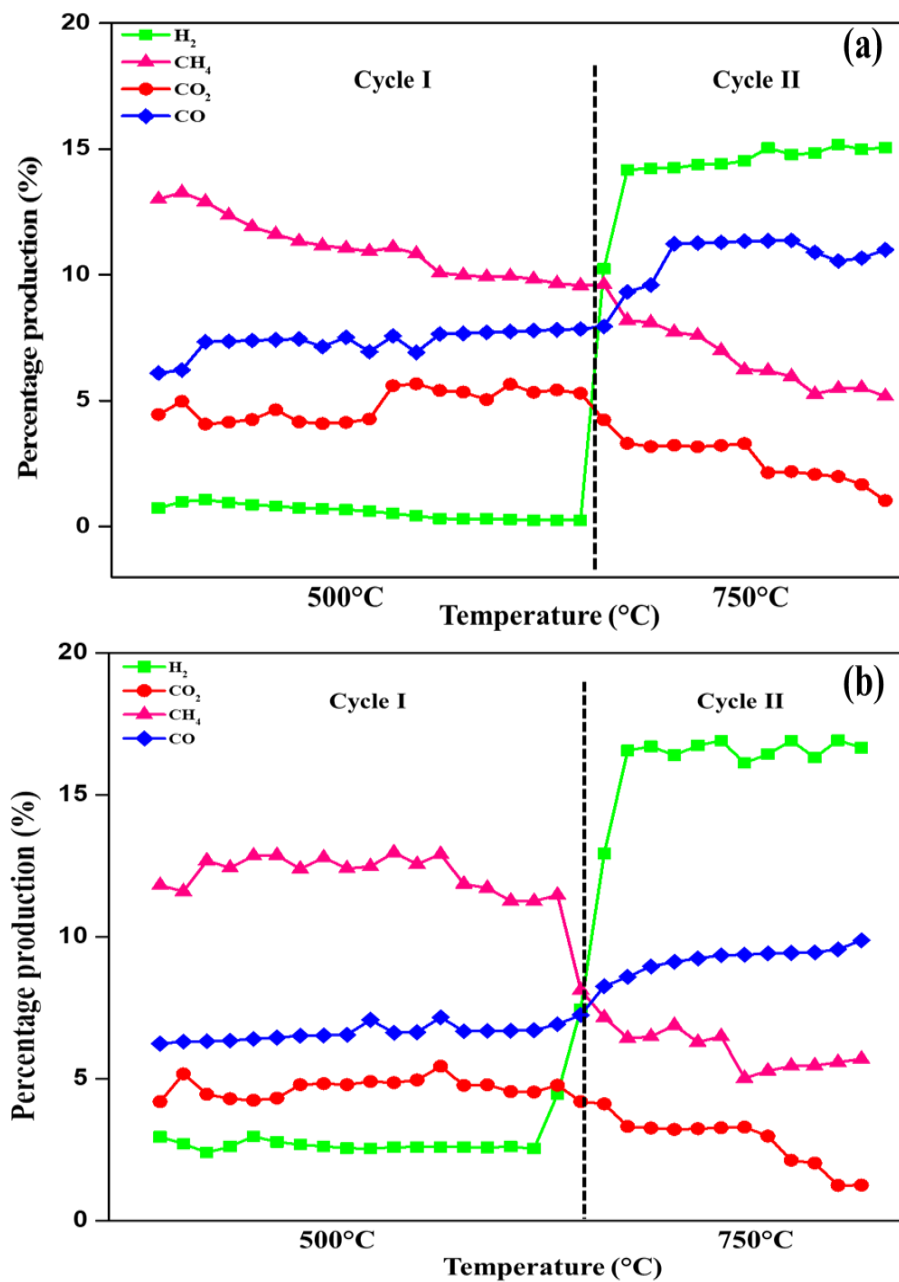
Fig 4.11 Product analysis from (a) C80-RH20 and (b) C60-RH40. (Cycle I: co-pyrolysis, Cycle II: co-gasification)

Table 4. 6 Summary of some literature on co-pyrolysis of coal-biomass blends

Coal/biomass type	Blending ratios (Coal: biomass)	Heating rate	Remarks	Ref
Lignite/rice husk	95:5 90:10 85:15 80:20 70:30	5°C/min	Gas and water yields were higher because of combination of hydrogen free radicals. RH produced more hydrogen and thus more methane was produced from RH as compared to coal. AAEM species in RH promoted transfer of hydrogen and also increased secondary tar cracking.	[59]
Lignite/rice husk	1:1	10°C/min	Fixed bed reactor was employed to pyrolyze rice husk, coal and their blend. Results depicted significant synergy during co-pyrolysis. Addition of RH increased gas yield and facilitated gasification of char.	[60]
Indonesian(sub-bituminous) coal/rice straw (RS)	1:0 3:1 1:1 1:3 0:1	33°C/s for steam gasification	Synergy was observed in the blending ratio of 1:1. It was due to transfer of H and OH radicals and presence of AAEM (specially potassium) from rice straw (RS). Steam gasification produced highly reactive char.	[36]

Shenfu bituminous coal/ rice straw (RS)	1:4 1:1 4:1 *(by mass ratios)	N/A	Synergy was observed at blending ratio of (RS/SB= 1:4) indicating higher volatile yield. It was also observed that increase in ration of RS in the blend decreased the synergy as well as reduced gasification rates.	[33]
Shenfu bituminous coal/ rice straw (RS)	100:0 25:75 50:50 75:25 0:100	N/A	Rice straw was torrefied which increased its C/H and C/O ratio. Very slight synergistic effect was observed in the blends. The secondary pyrolysis of coal after 700°C was prevented on addition of biomass	[61]
Peat (PT) /pine branch (PB)	1:3 3:1 1:1	5, 10, 20, 40, 80 °C/min	A slightly weak interaction was observed between both feedstocks in terms of volatile release. Activation energies were considerably higher with higher linear correlation	[58]
Sub-bituminous coal (SB) /pine saw dust (SD)	50:50	25°C/min	TGA weight loss behaviours of coal and biomass show three stages of devolatilization in TGA. Coats-Redfern method was used for determination of kinetic and thermodynamic parameters of blends	[62]

Summary

This chapter describes the results and discussions about the co-pyrolysis of coal and rice husk blends in detail. The effect of blending on chemical properties of blends was discussed. Blends having lower RH blending ratios depicted higher calorific values. Thermogravimetric behaviour of blends was studied which revealed the weight loss behavior, degradation temperatures, percent residue of the blends at heating rate of 20°C/min. Blends with higher RH percentage (C20-RH80) and (C40-RH60) showed greater weight loss and higher reactivity. Kinetic parameters were calculated using F_1, $F_{1.5}$, D_1 and S_1 models. C80-RH20 showed lowest activation energy among all other blends, and it was revealed that the activation energies increased on increasing the RH blending. Thermodynamic analysis showed that all of the models depicted positive ΔH values except in some cases for the stage B. ΔS values were negative for all the blends among all models. positive synergistic effect was observed in C80-RH20 and C60-RH40. These two blends also depicted higher calorific values and lower activation energies. C80-RH20 and C60-RH40 were then pyrolyzed in a fixed bed reactor at temperature of 500°C, and after two hours steam was introduced through the HPLC pump for co-gasification. Characterization of the produced products revealed a honey-comb like bio-char structure through SEM analysis which could be further used as an adsorbent, storage, and other applications. EDS analysis depicted presence of many catalytic active species which enabled the usage of biochar as a catalyst with little upgradation. TGA and FTIR analysis was performed to investigate the weight loss behavior and changes in chemical composition after co-pyrolysis. Bio-char was analyzed through GC-MS which exhibited yields of phenols (23%), acids (11%), and methoxy phenols for the C60-RH40 fuel blend. Product gas analysis showed that the product gas composition of 2% H_2, 14% CH_4, and 4% CO_2 for the C80-RH20 blend increased to 3% H_2, 12% CH_4, and 5% CO_2 for the C60-RH40 fuel blend. The co-gasification process substantially increased the production of H_2 up to 14%-17% when compared to co-pyrolysis results.

References

1] S.V. Vassilev, D. Baxter, L.K. Andersen, C.G. Vassileva, An overview of the chemical composition of biomass, Fuel, 89 (2010) 913-933.

[2] S.U. Patel, B. Jeevan Kumar, Y.P. Badhe, B.K. Sharma, S. Saha, S. Biswas, A. Chaudhury, S.S. Tambe, B.D. Kulkarni, Estimation of gross calorific value of coals using artificial neural networks, Fuel, 86 (2007) 334-344.

[3] G. Wang, J. Zhang, J. Shao, Z. Liu, G. Zhang, T. Xu, J. Guo, H. Wang, R. Xu, H. Lin, Thermal behavior and kinetic analysis of co-combustion of waste biomass/low rank coal blends, Energy Conversion and Management, 124 (2016) 414-426.

[4] R.K. Mishra, K. Mohanty, Characterization of non-edible lignocellulosic biomass in terms of their candidacy towards alternative renewable fuels, Biomass Conversion and Biorefinery, 8 (2018) 799-812.

[5] X. Chen, L. Liu, L. Zhang, Y. Zhao, P. Qiu, Pyrolysis characteristics and kinetics of coal–biomass blends during co-pyrolysis, Energy & Fuels, 33 (2019) 1267-1278.

[6] D. Chen, J. Zhou, Q. Zhang, Effects of torrefaction on the pyrolysis behavior and bio-oil properties of rice husk by using TG-FTIR and Py-GC/MS, Energy & Fuels, 28 (2014) 5857-5863.

[7] S.B. Daffalla, H. Mukhtar, M.S. Shaharun, Preparation and characterization of rice husk adsorbents for phenol removal from aqueous systems, PloS one, 15 (2020) e0243540.

[8] W.-H. Chen, J.-S. Wu, An evaluation on rice husks and pulverized coal blends using a drop tube furnace and a thermogravimetric analyzer for application to a blast furnace, Energy, 34 (2009) 1458-1466.

[9] D. Vamvuka, E. Kakaras, E. Kastanaki, P. Grammelis, Pyrolysis characteristics and kinetics of biomass residuals mixtures with lignite☆, Fuel, 82 (2003) 1949-1960.

[10] A. Blazej, M. Kosik, Phytomass, England: Ellis Horwood, (1993).

[11] K.L. Smith, L.D. Smoot, T.H. Fletcher, R.J. Pugmire, The structure and reaction processes of coal, Springer Science & Business Media1994.

[12] S. Munir, S.S. Daood, W. Nimmo, A.M. Cunliffe, B.M. Gibbs, Thermal analysis and devolatilization kinetics of cotton stalk, sugar cane bagasse and shea meal under nitrogen and air atmospheres, Bioresource Technology, 100 (2009) 1413-1418.

[13] X. Chen, L. Liu, L. Zhang, Y. Zhao, Z. Zhang, X. Xie, P. Qiu, G. Chen, J. Pei, Thermogravimetric analysis and kinetics of the co-pyrolysis of coal blends with corn stalks, Thermochimica Acta, 659 (2018) 59-65.

[14] G. Zheng, J.A. Koziński, Thermal events occurring during the combustion of biomass residue, Fuel, 79 (2000) 181-192.

[15] Y. Hu, S. Naito, N. Kobayashi, M. Hasatani, CO2, NOx and SO2 emissions from the combustion of coal with high oxygen concentration gases, Fuel, 79 (2000) 1925-1932.

[16] A.K. Sadhukhan, P. Gupta, T. Goyal, R.K. Saha, Modelling of pyrolysis of coal–biomass blends using thermogravimetric analysis, Bioresource Technology, 99 (2008) 8022-8026.

[17] Z.B. Laougé, H. Merdun, Investigation of thermal behavior of pine sawdust and coal during co-pyrolysis and co-combustion, Energy, 231 (2021) 120895.

[18] A. Saddawi, J. Jones, A. Williams, M. Wojtowicz, Kinetics of the thermal decomposition of biomass, Energy & fuels, 24 (2010) 1274-1282.

[19] A.A.D. Maia, L.C. de Morais, Kinetic parameters of red pepper waste as biomass to solid biofuel, Bioresource Technology, 204 (2016) 157-163.

[20] H. Merdun, Z.B. Laougé, Kinetic and thermodynamic analyses during co-pyrolysis of greenhouse wastes and coal by TGA, Renewable Energy, 163 (2021) 453-464.

[21] I. Mian, X. Li, Y. Jian, O.D. Dacres, M. Zhong, J. Liu, F. Ma, N. Rahman, Kinetic study of biomass pellet pyrolysis by using distributed activation energy model and Coats Redfern methods and their comparison, Bioresource Technology, 294 (2019) 122099.

[22] T. Wu, M. Gong, E. Lester, P. Hall, Characteristics and synergistic effects of co-firing of coal and carbonaceous wastes, Fuel, 104 (2013) 194-200.

[23] J. Oladejo, S. Adegbite, X. Gao, H. Liu, T. Wu, Catalytic and non-catalytic synergistic effects and their individual contributions to improved combustion performance of coal/biomass blends, Applied Energy, 211 (2018) 334-345.

[24] Z. Wu, S. Wang, J. Zhao, L. Chen, H. Meng, Thermochemical behavior and char morphology analysis of blended bituminous coal and lignocellulosic biomass model

compound co-pyrolysis: Effects of cellulose and carboxymethylcellulose sodium, Fuel, 171 (2016) 65-73.

[25] K.-M. Lu, W.-J. Lee, W.-H. Chen, T.-C. Lin, Thermogravimetric analysis and kinetics of co-pyrolysis of raw/torrefied wood and coal blends, Applied Energy, 105 (2013) 57-65.

[26] R.M. Soncini, N.C. Means, N.T. Weiland, Co-pyrolysis of low rank coals and biomass: Product distributions, Fuel, 112 (2013) 74-82.

[27] H.M. Jeong, M.W. Seo, S.M. Jeong, B.K. Na, S.J. Yoon, J.G. Lee, W.J. Lee, Pyrolysis kinetics of coking coal mixed with biomass under non-isothermal and isothermal conditions, Bioresource Technology, 155 (2014) 442-445.

[28] N. Ellis, M.S. Masnadi, D.G. Roberts, M.A. Kochanek, A.Y. Ilyushechkin, Mineral matter interactions during co-pyrolysis of coal and biomass and their impact on intrinsic char co-gasification reactivity, Chemical Engineering Journal, 279 (2015) 402-408.

[29] S. Li, X. Chen, A. Liu, L. Wang, G. Yu, Co-pyrolysis characteristic of biomass and bituminous coal, Bioresource Technology, 179 (2015) 414-420.

[30] A.H. Tchapda, S.V. Pisupati, A review of thermal co-conversion of coal and biomass/waste, Energies, 7 (2014) 1098-1148.

[31] X. Chen, L. Liu, L. Zhang, Y. Zhao, P. Qiu, R. Ruan, A review on the properties of copyrolysis char from coal blended with biomass, Energy & Fuels, 34 (2020) 3996-4005.

[32] T. Abbas, P. Costen, N.H. Kandamby, F.C. Lockwood, J.J. Ou, The influence of burner injection mode on pulverized coal and biomass co-fired flames, Combustion and Flame, 99 (1994) 617-625.

[33] S. Yuan, Z.-h. Dai, Z.-j. Zhou, X.-l. Chen, G.-s. Yu, F.-c. Wang, Rapid co-pyrolysis of rice straw and a bituminous coal in a high-frequency furnace and gasification of the residual char, Bioresource Technology, 109 (2012) 188-197.

[34] D.K. Park, S.D. Kim, S.H. Lee, J.G. Lee, Co-pyrolysis characteristics of sawdust and coal blend in TGA and a fixed bed reactor, Bioresource Technology, 101 (2010) 6151-6156.

[35] N. Howaniec, A. Smoliński, K. Stańczyk, M. Pichlak, Steam co-gasification of coal and biomass derived chars with synergy effect as an innovative way of hydrogen-rich gas production, International journal of hydrogen energy, 36 (2011) 14455-14463.

[36] S. Krerkkaiwan, C. Fushimi, A. Tsutsumi, P. Kuchonthara, Synergetic effect during co-pyrolysis/gasification of biomass and sub-bituminous coal, Fuel processing technology, 115 (2013) 11-18.

[37] H. Li, S.-l. Niu, C.-m. Lu, S.-q. Cheng, Comparative evaluation of thermal degradation for biodiesels derived from various feedstocks through transesterification, Energy Conversion and Management, 98 (2015) 81-88.

[38] S.C. Turmanova, S. Genieva, A. Dimitrova, L. Vlaev, Non-isothermal degradation kinetics of filled with rise husk ash polypropene composites, Express Polymer Letters, 2 (2008) 133-146.

[39] L. Huang, J. Liu, Y. He, S. Sun, J. Chen, J. Sun, K. Chang, J. Kuo, X.a. Ning, Thermodynamics and kinetics parameters of co-combustion between sewage sludge and water hyacinth in CO2/O2 atmosphere as biomass to solid biofuel, Bioresource Technology, 218 (2016) 631-642.

[40] B.V. Babu, A.S. Chaurasia, Parametric study of thermal and thermodynamic properties on pyrolysis of biomass in thermally thick regime, Energy Conversion and Management, 45 (2004) 53-72.

[41] Y.S. Kim, Y.S. Kim, S.H. Kim, Investigation of thermodynamic parameters in the thermal decomposition of plastic waste− waste lube oil compounds, Environmental science & technology, 44 (2010) 5313-5317.

[42] S.R. Naqvi, R. Tariq, Z. Hameed, I. Ali, M. Naqvi, W.-H. Chen, S. Ceylan, H. Rashid, J. Ahmad, S.A. Taqvi, Pyrolysis of high ash sewage sludge: Kinetics and thermodynamic analysis using Coats-Redfern method, Renewable energy, 131 (2019) 854-860.

[43] T. Sonobe, N. Worasuwannarak, S. Pipatmanomai, Synergies in co-pyrolysis of Thai lignite and corncob, Fuel Processing Technology, 89 (2008) 1371-1378.

[44] Z. Wu, W. Yang, L. Chen, H. Meng, J. Zhao, S. Wang, Morphology and microstructure of co-pyrolysis char from bituminous coal blended with lignocellulosic

biomass: Effects of cellulose, hemicellulose and lignin, Applied Thermal Engineering, 116 (2017) 24-32.

[45] J. Wei, Y. Gong, Q. Guo, X. Chen, L. Ding, G. Yu, A mechanism investigation of synergy behaviour variations during blended char co-gasification of biomass and different rank coals, Renewable energy, 131 (2019) 597-605.

[46] J. Wei, Y. Gong, Q. Guo, L. Ding, F. Wang, G. Yu, Physicochemical evolution during rice straw and coal co-pyrolysis and its effect on co-gasification reactivity, Bioresource technology, 227 (2017) 345-352.

[47] Y. Zhang, Y. Zheng, M. Yang, Y. Song, Effect of fuel origin on synergy during co-gasification of biomass and coal in CO2, Bioresource technology, 200 (2016) 789-794.

[48] J. Wang, S. Wang, Preparation, modification and environmental application of biochar: a review, Journal of Cleaner Production, 227 (2019) 1002-1022.

[49] X. Chen, L. Liu, L. Zhang, Y. Zhao, R. Ruan, P. Qiu, Physicochemical properties and AAEM retention of copyrolysis char from coal blended with corn stalks, Energy & Fuels, 33 (2019) 11082-11091.

[50] M. Wang, J. Tian, D.G. Roberts, L. Chang, K. Xie, Interactions between corncob and lignite during temperature-programmed co-pyrolysis, Fuel, 142 (2015) 102-108.

[51] Q. Lu, X.-l. Yang, X.-f. Zhu, Analysis on chemical and physical properties of bio-oil pyrolyzed from rice husk, Journal of Analytical and Applied Pyrolysis, 82 (2008) 191-198.

[52] M.S. Abu Bakar, J.O. Titiloye, Catalytic pyrolysis of rice husk for bio-oil production, Journal of Analytical and Applied Pyrolysis, 103 (2013) 362-368.

[53] N.T. Weiland, N.C. Means, B.D. Morreale, Product distributions from isothermal co-pyrolysis of coal and biomass, Fuel, 94 (2012) 563-570.

[54] J. Wang, Q. Yan, J. Zhao, Z. Wang, J. Huang, S. Gao, S. Song, Y. Fang, Fast co-pyrolysis of coal and biomass in a fluidized-bed reactor, Journal of Thermal Analysis and Calorimetry, 118 (2014) 1663-1673.

[55] Ö. Onay, E. Bayram, Ö.M. Koçkar, Copyrolysis of seyitömer− lignite and safflower seed: influence of the blending ratio and pyrolysis temperature on product yields and oil characterization, Energy & fuels, 21 (2007) 3049-3056.

[56] Y. Qian, J. Zhang, J. Wang, Pressurized pyrolysis of rice husk in an inert gas sweeping fixed-bed reactor with a focus on bio-oil deoxygenation, Bioresource technology, 174 (2014) 95-102.

[57] G. Bensidhom, A. Ben Hassen-Trabelsi, K. Alper, M. Sghairoun, K. Zaafouri, I. Trabelsi, Pyrolysis of Date palm waste in a fixed-bed reactor: Characterization of pyrolytic products, Bioresource Technology, 247 (2018) 363-369.

[58] Y. Li, H. Zhao, X. Sui, X. Wang, H. Ji, Studies on individual pyrolysis and co-pyrolysis of peat–biomass blends: Thermal decomposition behavior, possible synergism, product characteristic evaluations and kinetics, Fuel, 310 (2022) 122280.

[59] Y. Li, S. Huang, Q. Wang, H. Li, Q. Zhang, H. Wang, Y. Wu, S. Wu, J. Gao, Hydrogen transfer route and interaction mechanism during co-pyrolysis of Xilinhot lignite and rice husk, Fuel Processing Technology, 192 (2019) 13-20.

[60] X. Yang, C. Yuan, J. Xu, W. Zhang, Co-pyrolysis of Chinese lignite and biomass in a vacuum reactor, Bioresource Technology, 173 (2014) 1-5.

[61] Q. He, Q. Guo, L. Ding, Y. Gong, J. Wei, G. Yu, Co-pyrolysis behavior and char structure evolution of raw/torrefied rice straw and coal blends, Energy & Fuels, 32 (2018) 12469-12476.

[62] M.S. Masnadi, R. Habibi, J. Kopyscinski, J.M. Hill, X. Bi, C.J. Lim, N. Ellis, J.R. Grace, Fuel characterization and co-pyrolysis kinetics of biomass and fossil fuels, Fuel, 117 (2014) 1204-1214.

Chapter 5

Conclusions and Recommendations

5.1 Conclusions

The mixing of biomass (RH) into coal exhibited an interactive impact on co-pyrolysis as well as co-gasification processes, especially for the most appropriate blending ratio. The optimum temperature range of about 410 °C-560 °C was identified for co-pyrolysis reactions on the basis of four different reaction mechanisms, applied to calculate apparent energy of activation from the non-isothermal TGA data. The thermo-kinetic analysis exhibited convergence of all four reaction mechanisms with the TGA data except the diffusional reaction mechanism in the case of the C20-RH80 fuel blend. The average apparent values of E_a increased with an increasing ratio of RH for 250 °C-400 °C but later the energy barrier decreased with further increase in temperature, hence 500 °C and above was selected for fixed bed reactor tests. Comparative analysis of the reaction models revealed similar order; $D_1 > F_1 > F_{1.5} > S_1$ despite dissimilar values of Ea for C, RH, and their blends. The experimental weight loss value is greater than calculated weight loss value for C80-RH20 and C60-RH40, which is a major indication of presence of synergistic effect.

Co-pyrolysis proved to be effective in the transfer of catalytically active species from RH to coal and thus the produced biochar has a honeycomb structure useful in adsorption and various applications. Bio-oil consisted of phenols, acids, methoxy phenols, creosols, ethenone, cyclopentene, and acetaldehydes. The product gas fraction consisted of CH_4, H_2, and CO_2. The early evolution of CH_4 and H_2 is evidence of the interaction between coal and RH through the transfer of hydrogen radicals. Co-gasification configuration produced a significant increase in H_2 production; however, further future research is required to utilize these by-products with little up-gradation for other commercial-level applications.

5.2 Recommendations

- In this study, thermal, kinetic, and thermodynamic behavior of co-pyrolysis was studied followed by the characterization of co-pyrolysis products and co-gasification of the product gases. In future, further research can be conducted on downstream operations such as Fischer-Tropsch synthesis coupled with water gas shift reactors which will allow to adjust the amount of CO and H_2. So, a technique having co-pyrolysis and co-gasification coupled with these downstream systems is needed to be studied.

- An in-depth Economic and cost analysis is required for using this combination of feedstocks and this technology on commercial level

- Other models including ASPEN and hydrodynamic models (1-D, 2-D) are needed to develop for co-gasification of these feedstocks.

- Detailed investigation involving the energy balance estimation for co-gasification plants needs to be studied.

- To increase the knowledge of synergy, it is also suggested that the blends be processed in different atmospheres like CO_2, air etc.

- In order to produce more synergistic effects, a catalyst must be used that might lower the activation energy of the coal pyrolysis so that the pyrolysis process would correspond at a similar temperature as the biomass so that their in-between radicals will have the capacity to react with one another forming more products.

Appendix A

Research Article

Contents lists available at ScienceDirect

Fuel

journal homepage: www.elsevier.com/locate/fuel

Full Length Article

Thermokinetics synergistic effects on co-pyrolysis of coal and rice husk blends for bioenergy production

Maham Tauseef [a], Abeera Ayaz Ansari [a], Asif Hussain Khoja [a,*], Salman Raza Naqvi [b], Rabia Liaquat [a], William Nimmo [c], Syed Sheraz Daood [d,e,*]

[a] U.S.-Pakistan Centre for Advanced Studies in Energy (USPCAS-E), National University of Sciences & Technology (NUST), Sector H-12, Islamabad 44000, Pakistan
[b] School of Chemical and Materials Engineering (SCME), National University of Sciences & Technology (NUST), Sector H-12, Islamabad 44000, Pakistan
[c] Energy Engineering Group, Energy 2050, Department of Mechanical Engineering, University of Sheffield, Sheffield S3 7RD, United Kingdom
[d] Institute of Energy and Environmental Engineering, Faculty of Electrical, Energy and Environmental Engineering, University of the Punjab, Lahore 54590, Pakistan
[e] Energy Engineering Research and Development Centre, Faculty of Electrical, Energy and Environmental Engineering, University of the Punjab, Lahore 54590, Pakistan

ARTICLE INFO

ABSTRACT

In-depth thermodynamic and kinetic synergistic effects of the coal and rice husk blends on co-pyrolysis have been investigated for bioenergy production. The thermokinetic rate parameters were determined for chemical, one-dimensional diffusional, and phase interfacial reaction models especially when fitted to the Coats-Redfern method. The fitted models exhibited thermokinetic rate parameters. The thermogravimetric analysis in view of the thermodynamic parameters including enthalpy, Gibbs free energy, and entropy imparted the prominent degradation temperature ranges (Stage A: 200 °C-400 °C, Stage B: 410 °C-560 °C) for co-pyrolysis reactions of blends. The proportional increase of rise husk into coal for Stage A caused an increase in the apparent values of activation energy, enthalpy specifically for one-dimensional diffusional, and phase interfacial reaction models. In case of Stage B, the increasing share of rice husk into coal proved to be beneficial in decreasing values of activation energy and enthalpy. Positive synergies for 80:20 and 60:40 coal-rice husk blends were calculated. In addition to characterisation analysis of all samples; co-pyrolysis and co-gasification experiments were completed in a tubular fixed bed reactor at Stage B and onwards temperatures for synergised blends. The resultant co-pyrolysis biochar samples revealed honeycomb structure useful in adsorption applications. The gas chromatography-mass spectrometry analysis of the bio-oil yields 23% phenols, 11% acids, and methoxy phenols for the 60:40 coal-rice husk blend. The product gas composition of 2% H_2, 14% CH_4, and 4% CO_2 for the 80:20 coal-rice husk blend increased to 3% H_2, 12% CH_4, and 5% CO_2 for the 60:40 blend. The co-gasification process substantially increased the production of H_2 up to 14%-17% when compared to co-pyrolysis results. The approach used in this study can be utilized to capitalize on synergy to enhance co-pyrolysis of appropriate blends and their products can be used in further future applications upon upgradation.

1. Introduction

Growing population, rapid increase in industrialization concurrently complying to restrict the global warming to 1.5 °C raise potential challenges to sustainability and also increase the energy demand [1].

necessitates their continuing consumption. The premise of ongoing research and development in the energy and environment sector is to curb the increase of CO_2 whilst offsetting the consumption of fossil fuels without creating energy crises to meet energy and emission targets for the 21st century [2]. Coal still dominates the global primary energy consumption by resource; nevertheless, this conventional energy